Erratum

pg. 35 Tapping mode imaging avoids frictional forces and minimises adhesional forces; it is the preferred method for imaging soft samples.

pg. 89 We use a three dimensional Langevin simulation to examine the detachment of the chain and determine its corresponding force profile, as well as the effect of varying the strength of the surface/monomer interaction, the temperature of the system and the rate of retraction of the AFM tip.

Single Polymer Chains

Belinda Jean Haupt

A thesis submitted for the degree of
Doctor of Philosophy of the Australian National University

Research School of Chemistry
Institute of Advanced Studies

October 2001

Preface

This thesis is an account of research carried out at the Research School of Chemistry, Australian National University for the degree of Doctor of Philosophy.

Although the material presented herein is primarily my own independent research, several collaborators should be acknowledged for their contributions. The atomic force microscopy (AFM) experiments presented in Chapter 4 were performed with the help of Dr Tim Senden and Anthony Hyde is also thanked for his assistance in the design and construction of the inverted dewar used in these experiments. We thank Horst Neumann for his assistance with the synthesis of PNIPAM and in its characterization, Jelica Strauch at the Key Centre for Polymer Colloids, the University of Sydney for the GPC analysis of PNIPAM, used in AFM studies in Chapter 4. Dr David Williams contributed to the development of the simulation program used for generating the results presented in Chapter 6.

The work described in this thesis is original and has not previously been submitted for a degree or diploma in any other University or College.

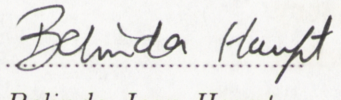

Belinda Jean Haupt.

Acknowledgements

There are many people whose assistance, guidance and friendship have not only made this thesis possible but my time at the A.N.U. memorable. I would specifically like to thank the following people for their invaluable contributions:

Firstly, my supervisor Dr. Edie Sevick, for her enthusiasm for science, insistence on overseas conferences, and her obsession with regular exercise (the result of which I am now a dedicated gym junkie). My temporary supervisor, Prof. David Williams, of the Department of Applied Mathematics, for his very, non-politically correct sense of humour and providing invaluable assistance with my research while Edie was away having their son, Max. I'd also like to thank Dr. Tim Senden, for his generous support with my experiments at the Department of Applied Mathematics and for introducing me to liquorice flavoured espressos.

Prof. Denis Evans, the Dean of the Research School of Chemistry, who gave me a real sense of hope in the future of science in Australia. Dr. Ray Withers, Graduate Convenor of the RSC and avid bush poetry fan, who together with Prof. Evans and the rest of the P&T group have made for some pretty interesting Morning and Afternoon Teas.

To the many people at the Research School of Chemistry and Department of Applied Mathematics, who made them enjoyable places to work. An incomplete list of names: Joanne Harvey, Keith Porter, Ken McRae, Leonie Chow, David Loong and Lasse Norén from the RSC and Ian Miller, Ira Cooke, Tristram Alexander, Chiara Neto, Vince Craig, Janey Wood, and Scott Miller from the Research School of Physical Sciences and Engineering.

To the computing staff for their invaluable support. Horst Neumann, from the RSC for his help with my one and only synthesis and Anthony Hyde, from the Department of Applied Mathematics, for his help in the necessary modifications to the instrument used in my experiments.

My friends here: Louise Sutherland, Doug Aberdeen, Cathie Menon, Tanya McKay, Bina D'Costa, and Wayne Solomon; and interstate/OS: Jennifer Clancy, Thuy Ho, Michael and Chris Noney, Jason Sky, David Carberry, Gemma Drew, Nikolai Tolich, Debbie Watson, Kevin Fleming, Freya Mearns and Felix Ho; who have been a great source of sanity, inspiration and fun.

Finally, my family, my parents Wendy and Heinz, my brother Karl and my sister Amanda, for their love and support throughout the years. Yes, you can call me a doctor now.

Abstract

Atomic Force Microscopy has been used to investigate the detachment of single polymer chains from surfaces and to measure the picoNewton forces required to extend the chain orthogonal to the surface. Such recent experiments show that the force-extension profiles provide interesting signatures which might be related to the progressive detachment of the chain from a surface.

We present experimental evidence of the Rayleigh instability of a single chain in poor solvent conditions using single molecule force microscopy. Poly-N-isopropyl-acrylamide (PNIPAM) and polyethylene oxide (PEO) are adsorbed onto silicon nitride surfaces in various solutions corresponding to poor and good solvent conditions. In good solvent conditions, the force-separation profile is identical to that described previously and attributed to the elastic stretching of single polymer chains. However, in poor solvent conditions, we see a dramatically different force profile, characterised by steps or plateaus of constant force. These plateaus signature the "pull-out" of chain segments from collapsed globules of polymer collected at each of the separating surfaces. A statistical analysis of the large number of force profiles collected indicates that these plateaus are stepped or quantised, suggesting pull-out of several chains of different length. Moreover, the frequency of the steps shows an interesting pattern which distinguishes pulled loops from pulled tails.

We also investigate theoretically the detachment of a single polymer chain from a weakly adsorbing surface. Using equilibrium scaling analysis and activation kinetics, we predict force versus extension profiles for various extension rates. The qualitative features that we predict, such as saw-tooth force-profiles with detachment forces which decrease with extension, maximal yielding forces at high extension rates, and featureless force profiles at large extension, are also seen in experiment.

Lastly, we use Langevin simulation to examine the detachment of the chain and determine its corresponding force profile, as well as the effect of varying the strength of the surface/monomer interaction, the temperature of the system and the rate of retraction of the AFM tip. Unlike our other studies, this work is not yet complete and will be the subject of further research. Consequently, we will only show examples of the possible measures with simulation and, where possible, contrast these results with those of theory and/or experiment.

Contents

List of Figures

List of Tables

Chapter 1

Introduction

1.1 Introduction

A polymer chain consists of a large number of identical chemical units which are referred to as monomers. The simplest polymer is polyethylene and consists of the chemical unit of $(-CH_2 - CH_2-)$. The total number of monomers in a chain is represented by N and is referred to as the degree of polymerisation. Polymers can be linear, branched or have ring configurations. Those that consist of only the one type of chemical unit are known as homopolymers. Alternatively, polymers can also consist of different monomers which can be in a random or regular sequence and are known as copolymers. Heteropolymers consist of several different types of monomers which occur in a non-regular pattern and are commonly found in biopolymers *e.g.*, nucleic acids, polysaccharides and proteins. Monomeric units may also be neutral or charged, those that carry a charge are called polyelectrolytes.

Polymer chains are large molecules, especially when compared to surrounding solvent molecules. In polymer liquids, any given polymer chain only experiences an average of its surrounding due to its many degrees of freedom and its ability to interact with its neighbours. Therefore only mean properties of an individual chain need to be determined. Macroscopic behaviour of polymer solutions are largely determined by the size of the chain. Due to this dependence, then if a few molecular sized parameters are equivalent, then different systems will behave the same. Hence, we consider polymer chains in terms of their molecular size and as being spaghetti-like.

Previously, the behaviour of polymers could only be studied using bulk methods which were limited in that they could only measure macroscopic ensemble averages and could not measure the elastic properties of polymers directly, relying on theoretical models. However, the development of new experimental techniques such as Atomic Force Microscopy (AFM)[1–30] and optical/magnetic tweezers[31–39] have enabled the study of individual chains and has led to an increase in their study

in recent years. These new techniques now make it possible to manipulate single polymer chains by imposing nanometer scale deformations and measuring forces on the scale of picoNewtons. Theoretical studies of perturbing a chain have also been conducted, the majority of these use models that are not atomistic, as the properties of interest are of the molecular scale. These compliment experimental studies, providing insight into experimentally obtained results and make predictions for experiments not yet conducted.

Single polymer chains are of interest to a wide variety of fields including biophysics, colloidal stabilisation, lubrication and adhesion.[1–9,31,32,40,41] The bioploymer DNA has been widely studied, this is due to its importance in biological processes, as it is important in transcription, replication and packaging into chromosomes.[33–35,42] An understanding of the physics of molecular interactions would therefore provide insight not only in biological interactions, but would be of use in the development of materials for specific industrial purposes and macroscopic properties.

We use the AFM to study the behaviour of synthetic polymer chains in different solvent conditions. Specifically, we study the stretching behaviour of adsorbed, single polymer chains in poor solvent. Over recent years, an ever increasing number of polymer systems, both biological and synthetic have been studied using both the AFM and optical tweezers, typically in good solvent conditions. Most notably, are the studies on the biopolymers DNA[3,10,32–35,38] and titin (the giant globular muscle protein),[27,36,39] which have been manipulated using both the AFM and optical tweezers and their mechanical properties determined. Some experimental studies measure the force required to detach a chain from an adsorbing surface and in many of these, the force versus extension profile exhibits sharp discontinuities which have been interpreted in terms of unadsorbed loops of the chain. A number of different single-chain systems have been studied using the AFM and include both synthetic polymers[7–9,11,13,16–25,29,30] and biopolymer chains.[4,10,12,14,26–28] From these studies, the adhesion and elasticity of individual polymer chains have been measured, also, and the structure and the unfolding/folding behaviour of individual domains in biopolymers been investigated.

We have also used scaling analysis, a theoretical treatment developed by deGennes[43] and discussed in greater detail in the following chapter, to investigate the physical behaviour of single polymer chains as they are detached from an adsorbing surface. The physics of polymers have been the studied since the synthesis of these molecules and most notably by deGennes, Flory, Doi, Edwards and Kuhn.[43–47] Of the numerous theoretical studies of polymer chains, there have been several that have investigated the stretching behaviour of a single polymer chain in solution under various solvent conditions.[43–53] The behaviour of a polymer chain adsorbed to a surface has also been studied and its behaviour is reasonably well understood.[43,44]

However, the compression with finite sized objects[54–58] has only recently been studied and is due to the advent and use of the AFM to probe surface bound chains. Similarly, theoretical treatments of AFM single chain experiments, where the surface adsorbed chains are extended have also recently received attention. The studies conducted have intended to explain experimentally obtained results for different polymer systems as well as make predictions for features observed in force extension curves.[9,18,59–62]

Simulation has also been used to study both the static and dynamic properties of single polymer chain under tension in this thesis. A number of different simulation techniques have been used to study the behaviour of a chain in solution, many of which confirm the results of theoretical studies.[63–69] The compression of polymer chains adsorbed or grafted to a surface has also been studied, where conformational transitions are found to occur when the object compressing the chain is of finite size *e.g.*, an AFM probe.[70–74] The stretching of surface bound chains orthogonal and perpendicular to a surface have also been investigated using simulation techniques.[75–78] These simulations were used to study the dynamics of the chains as they were extended and in some instances, detached from the surface.

The theme of this thesis has been the manipulation of single polymer chains using the atomic force microscope. In this thesis, we have combined theory with simulation and experiments to investigate the detachment of single polymer chains adsorbed to a surface.

1.2 Aims and Thesis Outline

Specifically, our aim has been to investigate the dynamics and physics of detaching a single polymer chain from an adsorbing surface using the AFM. In this thesis, we have used scaling analysis and activation kinetics to make predictions for the force profiles of single chain experiments using the AFM. We investigate how the detachment process and features observed in force versus extension profiles vary, depending on the rate of detachment of the chain. Following on from this is a study of the dynamics of single chain AFM experiments. Using simulation we are able to study the effect of a number of system parameters quite easily that would otherwise be quite difficult to do experimentally. The effect of varying the solvent quality on the force profile has also been investigated experimentally using a modified AFM. We have studied several different aqueous polymer systems in order to determine if differences in the force profiles for single chain experiments are attributable to the solvent conditions and not a specific polymer system.

The structure of this thesis is as follows. In the following chapter, we will discuss different theoretical polymer chain models used as well as the most common

simulation methods in use, in particular we will focus on the models and simulation techniques used in this thesis. In the next chapter we describe the atomic force microscope and how it is used to study single polymer chains. Chapter 4 contains the results and discussion of our investigation of the effects of solvency on features observed in force profiles for single chain AFM experiments. Chapter 5 is a theoretical study of using the AFM to probe single polymer chains adsorbed to a surface and specifically the effect of rate on the force extension profile. Chapter 6 uses simulation to the study of the dynamics this process and determines the effect of a number of system parameters on the behaviour of the chain. Lastly, Chapter 7 contains our conclusions from these studies and proposes suggestions for future work.

References

[1] Baumgartner, W.; Hinterdorfer, P.; Ness, W.; Raab, A.; Vestweber, D.; Schindler, H.; Drenckhahn, D. *Proceedings of the National Academy of Sciences of the United States of America* **2000**, *97*, 4005.

[2] Florin, E.-L.; Moy, V. T.; Gaub, H. E. *Science* **1994**, *264*, 415.

[3] Zlatanova, J.; Lindsay, S. M.; Leuba, S. H. *Progress in Biophysics and Molecular Biology* **2000**, *74*, 37.

[4] Oesterhelt, F.; Oesterhelt, D.; Pfeiffer, M.; Engel, A.; Gaub, H. E.; Müller, D. J. *Science* **2000**, *288*, 143.

[5] Müller, D. J.; Baumeister, W.; Engel, A. *Proceedings o f the National Academy of Sciences of the United States of America* **1999**, *96*, 13170.

[6] Camesano, T. A.; Logan, B. E. *Environmental Science and Technology* **2000**, *34*, 3354.

[7] Bemis, J. E.; Akhremitchev, B. B.; Walker, G. C. *Langmuir* **1999**, *15*, 2799.

[8] Courvoisier, A.; Isel, F.; François, J.; Maaloum, M. *Langmuir* **1998**, *14*, 3727.

[9] Hugel, T.; Grosholz, M.; Clausen-Schaumann, H.; Pfau, A.; Gaub, H. ; Seitz, M. *Macromolecules* **2001**, *34*, 1039.

[10] Strunz, T.; Oroszlan, K.; Schäfer, R.; H.-J. Güntherodt, H. -J. *Proc. Natl. Acad. Sci. USA* **1999**, *96*, 11277.

[11] Ortiz, C.; Hadziioannou, G. *Macromolecules* **1999**, *32*, 780.

[12] Marszalek, P. E.; Oberhauser, A. F.; Pang, Y. -P.; Fernandez, J. M. *Nature* **1998**, *396*, 661.

[13] Senden, T. J.; di Meglio, J. -M.; Auroy, P. *Eur. Phys. J. B* **1998**, *3*, 211.

[14] Rief, M.; Oesterhelt, M. F.; Heymann, B.; Gaub, H. E. *Science* **1997**, *275*, 1295.

[15] Bustamante, C.; Marko, J. F.; Siggia, E. D.; Smith, S. *Science* **1994**, *265*, 1599.

[16] Oesterhelt, F.; Rief, M.; Gaub, H. E. *New Journal of Physics* **1999**, *1*, 6.1.

[17] Zhang, W.; Zou, S.; Wang; C.; Zhang, X. *J. Phys. Chem. B* **2000**, *104*, 10258.

[18] Châtellier, X.; Senden, T. J.; Joanny, J. -F.; di Meglio, J. -M. *Europhysics Letters* **1998**, *41*, 303.

[19] Kikuchi, H.; Yokoyama, N.; Kajiyama, T. *Chemistry Letters* **1997**, *11*, 1107.

[20] Maaloum, M.; Courvoisier, A. *Macromolecules* **1999**, *32*, 4989.

[21] Li, H.; Liu, B.; Zhang, X.; Gao, C.; Shen, J.; Zou, G. *Langmuir* **1999**, *15*, 2120.

[22] Li, H.; Zhang, W.; Xu, W.; Zhang, X. *Macromolecules* **2000**, *33*, 465.

[23] Al-Maawali, S.; Bemis, J. E.; Akhremitchev, B. B.; Leecharoen, R.; Janesko, B. G.; Walker, G. C. *J. Phys. Chem.* **2001**, *105*, 3965.

[24] Garnier, L.; Gauthier-Manuel, B.; van der Vegte, E. W.; Snijders, J.; Hadzioannou, G. *Journal of Chemical Physics* **2000**, *113*, 2497.

[25] Yamamoto, S.; Tsujii, Y.; Fukuda, T. *Macromolecules* **2000**, *33*, 5995.

[26] Li, H.; Rief, M.; Oesterhelt, F.; Gaub, H. E. *Advanced Materials* **1998**, *3*, 316.

[27] Rief, M.; Gautel, M.; Oesterhelt, F.; Fernandez, J. M.; Gaub, H.E. *Science* **1997**, *276*, 1109.

[28] Carrion-Vazquez, M.; Oberhauser, A. F.; Fowler, S. B.; Marszalek, P. E.; Broedel, S. E.; Clarke, J.; Fernandez, J. M. *Proc. Natl. Acad. Sci. USA* **1999**, *96*, 3694.

[29] Senden, T. J. *Current Opinion in Colloid and Interface Science* **2001**, *6*, 95.

[30] Merkel, R. *Physics Reports* **2001**, *346*, 343.

[31] Carl, P.; Kwok, C. H.; Manderson, G.; Speicher, D. W.; Discher, D. E. *Proceedings of the National Academy of Sciences of the United States of America* **2001**, *98*, 1565.

[32] Shivashankar, G. V.; Feingold, M.; Krichevsky, O.; Libchaber, A. *Proceedings of the National Academy of Sciences of the United States of America* **1999**, *96*, 7916.

[33] Smith, S. B.; Finzi, L.; Bustamante, C. *Science* **1992**, *258*, 1122.

[34] Cui, Y.; Bustamante, C. *Proceedings of the National Academy of Sciences of the United States of America* **2000**, *97*, 127.

[35] Bennink, M. L.; Leuba, S. H.; Leno, G. H.; Zlatnova, J.; de Grooth, B. G.; Greve, J. *Nature Structural Biology* **2001**, *8*, 606.

[36] Tskhovrebova, L.; Trinick, J.; Sleep, A.; Simmons, R. M. *Nature* **1997**, *387*, 308.

[37] Smith, S. B.; Cui, Y.; Bustamante, C. *Science* **1996**, *271*, 795.

[38] Strick, T. R.; Croquette, V.; Bensimon, D. *Nature* **2000**, *404*, 901.

[39] Kellermayer, M. S. Z.; Smith, S. B.; Granzier, H. L.; Bustamante, C. *Science* **1997**, *276*, 1112.

[40] Krammer, A.; Lu, H.; Israelwitz, B.; Schulten, K.; Vogel, V. *Proceedings of the National Academy of Sciences of the United States of America* **1999**, *96*, 1351.

[41] Lasic, D. D. *Liposomes: from Physics to Applications*; Elsevier: Amsterdam and New York, 1993.

[42] Hansma, H. G.; Browne, K. A.; Bezanilla, M.; Bruice, T. C. *Biochemistry* **1994**, *33*, 8436.

[43] de Gennes, P. -G. *Scaling Concepts in Polymer Physics*; Cornell University Press: Ithaca, 197 9.

[44] Doi, M.; Edwards, S. F. *The Theory of Polymer Dynamics*; Oxford University Press: Oxford, 1986.

[45] Flory, P. J. *Principles of Polymer Chemistry*; Cornell University Press: Ithaca, 1992.

[46] Flory, P. J. *Statistical Mechanics of Chain Molecules*; Hanser Publishers: New York, 1989.

[47] Evans, D. F.; Wennerström, H. *The Colloidal Domain: Where Physics, Chemistry and Biology Meet*, 2nd. ed.; Wiley-VCH: New York, 1999.

[48] de Gennes, P. G. *Macromolecules* **1976**, *9*, 587.

[49] Pincus, P. *Macromolecules* **1976**, *9*, 386.

[50] Halperin, A.; Zhulina, E. B. *Europhys. Lett.* **1991**, *15*, 417.

[51] Buhot, A.; Halperin, A. *Physical Review Letters* **2000**, *84*, 2160.

[52] Marko, J. F. *Physical Review E* **1998**, *57*, 2134.

[53] Sarkar, A.; Léger, J.-F.; Chatenay, D.; Marko, J. F. *Physical Review E* **2001**, *63*, 051903-1.

[54] Subramanian, G.; Williams, S. R. M.; Pincus, P. A. *Macromolecules* **1996**, *29*, 4045.

[55] Guffond, M. C.; Williams, D. R. M.; Sevick, E. M. *Langmuir* **1997**, *13*, 5691.

[56] Ennis, J.; Sevick, E. M.; Williams, D. R. M. *Physical Review E* **1999**, *60*, 6906.

[57] Sevick, E. M. *Macromolecules* **2000**, *33*, 5743.

[58] Ennis, J.; Sevick, E. M. *Macromolecules* **2001**, *34*, 1908.

[59] Châtellier, X.; Joanny, J.-F., *Physical Review E* **1998**, *57*, 6923.

[60] Lubensky, D. K.; Nelson, D. R., *Physical Review Letters* **2000**, *85*, 1572.

[61] Tamashiro, M. N.; Schiessel, H., *Macromolecules* **2000**, *33*, 5263.

[62] Zhulina, E.; Walker, G. C.; Balazs, A. C., *Langmuir* **1998**, *14*, 4615.

[63] Hatfield, J. W.; Quake, S. R. *Physical Review Letters* **1999**, *82*, 3548.

[64] Kreitmeier, S.; Wittkop, M.; Göritz, D. *Physical Review E* **1999**, *59*, 1982.

[65] Wittkop, M.; Kreitmeier, S.; Göritz, D. *J. Chem. Soc., Faraday Trans.* **1996**, *92*, 1375.

[66] Wittkop, M.; Kreitmeier, S.; Göritz, D. *Physical Review E* **1996**, *53*, 838.

[67] Titantah, J. T.; Pierleoni, C.; Ryckaert, J.-P. *Physical Review E* **1999**, *60*, 7010.

[68] Sheng, Y.-J.; Lai, P.-Y. *Physical Review E* **1997**, *56*, 1900.

[69] Maurice, R. G.; Matthai, C. C. *Physical Review E* **1999**, *60*, 3165.

[70] Milchev, A.; Yamakov, V.; Binder, K. *Europhysics* **1999**, *47*, 675.

[71] Milchev, A.; Yamakov, V.; Binder, K. *Phys. Chem. Chem. Phys.* **1999**, *1*, 2083.

[72] Jimenez, J.; Rajagopalan, R. *Langmuir* **1998**, *14*, 2598.

[73] Jimenez, J.; Rajagopalan, R. *Physical Journal B* **1998**, *243*, 237.

[74] Murat, M. *Macromolecules* **1996**, *29*, 8282.

[75] Jimenez, J.; de Joannis, J.; Bitsanis, I.; Rajagopalan, R. *Macromolecules* **2000**, *33*, 7157.

[76] Stevens, F.; Lo, Y.-S.; Harris, J. M.; Beebe, T. P. *Langmuir* **1999**, *15*, 207.

[77] Kreuzer, H. J.,; Wang, R. L. C.; Grunze, M. *New Journal of Physics* **1999**, *1*, 1.

[78] Sevick, E. M.; Williams, D. R. M., *Physical Review Letters* **1999**, *82*, 2701.

Chapter 2

Background and Methodology: Tools used in this Thesis

In this thesis, we use theoretical models, simulation and the atomic force microscope (AFM) to investigate "pulling" single polymer chains off an adsorbing surface. This chapter provides the theoretical background and simulation techniques for studying single polymer chains. Firstly, we discuss polymer chain models and how they are used to represent a chain. In Section 2.2 we discuss the thermodynamics of a polymer system, different descriptions for stretching a chain, the compression of a chain and the effect of solvency on the size of the chain. Lastly, in Section 2.3 we compare and contrast the two simulation techniques of Molecular and Langevin Dynamics.

2.1 Polymer Chain Models

The simplest idealisation of a polymer chain is an ideal chain.[1–9] An ideal chain is analogous to an ideal gas in that we invoke the following assumptions, that (1) self-intersections are allowed and (2) there are no energetic interactions amongst components of the chain *i.e.*, there is no excluded volume and chains are "phantom". As reviewed below, the behaviour of an ideal chain can be modelled in a number of different ways. One example is the freely jointed chain[1–7,9] where links of constant length are joined and can rotate freely. This model is mathematical simple, providing formulas that are related to Gaussian statistics. However, this model is difficult to simulate and an equivalent model, the beads-springs model,[2,7] where the length of the links is allowed to vary, is used in simulation. Both models are used in this thesis and will be described in this chapter, followed by the thermodynamics of stretching and compressing a polymer chain and lastly the simulation techniques of molecular and Langevin dynamics.

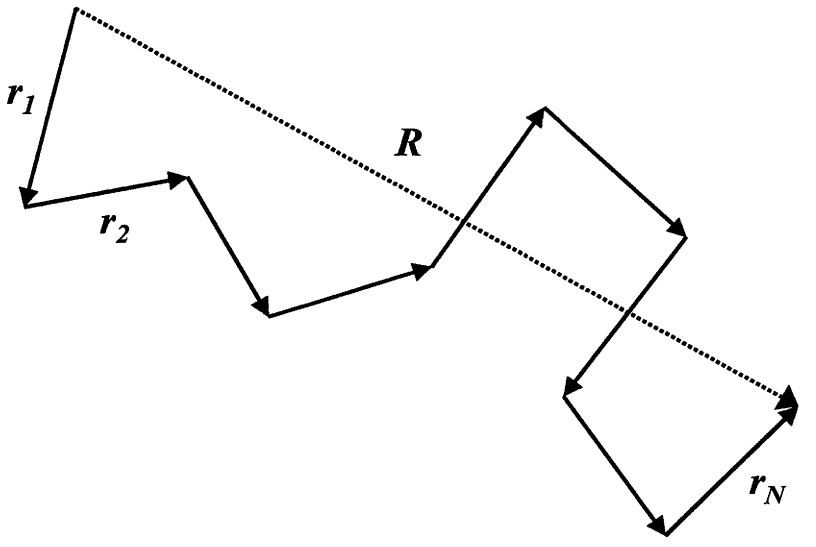

Figure 2.1: The freely jointed chain model consisting of N links of length a.

2.1.1 Freely Jointed Chain Model

A simple model used for polymer chains is the freely jointed chain (FJC) model,[1–7,9] Figure 2.1. The polymer chain is a series of N links of size a which orientate independently of each other. This is analogous to the trajectory of a random walk of fixed step size. The conformation of the chain can be described by either the set of the position vectors $\mathbf{R}_n = (\mathbf{R}_0...\mathbf{R}_N)$, or as the set of bond or step vectors $\mathbf{r}_n = (\mathbf{r}_1...\mathbf{r}_N)$ where

$$\mathbf{r}_n = \mathbf{R}_n - \mathbf{R}_{n-1}, n = 1, 2, ..., N. \tag{2.1}$$

and the magnitude of $\mathbf{r}_n$ is a, *i.e.*, $a = |\mathbf{r}_n|$ for all n. The size of the chain is determined by the end-to-end distance of the chain $\mathbf{R}$, and is shown to be

$$\mathbf{R} = \mathbf{R}_N - \mathbf{R}_0 = \sum_{n=1}^{N} \mathbf{r}_n \tag{2.2}$$

Since the probability of the end-to-end distance of the chain being $\mathbf{R}$ is the same as it being $-\mathbf{R}$, then the average $< \mathbf{R} >$ of $\mathbf{R}$ is zero. The size of the chain is determined from the average of the square of $\mathbf{R}$. Let R be

$$R =< \mathbf{R}^2 >^{1/2} \tag{2.3}$$

and $< \mathbf{R}^2 >$ given by

$$\begin{aligned} < \mathbf{R}^2 > &= \textstyle\sum_{n=1}^{N} \sum_{m=1}^{N} < \mathbf{r}_n.\mathbf{r}_m > \\ &= \textstyle\sum_{n=1}^{N} < \mathbf{r}_n^2 > + 2 \sum_{n>m} < \mathbf{r}_n.\mathbf{r}_m > \\ &= \textstyle\sum_{n=1}^{N} a^2 + 2 \sum_{n>m} < \mathbf{r}_n.\mathbf{r}_m > \\ &= Na^2 + 2 \textstyle\sum_{n>m} < \mathbf{r}_n.\mathbf{r}_m > \end{aligned} \tag{2.4}$$

where a is the step size. For a FJC, where the orientation of the vectors is completely uncorrelated, $< \mathbf{r}_n.\mathbf{r}_m >= 0$ and $n \neq m$. Therefore eq 2.4 is

$$< \mathbf{R}^2 >= Na^2 \tag{2.5}$$

Thus we say that the size of the freely jointed or ideal chain scales with N to the $1/2$ power, or

$$R = \sqrt{N}a. \tag{2.6}$$

Although the FJC model is simple, the result $< \mathbf{R}^2 >\sim Na^2$ is quite general and holds for other models such as the freely rotating chain (FRC) model.[2,4,9] The FRC model has a fixed angle between the bonds, therefore the orientation of the nearest neighbour vectors is correlated and $< \mathbf{r}_n.\mathbf{r}_m >\neq 0$ for $n \neq m$. However, as $|n - m|$ increases, $< \mathbf{r}_n.\mathbf{r}_m >$ approaches zero and $< \mathbf{R}^2 >\sim N$ is true for large N. For these models, the chain is not fully flexible and its flexibility is described by a term called the persistence length, l_p,

$$\begin{aligned} l_p &= a + \tfrac{1}{a}\textstyle\sum_{n>m} < \mathbf{r}_n.\mathbf{r}_m > \\ a(l_p - a) &= \textstyle\sum_{n>m} < \mathbf{r}_n.\mathbf{r}_m > \end{aligned} \tag{2.7}$$

which is the length scale over which the chain is rigid. Substituting this into eq 2.4 gives

$$\begin{aligned} < \mathbf{R}^2 >&= Na^2 + 2\textstyle\sum_n a(l_p - a) \\ < \mathbf{R}^2 >&= Na^2 + 2Na(l_p - a) \\ < \mathbf{R}^2 >&= Na^2(2(\tfrac{l_p}{a}) - 1) \end{aligned} \tag{2.8}$$

Therefore $< \mathbf{R}^2 >\sim Na^2$ for large N, with the prefactor, $(2(\frac{l_p}{a}) - 1)$, varying from unity in the FJC model, to a large value for chains where correlation persists over a number of sequential bonds.

Random walk statistics can be used to describe the probability functions of the FJC. The probability of finding a chain whose end-to-end distance is between R and dR is $p(R, N)dR$. The probability distribution function, $P(R, N)$, of R of a sufficiently long chain ($N >> 1$) is Gaussian:[2–4,7,9]

$$P(R, N) = (\frac{3}{2\pi Na^2})^{3/2} exp(-\frac{3R^2}{2Na^2}) \tag{2.9}$$

This general result comes from statistics and the central limit theorem.

The FJC model is very robust and mathematically simple to model. By having a equal to the persistence length, random walk statistics can be used. In Chapter 5, we use this model of an ideal chain for theory and scaling analysis. Although this model is ideal for theoretical treatments, it is not trivial to use in simulations.

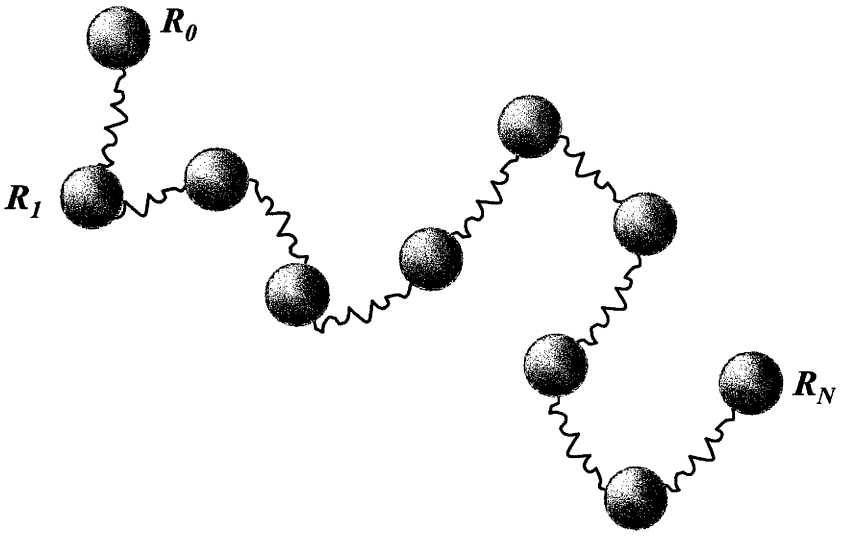

Figure 2.2: The beads-spring model.

The inherent difficulty lies in maintaining the $N-1$ constraints of $|\mathbf{R}_n - \mathbf{R}_m| = a$, while tracking the positions of N beads. The solution is to change the links from a fixed length to a variable length which is selected from a Gaussian distribution. This model is referred to as the beads-springs model[2,7] which recovers the random walk statistics and consequently still mimics an ideal chain. In simulation this model is the base upon which other potential interactions can be added, as for example interactions between the beads.

2.1.2 The Gaussian Chain and the Bead-Spring Model

A continuum model which is mathematically simple to model is the Gaussian chain model. This model makes the assumption that the bond vector or link $\mathbf{r}$ has a bond length chosne from the distribution

$$p(r) = (\frac{3}{2\pi a^2})^{3/2} exp(-\frac{3r^2}{2a^2}) \tag{2.10}$$

For a Gaussian chain, the position vector of the nth link can be written as $\mathbf{R}_n$ (similar to the models previously described), then eq 2.10 gives the distribution of the bond vector, $\mathbf{r}_n$. The probability distribution of a chain with an end-to-end distance $\mathbf{R}_n$, $P(\mathbf{R}_n)$, is given by

$$P(\mathbf{R}_n) = (\frac{3}{2\pi a^2})^{3N/2} exp(-\frac{3}{2a^2}\sum_{n=1}^{N}(\mathbf{R}_n - \mathbf{R}_{n-1})^2) \tag{2.11}$$

The Gaussian chain is most commonly described by the beads-springs model,[2,7] Figure 2.2. The polymer chain is depicted as a series of N beads connected by har-

monic springs, with an individual bead-spring component representing a statistical monomer unit of size a. If we let the spring constant be k, then the energy, U_{spring}, of the chain is,

$$U_{spring} = \frac{1}{2}k\sum_{n=1}^{N}(\mathbf{R}_n - \mathbf{R}_{n-1})^2) \tag{2.12}$$

At equilibrium the distribution function of the chain is proportional to $exp(-U/k_BT)$ and k is

$$k = \frac{3k_BT}{a^2} \tag{2.13}$$

where k_B is Boltzmann's constant and T is the temperature. Then the equilibrium distribution of the chain will be equivalent to eq 2.11. The Gaussian chain model depicted as beads-springs describes the properties of polymer chains on large length scales and is used quite frequently in polymer chain simulation.

2.2 Thermodynamics and the Polymer System

An important quantity for analysis of a thermodynamic system is the determination of the Helmholtz free energy, $\triangle F$, and consists of both entropic and enthalpic contributions ($\triangle F = \triangle E - T\triangle S$).[1] The entropic term, $T\triangle S$, describes the change in randomness that arises from the number of possible configurations of the chain, and the energy term, $\triangle E$, describes the interactions of monomers within the chain or with other chains or surfaces. An ideal chain has no interactions amongst the monomers, hence there is no change in the interactions between the monomers and $\triangle E = 0$. Therefore the ideal chain is purely entropic and is analogous to an ideal gas. The entropy, S is defined by Boltzmann's principle as

$$S \sim k_B ln(W) \tag{2.14}$$

where W is the number of possible configurations of the polymer chain. The entropy change upon stretching and confining a chain is used in a theoretical treatment in this thesis. Therefore we will discuss this in the following sections.

2.2.1 Stretching a Polymer Chain

Consider grabbing the ends of a chain and holding these ends a distance R apart. If R is increased from $\sqrt{N}a$ to a distance approaching the contour length of the chain, Na, we would be stretching the chain, resulting in a change in the chain's entropy. That is the number of configurations of a chain with ends fixed a distance R apart is smaller than the number of configurations when the ends are free. The

chain loses entropy or increases its free energy upon stretching according to[1]

$$\triangle F = -T\triangle S \sim -k_B T ln P(R) \tag{2.15}$$

We have already defined the probability distribution of R in eq 2.11, using this gives

$$\triangle F = \frac{3}{2}\frac{k_B T R^2}{Na^2} \tag{2.16}$$

the change in free energy with extension R.

The change in energy is equal to the work required to stretch a chain. Therefore, we can calculate the force for maintaining a given extension, R, by taking the derivative of eq 2.16 with respect to R,

$$f = \frac{dF}{dR} \sim (\frac{3k_B T}{Na^2})R \tag{2.17}$$

The stretching behaviour of the chain is of a Hookean spring where the spring constant is inversely proportional to N. This is valid for small extensions, *i.e.*, $R << Na$.

For large extensions of a polymer chain where the extension approaches the contour length of the chain, $R \Rightarrow Na$, the assumption of Gaussian statistics is not valid due to the small number of configurations available at such large extensions. A mathematical solution to this problem was to consider the distribution of **R** as electric dipoles being fully orientated by an applied field. This is applicable to extensions up to $R = Na$ and was adapted by Kuhn and Grün as well as James and Guth[3,4] and is simply the FJC of a finite number of inextensible links. Consider applying a force, **f**, in the x-direction to a single bond in the FJC. We let θ_n be the angle of the bond with the x-axis and the bond configuration as $x_n = acos\theta_n$. Thus the bond configurational energy is $-fx_n$, and the probability of its alignment value lying between x_n and $x_n + dx_n$ is proportional to

$$exp(fx_n/k_B T)dx_n \tag{2.18}$$

The average extension distance of the bond, $< x_n >$ is given by

$$< x_n >= \frac{\int_{-a}^{a} x_n exp(fx_n/k_B T)dx_n}{\int_{-a}^{a} exp(fx_n)/k_B T)dx_n)} = a[coth(fa/k_B T) - k_B T/fa] \tag{2.19}$$

The expression in the brackets may be rewritten as $\mathcal{L}(fa/k_B T)$, where $\mathcal{L}$ is the Langevin function. Thus,

$$< x_n >= a\mathcal{L}(fa/k_B T) \tag{2.20}$$

The average extension of the polymer chain is given as the sum of the average

projections of its N bonds on the x-axis and is

$$< x >= \sum_{n=1}^{N} < x_n >= L\mathcal{L}(fa/k_BT) \tag{2.21}$$

where L is the contour length of the chain. The force necessary for extending a polymer chain a fixed distance $< x >$ is

$$f = \frac{k_BT}{a}\mathcal{L}^{-1}(\frac{< x >}{L}) \tag{2.22}$$

It is only necessary to use a more accurate mathematical description for polymer chain extensions larger than $\sim (50N^{1/2})\%$ of $\sqrt{< \mathbf{R}^2 >}$. Note for this model, the parameter a is denoted as the Kuhn length which is $a =< \mathbf{R}^2 > /Na$.

Although the FJC model using the Langevin function is more accurate than the Gaussian function for high extensions, it has been modified so as to more closely match observed high force behaviour in single polymer chain experiments.[10,11] The extended FJC models involves the addition of the parameter, $k_{segment}$, which allows for the extensibility of the bonds as well as the alignment under an applied force. The expression for the extension of a polymer chain using the extended FJC model is,

$$x(f) = (L + \frac{Nf}{k_{segment}})[coth(\frac{fa}{k_BT}) - \frac{k_BT}{fa}] \tag{2.23}$$

Both the FJC and extended FJC model using the Langevin function are valid for fitting force curves for fully flexible polymer chains.

An alternative description of a polymer chain is the worm-like chain (WLC) model. This model was developed by Porod and Kratky[4] using the concept of continuous curvature of the chain and describes its trajectory as a smooth curve that randomly changes direction. It is similar to the freely rotating chain in that the bond angles are fixed. The WLC model uses persistence length, l_p instead of the Kuhn length for chain stiffness as well as the contour length as parameters for characterising the chain. In the absence of an applied force, the persistence length is equal to half the Kuhn length of the chain. Unlike the FJC model, there is no exact solution for the extension of the WLC by an applied force.[12] However, a numerical solution has been obtained by treating the system quantum mechanically, that is as a field applied to an electric dipole and solving a differential equation equivalent to Schrödinger's equation.[9] The summarized equation was given by Bustamante et al.,[13]

$$f = \frac{k_BT}{l_p}(\frac{1}{4}(1 - \frac{x}{L})^{-2} - \frac{1}{4} + \frac{x}{L}) \tag{2.24}$$

This model is used to characterise stiff chains, although not exclusively.

Figure 2.3 graphs the three different force laws: (1) the Gaussian chain with

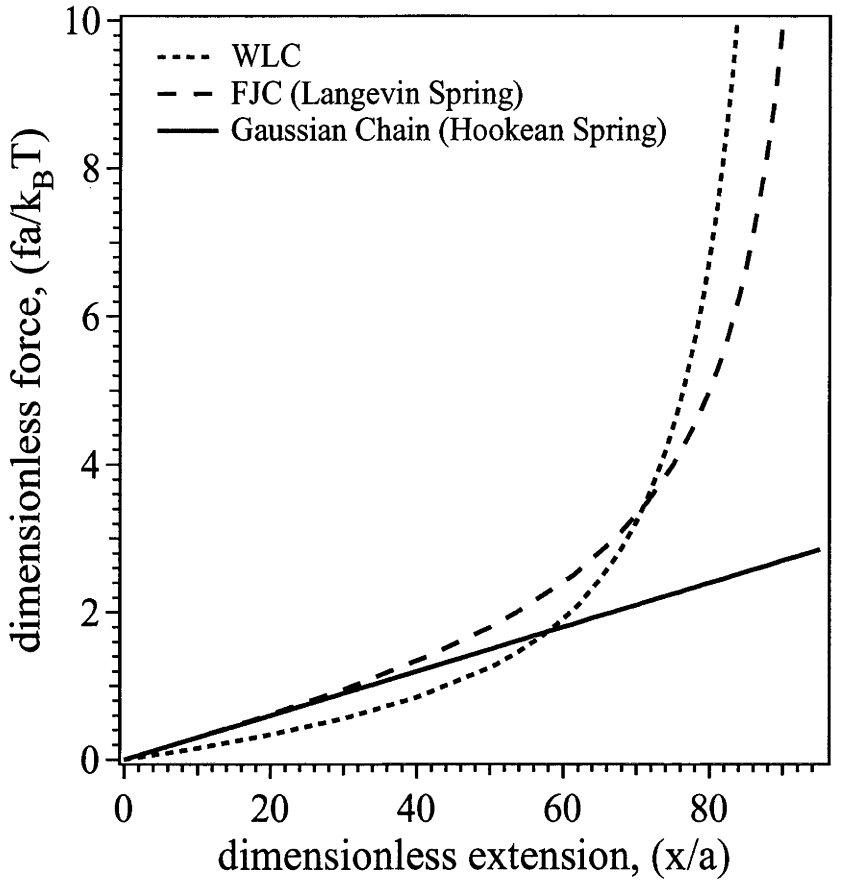

Figure 2.3: Dimensionless force, $fa/(K_BT)$, versus dimensionless extension, x/a, for the different models: (1) a simple Gaussian chain; (2) the FJC; and (3) the WLC.

Hookean springs; (2) the FJC with Langevin springs and (3) the WLC. Note for small chain extensions the simple model of a Gaussian chain is adequate for extensions up to $1/2Na$. For high extensions, the response of the polymer chain to an applied force is no longer linear and more sophisticated models are required such as the FJC and WLC models. For this reason the FJC and WLC models are used to fit force curves obtained in single molecule force microscopy experiments. We use the FJC, extended FJC and WLC models to fit our experimental force curves in Chapter 5.

2.2.2 Polymer Confinement

The reduction in conformational entropy when an ideal chain goes from solution where its size is unrestricted ($R \sim \sqrt{N}a$) to being confined within a slit of height H or a tube of diameter H is given by,

$$\triangle S \sim k_B \times \text{no. of times the chain "feels" a wall} \tag{2.25}$$

This comes from the notion that a monomer located along the chain that is situated in the middle of the pipe is unrestricted in its motion and behaves as in a random

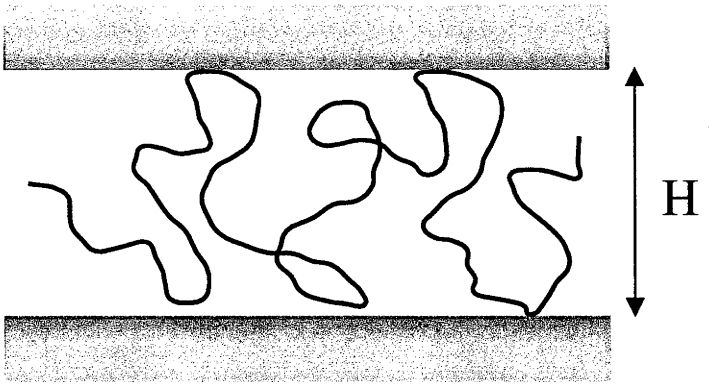

Figure 2.4: An ideal chain trapped between two walls that are a distance H apart.

walk. However, a monomer near the wall is restricted and effectively loses the ability to move in one direction *i.e.*, a three dimensional random walk is reduced to a two dimensional random walk. Therefore we need to count the number of times that the chain comes into contact with the walls. As the chain is ideal, we know that the size of the portion of a chain which does not feel the walls is

$$H \sim am^{1/2} \tag{2.26}$$

where m is the number of monomers in the portion between the two walls. Therefore the number of contacts is,

$$\frac{N}{m} = \frac{\text{no. of monomers in chain}}{\text{no. of monomers in bridge}} \tag{2.27}$$

and the change in entropy is

$$\triangle S \sim -k_B \frac{N}{m} \tag{2.28}$$

However, since $m \sim H^2/a^2$ then

$$\triangle S \sim -k_B \frac{Na^2}{H^2} \tag{2.29}$$

The compression of an ideal chain between two parallel plates of infinite size is analogous to a chain trapped in a pipe (see Figure 2.4). The free energy penalty of confinement is given by,[1,14]

$$F \sim k_B T \frac{Na^2}{H^2} \tag{2.30}$$

which increases as H decreases and is large for small separations. This is used in Chapter 5 for the theoretical study of detaching a single polymer chain from an adsorbing surface.

2.2.3 Polymer Solvent Types

All our previous sections have considered the polymer chain as ideal. However a polymer chain in solution rarely is ideal and its behaviour is greatly influenced by the solvent in which it is dissolved. There are three possible types of solvents or solutions for polymer chains which are nominally called good, poor or θ (an ideal chain). A good solvent has interactions between itself and the solvent molecules being energetically favourable which results in the chain becoming swollen. A poor solvent means the monomers in the chain prefer to interact with themselves, rather than with solvent molecules. This has the effect of causing the chain to collapse as the monomers in the chain minimise their contact with the solvent molecules. A θ solvent has a balance in the energy associated with repulsive (two-body) monomer-monomer interactions and the energy of monomer solvent interactions.

The interaction of a chain with itself is known as the excluded volume effect. Most notably it has been studied by Kuhn and Flory[2,3,6] who determined the relationship of R_g with N as,

$$R \approx N^{\nu} a \tag{2.31}$$

where ν is called the Flory exponent and varies according to temperature for a given polymer/solvent system.

The Flory argument for determining the size of a polymer chain in a good solvent involves balancing two effects, an excluded volume interaction which causes the coil to swell and an elastic energy that causes the chain to contract. We can therefore show this balance in the free energy of the chain:

$$F = U - TS \tag{2.32}$$

where U involves the excluded volume and monomer-solvent interactions and TS the entropy of an ideal chain. The repulsive interaction potential for excluded volume can be expressed as a virial expansion,

$$U = V k_B T (B\eta^2 + C\eta^3 + D\eta^4 + ...) \tag{2.33}$$

where V is the volume of the chain and is proportional to the chain size cubed ($V \sim R^3$), $\eta = N/V$ is the concentration of monomers, and B, C and D are virial coefficients. We can neglect the higher order terms as the density of monomers in the coil is small. Therefore, the repulsive interaction potential is,

$$U = V k_B T B \eta^2 \tag{2.34}$$

If we make the assumption that the entropy of a solvated chain differs very little

from that of an ideal chain, then using the result for the ideal chain (see eq 2.16) and eq 2.34, the total free energy of the chain is,

$$F/k_BT = VB\eta^2 + \frac{3}{2}\frac{R^2}{Na^2} \tag{2.35}$$

Introducing α, the swelling coefficient,

$$\alpha = \frac{R^2}{Na^2} \tag{2.36}$$

into eq 2.35 gives,

$$F/k_BT \sim \frac{B\sqrt{N}}{a^3\alpha^3} + \frac{3}{2}\alpha^2 \tag{2.37}$$

The size of the polymer chain can be estimated by finding the minimum of F with respect to α. For $dF/d\alpha = 0$, the size of the chain is

$$R \sim (\frac{B}{a^3})^{1/5} a N^{3/5} \tag{2.38}$$

The exponent 3/5 corresponds to the Flory exponent is $\nu = 3/5$ in eq 2.31.

A polymer chain in a poor solvent has the configuration of a spherical globule. This configuration minimises the surface area of the polymer chain and hence its interaction with the solvent. The volume of the spherical globule is $V = 4/3\pi R^3 \approx a^3N$, where R is the radius of the sphere and the size of the chain. Therefore the size of a polymer chain in a poor solvent scales as,[1,5]

$$R \approx aN^{1/3}. \tag{2.39}$$

For the ideal chain, the second virial coefficient is equal to zero ($B = 0$), resulting in the repulsive interaction potential, eq 2.34, being zero and the total free energy of the chain given by eq 2.16.

In summary the size of the polymer chains in the different solvents scales with N according to:[1–3,5–9,15]

$$\begin{aligned} R_g &\approx N^{3/5}a \quad \text{a swollen chain} \\ R_g &\approx N^{1/2}a \quad \text{an ideal chain} \\ R_g &\approx N^{1/3}a \quad \text{a globule} \end{aligned} \tag{2.40}$$

Due to the differences in the solvent types, not only does the size of the polymer chain vary but also its behaviour under an applied force. In Chapter 4, we use this to discuss the behaviour of a polymer chain under tension in poor solvent conditions and how dramatically different it is to the good solvent case.

2.3 Simulation Methods

Another method used in conjunction with theory to study single polymer chains is simulation. In our studies, we have used Langevin simulation exclusively. We will first discuss molecular dynamics as it is a more commonly used simulation, then the Langevin simulation comparing the two techniques and reasoning for our choice of simulation method.

2.3.1 Molecular Dynamics

Molecular Dynamics (MD) is able to calculate properties of a system, both static and dynamical by solving numerically Newton's laws of motion.[15–18] MD simulation involves a system of N particles placed within a cubic cell of constant volume, where the initial coordinates of the particles, $\mathbf{r}_i(0)$, are arbitrarily chosen. The trajectories of the particles which interact via a potential are tracked. The coordinates of the particles are then determined after a short timestep using Newton's equations of motion. An example of the scheme of an MD simulation is the following. Using the finite difference method, a prediction is made for time $t + \triangle t$, for the particles' coordinates, velocities and accelerations based on their current values. The forces and accelerations can then be calculated from the new coordinates using $\mathbf{f}_i = m_i\mathbf{a}_i$, where $\mathbf{f}_i$ is the force, m_i is the mass and $\mathbf{a}_i$ is the acceleration of a particle i. Using the new accelerations, the predicted coordinates, velocities etc. are corrected. Lastly, properties of the system such as energy, density are calculated before returning to the first step of making a prediction. This is one method of treating the equations of motion as first order differential equations.

A system is considered as equilibrated for an MD simulation, when the potential energy fluctuate closely around a constant mean value. A run of 10^3 time steps (excluding equilibration time) is typically enough to yield an energy with an uncertainty of about 1%.[17] Periodic boundary conditions are used to minimise effects of the particles being placed within the finite-sized simulation cell so as to more closely simulate an infinite system. The particles coordinates and momenta are stored during the course of the simulation, while other properties are stored as time averages. Difficulties inherent in this method is the limit of the number of particles (of order 10^3) it can simulate and the maximum time that can be simulated. When each particle is a molecule with more than 3 degrees of freedom, such as in a polymer, MD becomes even more limited with respect not only to the number of molecules and time, but also with respect to the size of the polymer. Also the numerical integration of the equations leads to small numerical errors and can result in a temperature drift. This can be corrected for by rescaling the velocities. Characteristically, MD simulations simulate for short timescales *i.e.*, a few femtoseconds. It cannot simulate

the collective motion of molecules which occurs in diffusion and hydrodynamic flow as these occur over much longer timescales. To do this requires the use of coarse grain models. These have large length scales where the fluid system behaves as a continuum. The following simulation method uses this model.

2.3.2 Langevin Dynamics

The Langevin Dynamics is often called Brownian Dynamics and uses a dynamical equation of motion to describe the interaction of a large Brownian particle with fluid molecules.[2,7,17] The time and length scales used in a Langevin simulation are sufficiently large that inertia of the particles is negligible. Therefore Newton's law of motion, $\mathbf{F} = m\mathbf{a}$, is $\mathbf{F} = \mathbf{0}$. The simulation calculates new coordinates of the Brownian particle with the sum of the forces acting on it are set to zero. This description is coarse grained and does describe the system microscopically but not to the same molecular detail as in MD. This is because the dynamical properties we are interested in calculating for a polymer system are mesoscopic, *i.e.*, the lengthscale we are interested in is not Ångstrom but of the micron scale. The solvent molecules are considered as a viscous continuum through which the particles move.

The behaviour of a Brownian particle in a solvent can be considered as a spherical particle that is buffeted by solvent molecules that collectively impart momentum to the particle. The particle motion was described by Einstein as a random walk with a root-mean-square displacement x at time t as[15]

$$x = (2Dt)^{1/2} \tag{2.41}$$

and D is the diffusion coefficient. The motion of the particle is also retarded by a frictional force F that is proportional to particle's velocity, V,

$$F = -\zeta V \tag{2.42}$$

where ζ is the friction constant. This holds for the condition that the particle is smooth and the velocity is not too large. An equation relating kinetic energy to both the diffusion coefficient and friction constant is[2,7,15]

$$D\zeta = k_B T \tag{2.43}$$

where $k_B T$ is the thermal energy and is known as the Einstein relation. For a spherical particle ζ is determined from Stoke's law,

$$\zeta = 6\pi\eta a \tag{2.44}$$

with a as the hydrodynamic radius. The combination of the last two equations yields

the Stokes-Einstein relation for a spherical particle diffusing through a medium

$$D = \frac{k_B T}{6\pi\eta a} \tag{2.45}$$

We then apply a continuous potential field $U(x)$ to the Brownian particle which experiences a force, $-\partial U/\partial x$. The particle then moves with an average velocity[7]

$$V = -\frac{1}{\zeta}\frac{\partial U}{\partial x} \tag{2.46}$$

through the solvent. If it is assumed that the effect of the Brownian motion is negligible, then from the last equation the particle displacement satisfies

$$\frac{dx}{dt} = -\frac{1}{\zeta}\frac{\partial U}{\partial x} \tag{2.47}$$

and the particle moves towards a decreasing potential, stopping when it reaches the minimum.

If there is Brownian motion, then the velocity of the particle fluctuates around the average value determined in eq 2.46. To account for these fluctuations, a probability function, $g(t)$, that randomly varies with time, is added to the right hand side of eq 2.47

$$\frac{dx}{dt} = -\frac{1}{\zeta}\frac{\partial U}{\partial x} + g(t) \tag{2.48}$$

If the velocity fluctuations is the same for both the presence and absence of a field, then the mean and variance of $g(t)$ is

$$< g(t) >= 0, < g(t)g(t') >= 2D\delta(t - t') \tag{2.49}$$

where D is diffusion coefficient and has the following relation,[7,19]

$$D = \frac{k_B T}{\zeta} \tag{2.50}$$

known as the Einstein relation. The distribution of $g(t)$ can then be assumed to be Gaussian. Equation 2.48 is known as the Langevin equation.

Equations 2.48 and 2.49 describe mathematically the motion of a Brownian particle in a potential field. If we integrate the Langevin equation from t to $t + \triangle t$, and discretise with respect to time then

$$x(t + \triangle t) = x(t) - \frac{1}{\zeta}\frac{\partial U}{\partial x}\triangle t + G(t) \tag{2.51}$$

where the probability distribution function, $G(t)$, comes from integrating $g(t)$ from

t to $t + \triangle t$ and has a mean and variance of

$$< G(t) >= 0, < G(t)G(t') >= 2D\delta_{tt'}\triangle t. \tag{2.52}$$

For determining how far a particle moves with time, t, we use the root mean square (r.m.s.) displacement $< x^2 >^{1/2}$ and not the mean displacement $< x >$ which is equal to zero. The r.m.s. displacement is analogous to the standard deviation of the Gaussian distribution function $G(t)$ and is[15,19]

$$< x^2 >^{1/2}= (2D\triangle t)^{1/2}. \tag{2.53}$$

In Chapter 6, we use Langevin Dynamics in our simulations for investigating the dynamical behaviour of a single polymer chain.

2.3.3 Radius of Gyration

In order to determine whether the chain has equilibrated or not, we calculate the radius of gyration, R_g, of the chain which is,[1–9,15]

$$R_g^2 = \frac{1}{2N^2}\sum_{n=1}^{N}\sum_{m=1}^{N} < (\mathbf{R}_n - \mathbf{R}_m)^2 > \tag{2.54}$$

The radius of gyration is equivalent to the square of the average distance between the centre of mass of the polymer and its segments. The location of the centre of mass is

$$\mathbf{R}_G = \frac{1}{N}\sum_{n=1}^{N}\mathbf{R}_n \tag{2.55}$$

and R_g can be written as

$$R_g^2 = \frac{1}{N}\sum_{n=1}^{N} < (\mathbf{R}_n - \mathbf{R}_G)^2 > \tag{2.56}$$

The chain is said to have equilibrated once the value of R_g is constant with respect to time.

2.4 Summary

The background theory and simulation techniques developed and used for studying single polymer chains presented in this chapter is used throughout this thesis. In Chapter 5, we use the simple model of an ideal chain discussed in Section 2.1 and the thermodynamics of a chain in Section 2.2 for investigating the physics of detaching a chain from a surface. In Chapter 6, we investigate the dynamics of the detachment process using Langevin Dynamics, discussed in Section 2.3, exclusively.

References

[1] de Gennes, P. -G. *Scaling Concepts in Polymer Physics*; Cornell University Press: Ithaca, 197 9.

[2] Doi, M.; Edwards, S. F. *The Theory of Polymer Dynamics*; Oxford University Press: Oxford, 1986.

[3] Flory, P. J. *Principles of Polymer Chemistry*; Cornell University Press: Ithaca, 1992.

[4] Flory, P. J. *Statistical Mechanics of Chain Molecules*; Hanser Publishers: New York, 1989.

[5] Evans, D. F.; Wennerström, H. *The Colloidal Domain: Where Physics, Chemistry and Biology Meet*, 2nd. ed.; Wiley-VCH: New York, 1999.

[6] Fleer, G. J.; Cohen Stuart, M. A.; Scheutjens, J. M. H. M.; Cosgrove, T.; Vincent, B. *Polymers at Interfaces*; Chapman & Hall: London, 1993.

[7] Doi, M. *Introduction to Polymer Physics*; Clarendon Press: Oxford, 1997.

[8] Israelachvili, J. *Intermolecular and Surface Forces*, 2nd. ed.; Academic Press: London, 1992.

[9] Yamakawa, H. *Modern Theory of Polymer Solutions*; Harper & Row: New York, 1971.

[10] Smith, S. B.; Cui, Y.; Bustamante, C. *Science* **1996**, *271*, 795.

[11] Rief, M.; Oesterhelt, F.; Heymann, B.; Gaub, H. E. *Science* **1997**, *275*, 1295.

[12] Fixman, M.; Kovac, J. *Journal of Chemical Physics* **1973**, *58*, 1564.

[13] Bustamante, C.; Marko, J. F.; Siggia, E. D.; Smith, S. *Science* **1994**, *265*, 1599.

[14] Guffond, M. C.; Williams, D. R. M.; Sevick, E. M. *Langmuir* **1997**, *13*, 5691.

[15] Hamley, I. W. *Introduction to Soft Matter*; John Wiley & Sons: New York, 2000.

[16] Heermann, D. W. *Computer Simulation Methods in Theoretical Physics*; Springer-Verlag: Berlin, 1986.

[17] Hansen, J. P.; McDonald, I. R. *Theory of Simple Liquids*, 2nd ed.; Academic Press: London, 1986.

[18] Allen, M. P.; Tildesley, D. J. *Computer Simulation of Liquids*; Clarendon Press: Oxford, 1990.

[19] Hunter, R. J. *Introduction to Modern Colloid Science*; Oxford University Press: Oxford, 1993.

Chapter 3

Atomic Force Microscope: The Instrument and Its Use

3.1 Introduction to the Atomic Force Microscope

The atomic force microscope (AFM), or as it is otherwise known the scanning force microscope, was invented by Binnig et al. in 1986.[1] The AFM is able to image surfaces and is an important technique used in a number of different fields including semiconductor processing, material science, polymers, biology and biomaterials, to name only a few. The AFM can also be used to probe the adhesive and elastic properties of sample surfaces and for nanomanipulation. As the AFM has a force sensitivity of only a few picoNewtons, it is capable of probing fundamental forces including attractive van der Waals forces, electrostatic forces, capillary forces and magnetic forces. The advent of the fluid cell has enabled the AFM to measure forces in a fluid environment enabling the study of electrostatic forces between dissolved ions and other charged species on the probe tip and sample surface,[4] biological materials,[3,5–11] colloidal forces[12–14] and the nanomanipulation of polymer chains.[13,15–26]

Figure 3.1 shows the essential components in an AFM. The AFM uses a probe consisting of a sharp tip attached to a flexible cantilever to determine the properties of a sample surface. Forces acting between the probe tip and sample cause the cantilever to deflect which is measured by bouncing a laser beam off the back of the cantilever. This detection method uses a laser beam deflection sensor and is known as the optical or light lever method. The AFM can create three dimensional images of a sample surface from these deflections with a spatial resolution of nanometers and a vertical resolution of Angstroms by raster scanning the sample plane in the x-y direction using a computer controlled piezoelectric stage. In addition, the AFM measures force curves by moving the probe tip perpendicular to the sample plane, *i.e.*, in the z-direction. The range of forces an AFM can detect and measure forces is of the order of $\sim$1pN to 10^{-7}N.[27]

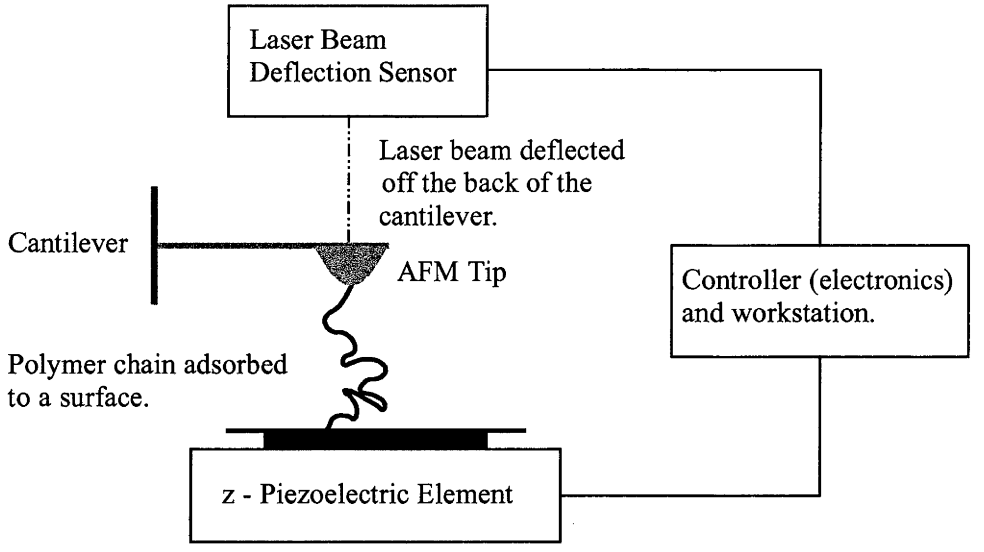

Figure 3.1: Schematic diagram of an atomic force microscope (AFM). The AFM tip is attached to a cantilever type spring. The sensor monitors any resulting deflections in the cantilever due to forces acting upon the tip. The force between the tip and the sample surface can be precisely controlled by the controller electronics and workstation using the output from the deflection sensor and the piezoelectric element to determine the height (z-displacement) of the AFM tip from the sample surface.

We have used the AFM to study single polymer chains and will briefly discuss the principles of using the AFM to measure forces while extending a single polymer chain. Figure 3.2 is a schematic representation of a single polymer chain AFM experiment where the polymer chain is end-tethered to the sample surface and to the AFM tip and is represented as a Hookean spring of length l, with a spring constant for the polymer as k_p, and the cantilever as k_c. When there is no interaction between the AFM probe tip and the sample surface, *e.g.*, there is no bridging chain between the surfaces, then the distance between these two surfaces is given by D, the z-displacement of the piezoelectric scanner. However, if there is a bridging chain between the two surfaces then as the displacement of the piezo is increased, the chain is elongated. As the z-displacement approaches the contour length of the chain, the force on the AFM tip increases resulting in the deflection of the cantilever that is equal to the distance x. At this point the distance between the AFM tip and sample surface is given by $l = D - x$ (see Figure 3.2) and is the length of the chain extended. As the rate of extension of the chain is slow compared the rate of its conformational rearrangement, it is essentially in mechanical equilibrium and the forces on the tip, F_c and the chain, F_p, balance $F_c = F_p$. In this case the cantilever should be the most compliant part of the system with $k_c << k_p$. If the spring is too stiff, $k_c > k_p$, then the deflection of the cantilever is too small and the force cannot be measured. As it is impossible to know the intrinsic deflection of the cantilever, it necessary that it

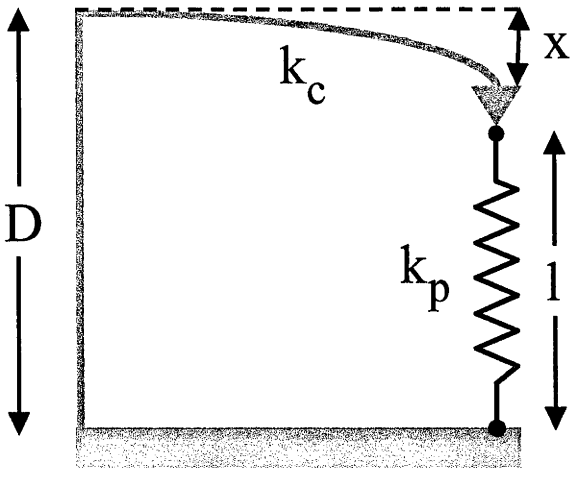

Figure 3.2: A schematic of the extension of an end-tethered chain using an AFM probe. D is the z-displacement of the piezo scanner, x is the deflection of the cantilever, k_c is the cantilever spring constant and k_p the polymer spring constant and l is the length of the polymer chain extended. When there is no interaction between the probe tip and the sample surface, the tip-sample separation is equivalent to D.

deflect a small distance x, so as to be able the measure the force. Since $x/D << l/D$, then tip-sample separation can be approximated as the z-displacement of the piezo, *i.e.*, $l \sim D$.

In this chapter we discuss in Sections 3.2-3.4 the essential components of the AFM including manufacturer specifications, limitations and calibration techniques. In Section 3.5 we briefly describe the various operational modes used for imaging and measuring forces using the AFM. Section 3.6 describes in detail the conversion of the raw data into force versus distance curves. The various sample surface cleaning techniques are described in Section 3.7 and lastly in Section 3.8 we describe experimental modifications made to the AFM in order to conduct our experiments.

3.2 Cantilever and Probe Tips

So as to be able to measure small forces, we require that the deflection of a cantilever by a force be as large as possible. Therefore it is necessary that the cantilever be soft so as to be deflected by such small forces and to also have a high resonant frequency in order to minimise vibrational noise. To sustain a high resonance frequency while reducing the spring constant, it is necessary to reduce the mass of the cantilever, *i.e.*, the length and width of the cantilever are small. For high resolution, a probe tip with a small radius of curvature is required. The probes we used were long, thin silicon nitride cantilevers with integral tips purchased from Digital Instruments, Inc. Santa Barbara. These cantilevers have a nominal spring constant of 6 pN/Å. However, variation in the thickness of the cantilever (the

manufacturer quotes a range of 0.4 to 0.7 μm) leads in a variation of the spring constants. As the spring constant is proportional to the thickness cubed, the spring constant would have a range from 0.017 to 0.095 Nm^{-1}. The specifications of the probe as stated by the manufacturer are as follows: the cantilever is v-shaped with a length of 200 μm, the leg width of the cantilever is 30 μm, the tip radius has a range of 20-60 nm and the resonant frequency is 5-50 kHz. Although a convenient way of measuring the force, there are inherent problems in this technique. Specifically, when the tip is under a load (in contact with the sample surface) it is no longer linear but describes an arc. This reduces the accuracy of the measured adhesion forces due to surface shearing. Also the vibrational modes of the cantilever are not simple, making theoretical treatments difficult.

3.2.1 Spring Constant Calibration

In determining the spring constant of the cantilever, it is important to note that the AFM can only measure a change in the deflection. The gravimetric method[30] measures the static deflection of a cantilever by by end-loading it with a known mass. This calibration technique has a reported error of $\sim$ 10%. An alternative method that also end-loads the cantilever measures the change in resonant frequency of the cantilever[31] and has an error range of $5 - 10\%$. The calibration of spring constants by resonant methods is a popular technique that is continually being refined both experimentally[32] and theoretically.[33]

We used the *in-situ* hydrodynamic drag method[34] to determine the spring constant of the cantilever for a given solution for our AFM experiments discussed in Chapter 4. This method uses a semi-empirical equation to relate the deflection of the cantilever by end-loading, to the deflection caused by laminar fluid flow. The compliance of the system is firstly determined by bringing the probe tip into contact with the sample surface. These are then separated a known distance (typically $> 20\mu$m) and the piezo scanner is cycled over this extension range. We record the difference between the deflection curves for extension and retraction, scaling it by the compliance. This is repeated for a number of speeds (eg. 4, 8 and 16 cycles/s) and a plot is made of half the difference in the deflection versus the speed. This process is repeated for another separation distance (see Figure 3.3(a)). The slopes of these curves are then converted to α-factors, where α is the ratio of the end-loaded force given by Hooke's law to the distributed force determined by Stoke's law and is dimensionless. This is achieved by dividing the slopes by both the viscosity of the solvent (0.00089 kg/ms^{-1} for water at 22°) and the cantilever length (0.0002 m for the long thin cantilever), and then multiplying by the nominal spring constant (6 pN/Å). The α-factors are plotted versus the separation distance and the corresponding model α-factors, are determined from the semi-empirical equation for a

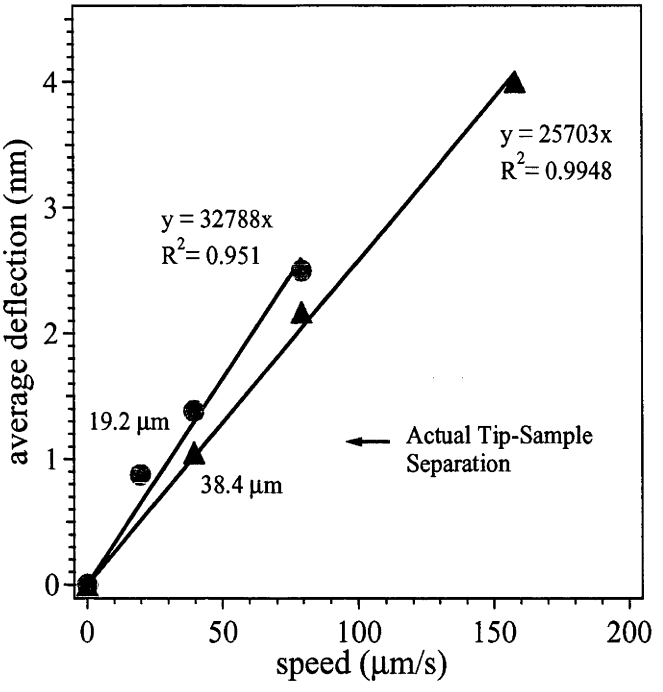

(a)

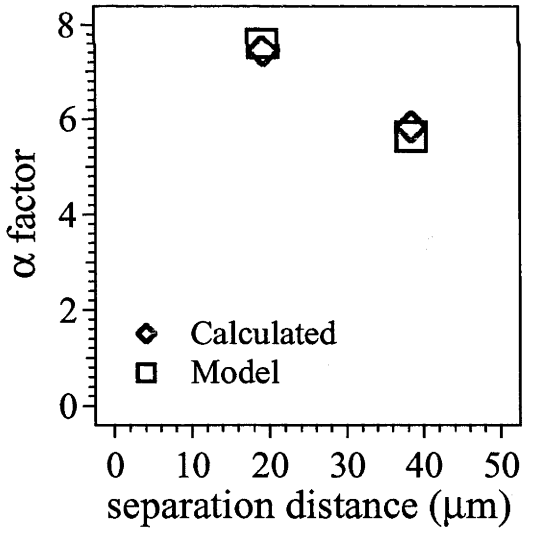

(b)

Figure 3.3: An example of the plots used to determine the spring constant of the cantilever for an AFM experiment. Figure (a) is the average deflection of the cantilever (nm) versus speed (μm/s) for different tip-sample separations. Figure (b) is a plot of α-factor versus the tip-sample separation (μm). In this instance, the solution was 0.3 wt% PEO in 0.45 M K_2SO_4.

model cantilever system,

$$\alpha(D) = 0.06818D^{-0.434} \tag{3.1}$$

where D is the tip-sample separation and plotted on the same graph (see Figure 3.3(b)). The spring constant is determined by adjusting the nominal value of the spring constant by performing a least-squares fit, minimising the difference between the experimental and model value of the parameter. From the example given, the spring constant was determined to be 0.042 N/m. This calibration technique has an inaccuracy of $5 - 10\%$ which is comparable to resonant methods.

3.3 Laser Beam Deflection Sensor

The laser beam deflection sensor was developed by Meyer et al.[28] and Alexander et al.[29] A laser beam is reflected off the rear side of the cantilever and the deflection is monitored with a position-sensitive detector (PSD). The signal-to-noise ratio, S/N, is given by

$$S/N = \frac{\sqrt{a^3 b}}{l} \frac{\sqrt{(IRR_S)}}{\sqrt{B}} \triangle z \tag{3.2}$$

where a and b are the dimensions of the mirror, l is the cantilever length, R is the mirror reflectivity, R_S is the spectral responsivity of the PSD, I the laser intensity B is the bandwidth and $\triangle z$ is the deflection of the cantilever. The Nanoscope IIIa uses a noncoherent, non-polarized semiconductor laser of 3 mW power and a red wavelength of 633 nm. Therefore the radiation force exerted by the laser beam on the cantilever is small (on the order of a few picoNewtons).

3.4 Piezoelectric Scanners

The piezoelectric scanner manufactured by Digital Instruments is a single tube consisting of five or more piezo-elements that are operated independently of each other. These devices respond to voltages applied to electrodes on the tube by moving a microscopic amount. The distance the piezo scanner moves is proportional to the applied voltage and whether it contracts or elongates depends on the polarity of the voltage. Therefore the piezo scanner used in AFM is capable of translating along the x, y and z-axes. All piezo ceramics exhibit some nonlinearity and hysteresis in their response to an applied voltage and this behaviour changes with time. No two piezo-elements are the same. This necessitates calibration and recalibration of the piezo scanner to compensate for these undesirable properties which we will discuss in Section 3.4.1. The piezo scanner we used was a Digital Instruments E scanner with a ± 220 V range, a lateral (x-y) range of 10 μm $\times$ 10 μm and a vertical (z)

range of 2.5 μm.

3.4.1 Piezo-element Calibration

Digital Instruments calibrates the piezo scanners by scanning a calibration standard of known dimensions and then adjusting the control electronics to compensate for any observed non-linearities. As the response of a piezo to an applied voltage changes over time, it is necessary to recalibrate the piezo. Typically, this is done every 6 months. Calibration using a single step height is an *ex-situ* technique commonly used by experimentalists.[35] It involves spreading layers of polystyrene-latex spheres of known diameter onto mica substrate and scanning the surface. This technique does not take into non-linearities in the piezo. Another technique involves laser interferometry[36] and is only valid for large displacements of the piezo *i.e.*, greater than the wavelength of the laser used, typically 632.8 nm (He-Ne laser).

We calibrated the piezoelectric element in the z-direction using an external calibration grid purchased from NT-MDT Co., Zelenograd Research Institute of Physical Problems, 103460 Moscow, Russia. The silicon diffraction grating used is a 3 $\times$ 3 mm array, with a pitch of 3 μm and a step height of 516 $\pm$ 2 nm (see Figure 3.4). This grating was scanned using the AFM and the measured value was compared to the known step height in order to calibrate the piezo scanner.

3.5 Modes of Operation

As previously stated, the AFM is typically used to image sample surfaces and to measure forces. Firstly, we discuss the several different modes available for imaging using a commercial AFM instrument. The most commonly used are contact mode, non-contact mode and tapping mode imaging. In contact mode the probe tip is in contact with the surface while it raster scans. This technique is problematic due to adhesional and frictional forces between the tip and sample surface that can distort images and damage samples. Soft samples, such as polymers physisorbed to a surface, can be displaced due to the action of the tip. Non-contact mode attempts to minimise damage to the sample by holding the probe tip a distance above the surface and measures the attractive Van der Waals forces of the tip with the sample surface. As these forces are so small, it is impractical for imaging in a fluid environment. The last imaging mode we will discuss is tapping mode imaging. When scanning the surface, the probe tip is oscillated and alternately placed in contact with the sample surface. This technique monitors the amplitude of oscillation of the tip. Due to interactions between the tip and sample, the height of the tip is adjusted to maintain a constant amplitude. Tapping mode imaging avoids frictional and

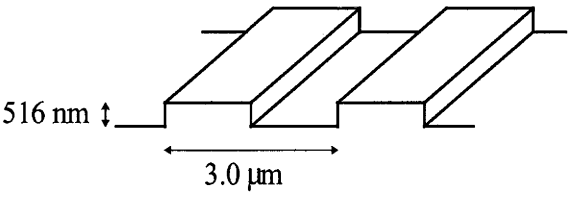

Figure 3.4: A schematic of the silicon calibration grating model TGZ03. It consists of a 1-D array of rectangular steps 516±2 nm in height with a pitch of 3 μm.

adhesive forces and is the preferred method for imaging soft samples.

The AFM also has different modes of operation for measuring forces, and are either static (contact mode) or dynamic. In contact mode, the tip can be cycled towards the surface until it makes contact and then retacted from it by applying a triangle-wave voltage at a given frequency to the electrodes in the $z-$ direction of a (x,y,z) piezoelectric scanner. Dynamic mode operates by oscillating the cantilever while it moves towards and away from the sample surface. The reduced amplitude of the oscillating cantilever is measured and is a result of the probe tip and sample interaction. As our experiments were conducted exclusively using static mode (see Chapter 4), we will not further concern ourselves with discussion of the dynamic mode.

3.6 Force versus Distance Curves

To obtain force-distance curves (see Figure 3.5) the AFM measures the deflection of the cantilever as a function of the sample displacement. The deflection signal (in arbitrary units) is the difference of signals across two photodiodes, normalised by the total signal $(A-B)/(A+B)$. It is assumed that at large distance of separation the surface force is zero and the cantilever does not deflect *i.e.*, the probe and sample do not interact and the change in the distance between the surfaces is the piezo z-displacement. This changes when there is an interaction of the probe and tip, which causes the cantilever to deflect. The change in separation of the two surfaces is then a combination of the piezo-element z-displacement and the cantilever deflection. If the interaction between the probe and the sample is strongly attractive, a spring instability can occur and the surfaces "jump" in to contact. The jump is a zone where the gradient of the force exceeds the spring constant and the cantilever accelerates towards the next point of lower or equal force gradient, usually the "contact" position.

When the tip and the sample are in contact, then their motion is directly coupled, *i.e.*, every nanometre displacement of the piezo leads to a proportional change in the deflection signal. This is termed as "compliance". The optical sensitivity of the

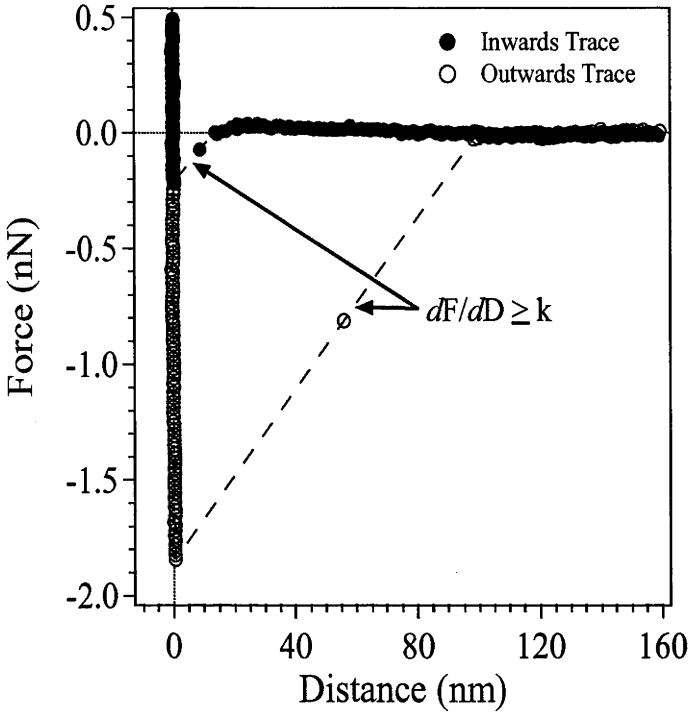

Figure 3.5: A typical force curve for Milli-Q pure water, a silicon nitride substrate and AFM tip. A spring instability, $d\,\mathrm{F}/d\,\mathrm{D} \geq \mathrm{k}$, occurs on the approach cycle and is due to the two surfaces jump into contact. Another also occurs on retracting the z-piezo and is due to the adhesion of the AFM tip to the substrate. A dashed line is used to highlight the region of instability. The adhesive force of the two surfaces in water is $\approx$ 1.8 nN.

detector can then be measured directly from the deflection of the cantilever. The compliance measurement is simply the slope of the deflection versus displacement curve when the diode is non-zero and linear. The deflection signal can then be converted to units of distance using the compliance. Hooke's law ($F = -kd$, F is the force, k is the spring constant and d is the deflection of the cantilever) is then used to calculate the force.

As the surfaces are separated by retracting the piezo, a primary adhesion may occur. This persists until there is another spring instability. Any adhesion events that occur after this are denoted as secondary adhesions as they occur when the surface are no longer in contact and are typically due to bridging polymer chains.[13] Separation of the surface assumes two things: firstly that the separation is a result of the deflection of the cantilever and the displacement of the sample; secondly that the linear compliance regime marks the closest point of approach. The second point is often assumed to be the "contact" position, however because of the ambiguity of whether actual contact has been achieved, it is wrong to assume this. The zero of separation seen in all force curves is always assumed. Having measured the slope

of the compliance regime and converting the deflection into units of distance, the deflection due to the surface force can be subtracted from the displacement at each point recorded in the data. The sign of the deflection is important; a repulsion will mean that the separation changes less rapidly with displacement. To further improve the distance axis relative to the "zero" position, the intercept line of compliance calibration made with the distance axis is subtracted from all data points. This method was used to obtain Figure 3.5 and the force-distance curves presented in Chapter 4.

Lastly, it is assumed that the measurement taken is at the mechanical equilibrium. This is largely true, except when the surface force is very attractive in which case a jump occurs. It is assumed that the deflections of the cantilever are small enough to make an angle equal to the tangent of the angle. This is a reasonable assumption considering the deflections are usually around 10 nm and the cantilever is $100 - 200\mu$m in length. The quality of the force curve is assessed by looking at the scatter in the compliance data at zero separation.

3.7 Sample Preparation

To ensure reproducibility of results, it is necessary for both the sample substrate and the tip to be free of contaminants. Techniques available for cleaning include $O_2/H_2O/Ar$ plasmas,[37,38] CO_2 snow, wet oxidation,[39] UV/ozone/NO_x, or solvents.[38,39] However, it is not necessary for such care in all systems studied eg. in concentrated polymer solutions, the adsorbing chains would easily displace all minor contaminants on the surfaces. All surfaces used in our experiments in Chapter 4 were H_2O plasma treated to ensure the surfaces were clean and hydrophilic.

3.8 Instrument Modification

In order maintain a constant temperature for our experiments presented in Chapter 4, it was necessary to thermally isolate the Digital Instruments Nanoscope IIIa Force Microscope. This was achieved by placing a large inverted vacuum dewar over the instrument. Figure 3.6 contains a schematic diagram of the inverted dewar. By circulating water through a copper coil that was wrapped around the microscope head, the temperature inside the dewar could be set. A Frigomix julabo VC water bath from Crown Scientific Pty. Ltd. was used to control the temperature of the circulating water and the temperature inside the dewar was measured using a thermistor attached to a multimeter. So as be able to convert resistance into temperature measurement, the resistance of the thermistor was measured by the multimeter and was calibrated against a MMS 3000 MultiMeasurement System Model T6V4 from

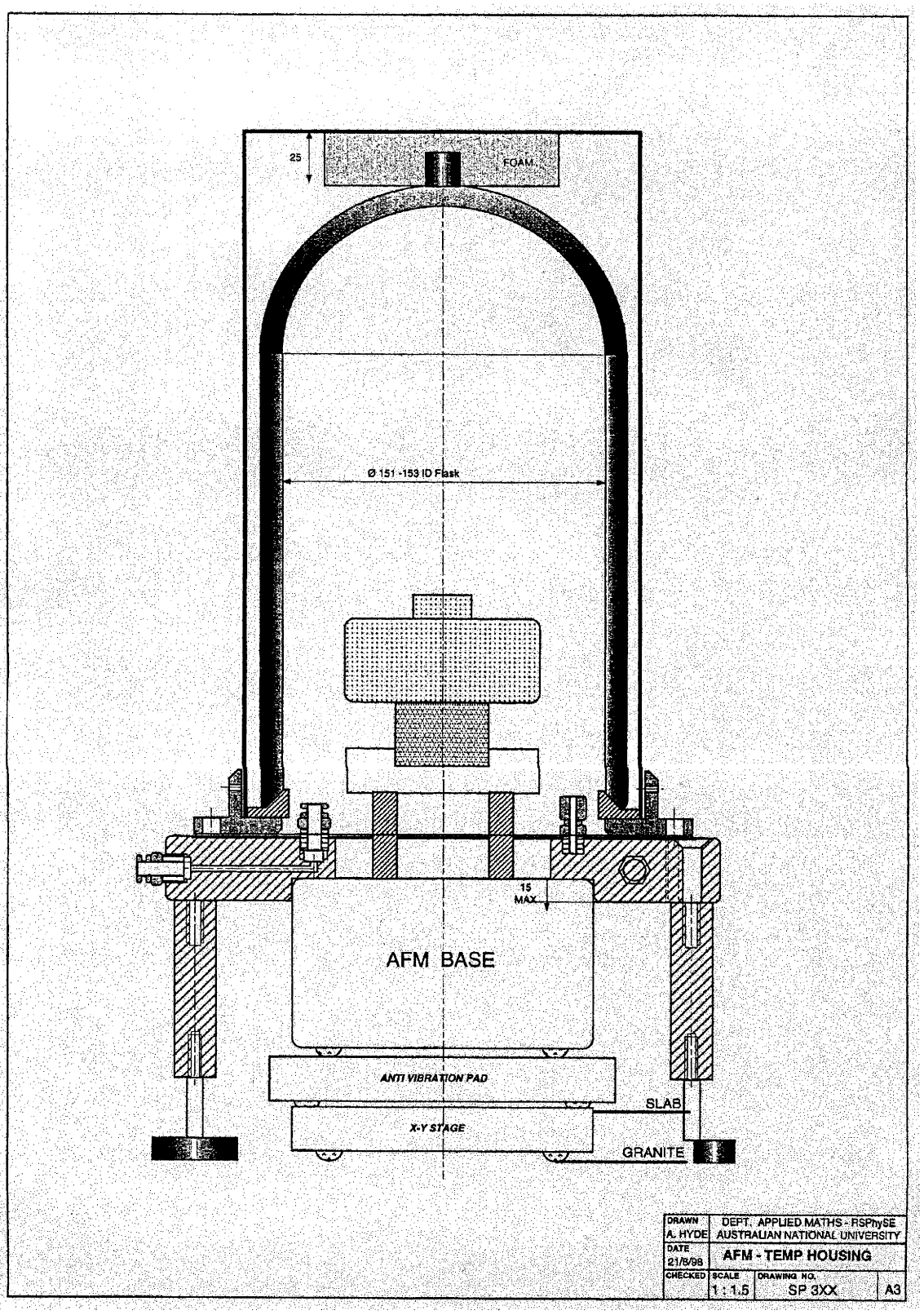

Figure 3.6: A schematic diagram of the inverted vacuum dewar by A. Hyde, Department of Applied Mathematics, Research School of Physical Sciences and Engineering, Australian National University.

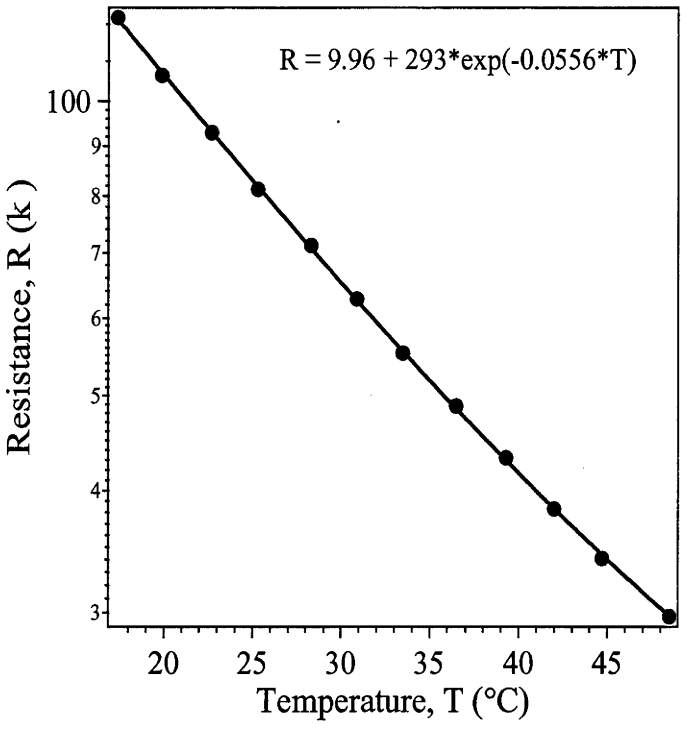

Figure 3.7: The calibration graph for the thermistor with resistance (kΩ) versus temperature (°C).

Commtest Instruments Ltd. New Zealand (see Figure 3.7). The reported accuracy for the MMS 3000 for measuring temperature is ±0.1% of the reading. This modification allowed the temperature of the system to be maintained to within 0.1°C of a desired temperature.

References

[1] Binnig, G.; Quate, C. F. *Physical Review Letters* **1986**, *56*, 930.

[2] Meyer, E.; Heinzelmann, H. *Scanning Tunneling Microscopy II*, 2nd. ed.; Springer: Berlin, 1995; Chapter 4.

[3] Zlatanova, J.; Lindsay, S. M.; Leuba, S. H. *Progress in Biophysics and Molecular Biology* **2000**, *74*, 37.

[4] Butt, H. -J.; Jaschke, M.; Ducker, W. A. *Bioelectrochemistry and Bioenergetics* **1995**, *38*, 191.

[5] Lal, R.; John, S. A. *American Physiological Society* **1994**, *266*, C1.

[6] Clausen-Schaumann, H.; Seitz, M.; Krautbauer, R.; Gaub, H. E. *Current Opinion in Chemical Biology* **2000**, *4*, 524.

[7] Fisher, T. E.; Marszalek, P. E.; Oberhauser, A. F.; Carrion-Vazquez, M.; Fernandez, J. M. *Journal of Physiology* **1999**, *520.1*, 5.

[8] Oesterhelt, F.; Oesterhelt, D.; Pfeiffer, M.; Engel, A.; Gaub, H. E.; Müller, D. J. *Science* **2000**, *288*, 143.

[9] Carrion-Vazquez, M.; Oberhauser, A. F.; Fowler, S. B.; Marszalek, P. E.; Broedel, S. E.; Clarke J.; Fernandez, J. M. *Proc. Natl. Acad. Sci. USA* **1999**, *96*, 3694.

[10] Rief, M.; Gautel, M.; Oesterhelt, F.; Fernandez, J. M.; Gaub, H. E. *Science* **1997**, *276*, 1109.

[11] Li, H. B.; Reif, M.; Oesterhelt, F.; Gaub, H. E. *Advanced Materials* **1998**, *10*, 316.

[12] Ducker, W. A.; Senden, T. J.; Pashley, R. M. *Nature* **1991**, *353*, 239.

[13] Senden, T. J. *Current Opinion in Colloid and Interface Science* **2001**, *6*, 95.

[14] Craig, V. S. J.; Neto, C.; Williams, D. R. M. *Physical Review Letters* **2001**, *87*, 054504.

[15] Strunz, T.; Oroszlan, K.; Schäfer, R.; H.-J. Güntherodt, H. -J. *Proc. Natl. Acad. Sci. USA* **1999**, *96*, 11277.

[16] Bemis, J. E.; Akhremitchev, B. B.; Walker, G. C. *Langmuir* **1999**, *15*, 2799.

[17] Ortiz, C.; Hadziioannou, G. *Macromolecules* **1999**, *32*, 780.

[18] Marszalek, P. E.; Oberhauser, A. F.; Pang, Y. -P.; Fernandez, J. M. *Nature* **1998**, *396*, 661.

[19] Senden, T. J.; di Meglio, J. -M.; Auroy, P. *Eur. Phys. J. B* **1998**, *3*, 211.

[20] Rief, M.; Oesterhelt, M. F.; Heymann, B.; Gaub, H. E. *Science* **1997**, *275*, 1295.

[21] Bustamante, C.; Marko, J. F.; Siggia, E. D.; Smith, S. *Science* **1994**, *265*, 1599.

[22] Courvoisier, A.; Isel, F.; Maaloum, M. *Langmuir* **1998**, *14*, 3727.

[23] Oesterhelt, F.; Rief, M.; Gaub, H. E. *New Journal of Physics* **1999**, *1*, 6.1.

[24] Zhang, W.; Zou, S.; Wang; C.; Zhang, X. *J. Phys. Chem. B* **2000**, *104*, 10258.

[25] Châtellier, X.; Senden, T. J.; Joanny, J. -F.; di Meglio, J. -M. *Europhysics Letters* **1998**, *41*, 303.

[26] Hugel, T.; Grosholz, M.; Clausen-Schaumann, H.; Pfau, A.; Gaub, H. E.; Seitz, M. *Macromolecules* **2001**, *34*, 1039.

[27] http://www.di.com

[28] Meyer, G.; Amer, N. M. *Applied Physics Letters* **1988**, *53*, 1045.

[29] Alexander, S.; Hellemans, L.; Marti, O.; Schneir, J.; Eilings, V.; Hansma, P. K.; Longmire, M.; Gurley, J. *Journal of Applied Physics* **1989**, *65*, 164.

[30] Senden, T. J.; Ducker, W. A. *Langmuir* **1994**, *10*, 1003.

[31] Cleveland, J. P.; Manne, S.; Bocek, D.; Hansma, P. K. *Review of Scientific Instruments* **1993**, *64*, 403.

[32] Sader, J. E.; Chon, J. W. M.; Mulvaney, P. *Review of Scientific Instruments* **1999**, *70*, 3967.

[33] Sader, J. E. *Journal of Applied Physics* **1998**, *84*, 64.

[34] Maeda, N.; Senden, T. J. *Langmuir* **2000**, *16*, 9282.

[35] Li, Y.; Lindsay, S. M. *Review of Scientific Instruments* **1991**, *62*, 2631.

[36] van de Leemput, L. E. C.; Rongen, P. H. H.; Timmerman, B. H.; van Kempen, H. *Review of Scientific Instruments* **1995**, *66*, 1258.

[37] Senden T. J.; di Meglio, J. -M.; Auroy, P. *European Physical Journal B* **1998**, *3*, 211.

[38] Bowen, W. R.; Hilal, N.; Lovitt, R. W.; Wright, C. J. *Colloids and Surfaces A: Physiochemical and Engineering Aspects* **1999**, *157*, 117.

[39] Lo, Y. -S.; Huefner, N. D.; Chan, W. S.; Dryden, P.; Hagenhoff, B.; Beebe, T. P. *Langmuir* **1999**, *15*, 6522.

Chapter 4

AFM Evidence of the Rayleigh Instability in Single Polymer Chains

4.1 Introduction

The majority of single chain studies using the atomic force microscope (AFM)[1–12] conducted over the last few years have been almost exclusively in the good solvent case. In these conditions the chains are swollen by the solvent and form loose coils. The loops or tails of the adsorbed polymer chain can then be "grabbed" by an adsorbing AFM tip. As the AFM tip and surface are separated, a tension is produced in the bridging polymer which is measured and characterises the elasticity of the chain. At weak extensions, the stretching of the chain is purely entropic but at higher extensions, there is an additional enthalpic cost from straightening the chain. A number of different models have been fitted to the stretching forces obtained from AFM single chain experiments, including the freely-jointed chain (FJC)[16] and worm-like chain (WLC)[7] models, along with variations of these[15] (see Chapter 2, Section 2.2.1). These stretching forces increase monotonically with extension until the adsorption site or monomer-surface contact is broken, typically at extensions of the order of hundreds of nanometres.

Much less attention has been placed upon the stretching of single chains in poor solvent. The stretching of chains which are collapsed in poor solvent was first studied theoretically by Halperin and Zhulina[17] who argued that at weak extensions the globule deforms into an ellipse and then into a cylinder. At a critical extension the polymer undergoes a sharp first-order transition into a "ball-string" configuration. This transition is analogous to the surface tension driven break-up of a column of liquid into a series of droplets, referred to as the Rayleigh-Plateau instability.[18] However in the polymer case, the applied tension draws out a thin filament rather

than a series of disconnected droplets, owing to the constraint of connectivity of the monomers. The force required to pull the chain beyond this critical extension, or to "pull-out" the chain monomer-by-monomer from the collapsed globule, is constant and independent of extension. Computer simulations[19,20] of the extension of a single polymer chain in poor solvent have verified the existence of this ball-string configuration.

A polymer chain in a poor solvent wants to avoid any interactions with the solvent molecules. It does this by minimising its surface area, forming a spherical ball or globule with a radius $R_0 \approx N^{1/3}a$, where N is the number of monomers in the chain and a is the monomer size. The free energy of the unperturbed chain is $F \approx \zeta \triangle A$, where $\zeta \approx k_B T/a^2$ is the surface tension between the polymer and the solvent molecules and $\triangle A$ is the change in the surface area. For weak extensions, ($Na > L > R_0$, where L is the extension distance) the configuration of the polymer chain deforms from a sphere to an ellipse, with $\triangle A \approx (L - R_0)^2$ and $F \approx \zeta(L - R_0)^2$. For strong deformation the chain completely unravels as $L \to Na$. In this regime, the deformation of the chain is simply Gaussian stretching. The ball-string configuration is an equilibrium state between the deformed sphere and fully extended chain. The free energy of extending the ball-string is the energy required to pull a monomer out of the spherical globule into the solvent, lengthening the string and is $F \approx \zeta(L - R_0)$. If we compare the free energy of the ellipse and the ball-string, we find that at $L = R_0$, they are equivalent as the chain has been perturbed and is simply a sphere with no tethers. Figure 4.1(a) graphs the free energy of stretching an ellipse, $F_{ellipse}$ and that of the ball-string, $F_{ball-string}$ for a polymer chain consisting of $N = 1000$ monomers of size $a = 1$. It is clear from Figure 4.1(a) that $F_{ellipse} < F_{ball-string}$ for extension distances $L < L*$, while $F_{ellipse} > F_{ball-string}$ for $L > L*$, where $L*$ is the crossover and is $L* \approx R_0 - a$, *i.e.*, $L*$ is proportional to the natural size of the chain in poor solvent. This indicates that the chain undergoes a first order configurational transition from an ellipse to a ball-string configuration at the critical extension distance of $L*$. Figure 4.1(b) is the theoretically predicted force profile for extending a chain in poor solvent conditions obtained from taking the derivative of the free energy with respect to the extension distance. It shows that the force increases linearly with extension distance until it reaches a critical extension distance after which it is a constant force.

Halperin and Zhulina[17] explained the same phenomena in terms of van der Waals loops. They showed that as the chain was deformed from a sphere to an ellipse, to a cylinder and then to a chain that the force scaled as $f \sim L$, $f \sim L^{-1/2}$ and $f \sim L$.

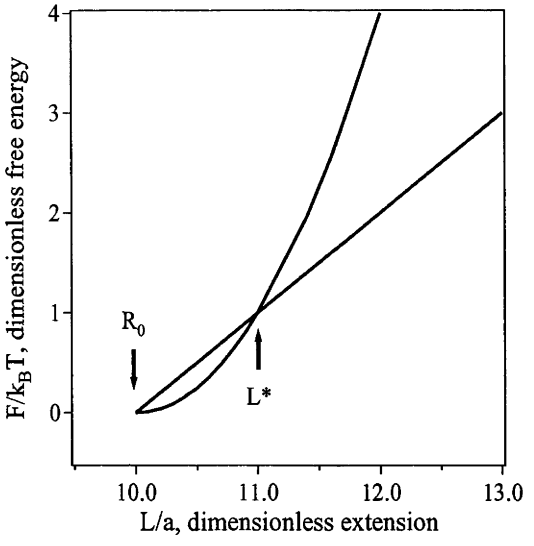

(a)

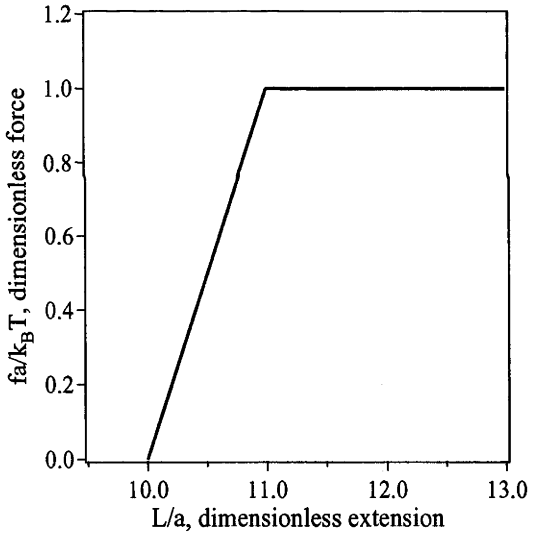

(b)

Figure 4.1: The theoretically predicted (a) free energy profile of dimensionless free energy, F/k_BT, versus dimensionless extension, L/a, of a single polymer chain in a poor solvent. Th two traces correspond to an ellipse, $F_{ellipse} \approx \zeta(L - R_0)^2$, and a ball-string, $F_{ball-string} \approx \zeta(L - R_0)$. The free energies of these two different configurations are equivalent when $L = R_0$, where R_0 is the unperturbed size of the chain and at $L*$. Clearly, $F_{ellipse} < F_{ball-string}$ for $R_0 > L > L*$ and $F_{ball-string} < F_{ellipse}$ for $L > L*$. Figure (b) is theoretically predicted force profile with dimensionless force, fa/k_BT, versus dimensionless extension, L/a. From $R_0 > L > L*$, the force increases linearly with extension. For $L > L*$, the force is constant with extension.

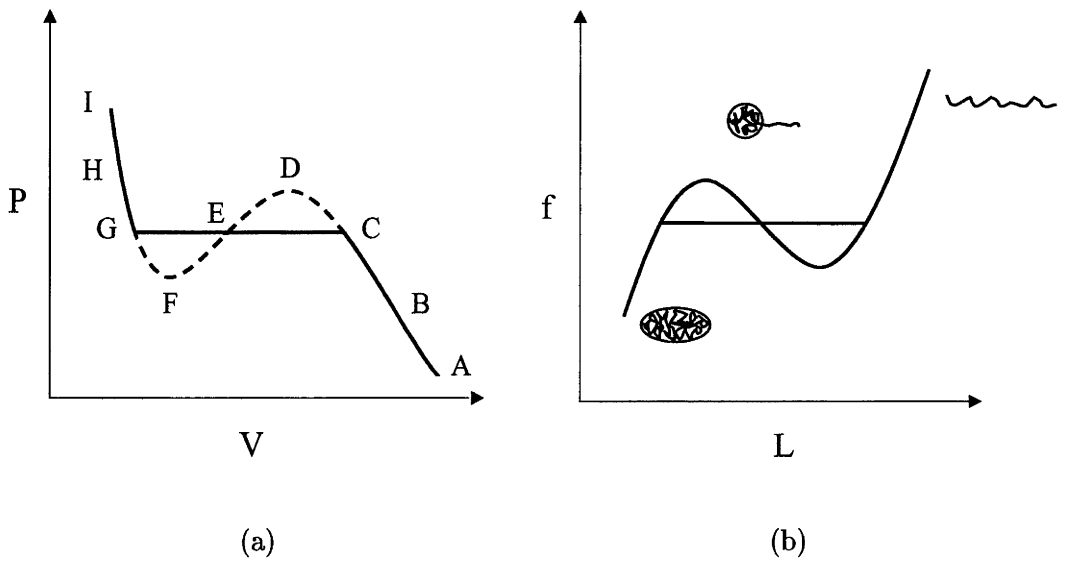

Figure 4.2: (a) The van der Waals isotherm, where IGFEDCA is the hypothetical isotherm and IGECA is the physically stable isotherm converted from the hypothetical isotherm by Maxwell's equal area construction. (b) The theoretically predicted force profile of force, f, versus extension distance, L, for extending a polymer chain in a poor solvent.

An analogy can be made to an unphysical P-V isotherm constructed from the energy of the gas/liquid system. The van der Waals isotherm of IGFEDCA shown in Figure 4.2(a) does not show mechanical stability everywhere, violating the condition of $(\partial P/\partial V)_T < 0$ over the section DEF of the isotherm[21] and a first order phase transition occurs. The physical isotherm of IGECA also shown in Figure 4.2(a), was constructed from the hypothetical isotherm using Maxwell's equal-area construction, where $\int_C^G v(P)dP = 0$. This isotherm now contains three regions, with the region IG being a liquid phase and the region CA exclusively the gas phase. The flat region GEC corresponds to a mixture of these two phases, the fraction of each state for points along this section being governed by the lever rule.[21] Using this analogy it was argued by Halperin and Zhulina[17] that the cylinder phase was unphysical and not attained, instead there existed a coexistence regime and the polymer chain under would undergo a first order phase transition at a critical extension distance, forming the ball-string configuration, Figure 4.2(b).

In this chapter we present for the first time experimental evidence of the Rayleigh instability of a single chain using single molecule force microscopy. In a simple experiment, we adsorb polymer onto a flat surface and use the adsorbing tip of an AFM to probe the polymer. This involves repeatedly bringing the surface and AFM tip into contact and separating them again, while simultaneously measuring the force on the tip. This results in chains forming bridges between the two adsorbing surfaces. The resulting force versus separation profile is often relatively featureless,

showing only a primary adhesion upon retraction. However, over many separation cycles we find two distinct types of force profiles, depending upon the solvent conditions. The characteristics of the first type of force profile are identical to that observed by previous authors and have been interpreted as the elasticity of various polymers.[1–15] This characteristic force profile is referred to as a "Langevin" event as it has been fitted to various elasticity models. In poor solvent, we see a new, second type of profile. It is characterized by "steps" or plateaus of constant force which extend over separation distances which are comparable to the Langevin events. At these separation distances, polymer-solvent contact is minimised by the formation of surface-bound polymer globules at each surface, connected by a polymer filament, Figure 4.3. This is the analog of the ball-string configuration of the single chain Rayleigh instability. As the surfaces are separated further, monomers are pulled out of the surface bound globules and incorporated into the lengthening filament. The force of extension of the filament, measured as the force on the AFM tip, is constant over the separation distance, reflecting the constant rate of monomer extracted from the surface bound globules. This polymer filament may contain several chains and surface separation can completely pull-out the shorter chains. With each pull-out, the plateau force drops discontinuously in a "step-like" manner, until the last single chain in the filament is pulled out and the force between the surfaces returns to zero. We refer to such constant force events as "Plateau" events after Plateau's work in instabilities as well as the physical description of the force versus distance profile.

The remainder of the chapter is organised in the following manner. In the next section we describe the chains investigated, poly-*N*-isopropylacrylamide (PNIPAM) and polyethylene oxide (PEO), and the AFM experimental procedure. In Section 4.3 we present force profiles for single chain PNIPAM stretching, focusing first upon the Langevin events observed in good solvent conditions and then the new Plateau events observed in poor solvent. For the PNIPAM experiments, the solvency condition is changed *in-situ* by elevating the temperature of the aqueous solvent above the lower critical solution temperature. PEO in various concentrated electrolyte solutions provides another view of the same phenomena and these PEO results are presented and discussed in Section 4.4. Although the PEO profiles are very similar in character to those of the PNIPAM profiles, the PEO profiles contain a much larger number of Plateau events which allow a statistical analysis. From this we find that the plateau force is quantised and that the frequency of these quantised steps shows an interesting pattern. This implies that we can distinguish the number of chains that are being pulled in poor solvent and distinguish loops from tails by the frequency of Plateau events.

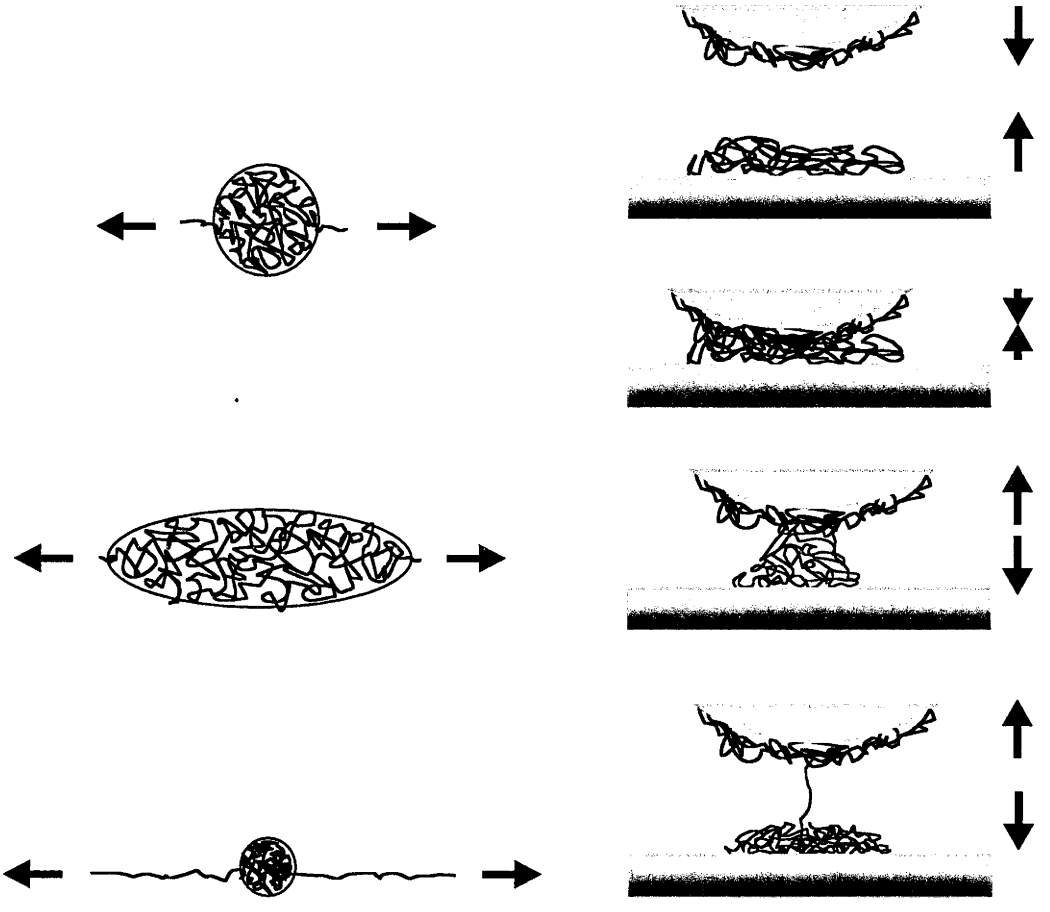

Figure 4.3: Schematic of the Rayleigh instability for a single polymer chain in a poor solvent. Theory and simulation show that the extension of the ends of a collapsed chain or globule leads to the configurations depicted in (a). The collapsed polymer or globule deforms into an elliptical shape and at a critical extension, forms a "ball-string" configuration. Extension of the strings from the ball occurs with a constant force. These configurations arise due to the high polymer-solvent interfacial energy. Experimentally, it is difficult to "grab" the ends of a single chain; so we use (b) a flat surface and an AFM tip to produce an analog of the Rayleigh instability. The surface-adsorbing polymer is sandwiched between the flat surface and AFM tip. Upon separation the polymer "necks", forming a bridge between in the surfaces and at a critical separation, the high surface energy favours the formation of surface-bound globules which are connected by a polymer filament. This filament can contain one or a few chains. Further separation draws monomers out of the globules and into the filament. The surface energy penalty is proportional to the length of the filament and consequently, the extensional force is constant and independent of surface separation.

4.2 Experimental Section

4.2.1 Materials

Two different model polymers were studied: poly-*N*-isopropylacrylamide (PNIPAM) and polyethylene oxide (PEO). PNIPAM was synthesized according to the reaction scheme of Zhou et al.[22] (see Figure 4.4(a)), then precipitated twice from acetone/n-hexane, and confirmed from a ^{13}C n.m.r spectra obtained from a Gemini BB n.m.r. spectrometer operating at 300 MHz (see Figure 4.4(b)). The weight-average molecular weight, determined by GPC, is $M_W = 5035$ with a high polydispersity index of 2.1. PEO with an average molecular weight of 10^6 was purchased from Aldrich Chemicals and purified by reprecipitation twice from dichloromethane/ diethylether. The salts used in this study, K_2SO_4 and KNO_3, were purchased from MERCK Pty. Ltd. and BDH Laboratory Supplies, respectively and used without further purification.

The aqueous solutions of PNIPAM and PEO were prepared by gentle shaking in milli-Q water for approximately 12 hours, diluted to about 0.001% and 0.3% by weight, respectively, and filtered through pre-wet 0.2 μm teflon membranes. For our studies of PEO in salt solutions, K_2SO_4 or KNO_3 were added to make the a salt concentration 0.45 M and 0.25 M, respectively and filtered prior to injection. The polymer solution was injected into the AFM fluid cell from which measurements are made at a specified and controlled temperature. The base of the fluid cell is chemical vapour deposited silicon nitride[23] that was water-plasma treated immediately prior to the experiment to ensure clean surfaces amenable to polymer adsorption. Both of the polymers readily adsorb via H-bonding to the silicon nitride surfaces. Additionally, both are above their glass temperature temperatures and hence have sufficient mobility to vary their degree of surface aggregation.

The polymer solutions were allowed to equilibrate in the fluid cell for 1-2 hours before flushing with milli-Q water at the same temperature. In the case of the salt studies, we flushed the cell with filtered 0.5 M K_2SO_4 or 0.25 M KNO_3 solution. This final flushing removes excess and poorly adsorbed polymer and results in a sparsely covered surface.

4.2.2 Equipment and Technique

Force measurements were made using a Digital Instruments NanoScope IIIa Force Microscope which was thermally isolated by placing a large inverted vacuum dewar over the instrument. By circulating water through a copper coil around the microscope head, the desired temperature can be maintained to within 0.1°C. In this way, we are able to maintain the temperature of the polymer system as it adsorbs

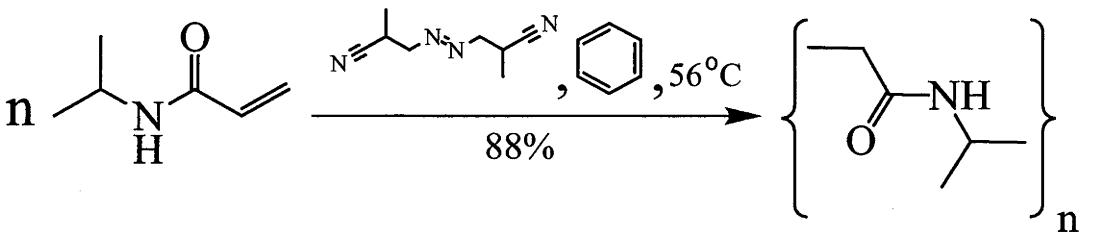

(a)

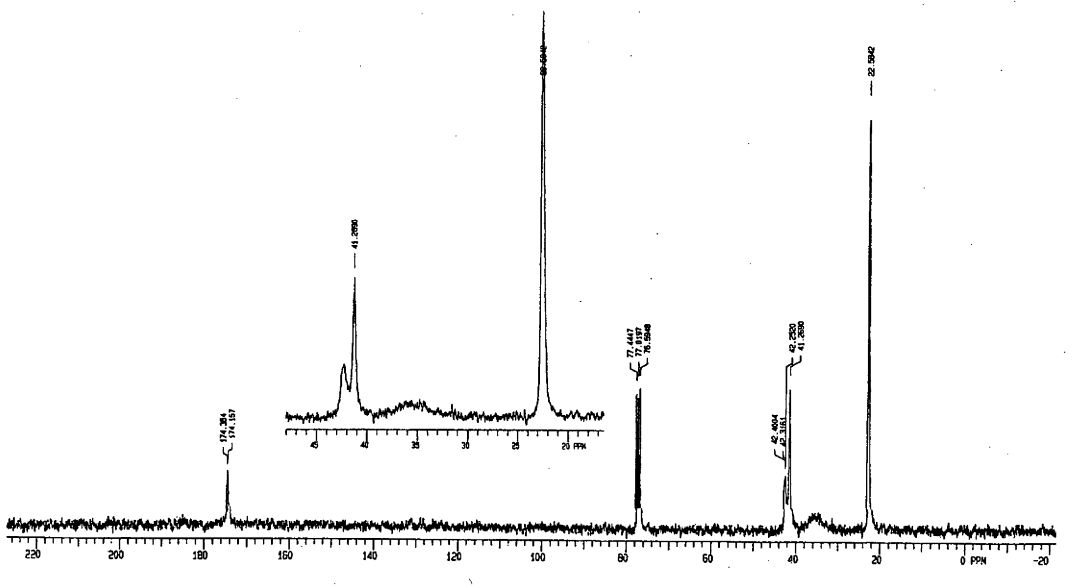

(b)

Figure 4.4: The reaction scheme for the synthesis of poly(*N*-isopropylacrylamide) (a) and the ^{13}C n.m.r. spectra of PNIPAM (b).

to the substrate, throughout equilibration, and during the force measurements. Details of the force measurements are found elsewhere. Briefly, the force measurements are obtained by bringing the tip of AFM cantilever into contact with the polymer covered substrate. As both substrate and cantilever tip are made of the same material, polymer is adsorbed onto both surfaces. Upon separation or retraction of the surfaces, the polymer can bridge the two surfaces and the tension in this bridge causes a deflection in the cantilever spring which is monitored by the deflection of a laser beam reflected from the back of the cantilever. For each cantilever used, we determined the spring constant *in situ* using a hydrodynamic method[24] which allowed us to convert the deflection versus surface separation signals to force versus separation profiles. The spring constants varied from 0.019 Nm^{-1} to 0.062 Nm^{-1} (or 2 - 6 $pNÅ^{-1}$) and the cyclic rate of approach and retraction of the surfaces was set

at 1 Hz, corresponding to speeds of several hundred nanometres per second. Higher frequencies (10 Hz) did not affect the character of the force profiles.

4.3 Force profiles of PNIPAM

PNIPAM has an aqueous lower critical solution temperature (LCST) of 31-34°C;[25] that is, water is a good solvent at temperatures below the LCST and a poor solvent at temperatures above it. Thus, we are able to vary the solvent quality *in situ* by changing the temperature within this convenient range. Changes in the force profiles can then be attributed solely to the solvation conditions. Typical force profiles resulting from single chain stretching as the cantilever and the substrate are separated are shown in Figure 4.5 and 4.6. In these and following profiles, we use the convention that negative forces represent tension in the bridging polymer or an attractive force between the tip and substrate while a positive force represents repulsion between the surfaces. Figure 4.5(a) is a force profile obtained for aqueous PNIPAM at 12°C below the LCST, well within the good solvent regime. Note that within the first $\sim$ 50 nm of separation the force between the tip and substrate is strongly attractive or adhesive. This primary adhesion is non-specific and masks any forces which can be attributed the tension of a chain within this region. Following this primary adhesion, and in about 10-15% of the force profiles, we observe the typical saw-tooth features which have been attributed to single chain stretching. Each saw-tooth represents the stretching of a chain of fixed number of monomers which bridge the two surfaces: at weak extension the tension in the chain is linear with separation but as separation approaches the contour length of the chain, the force increases sharply until at a sufficiently large force, one end of the chain detaches from the surface and the tension abruptly disappears. This detachment force is, for the PNIPAM system, around 100 pN. Such force profiles have been fitted to a number of force laws, among them the Langevin force function and variations thereof. For that reason we refer to such saw-tooth features as "Langevin" events as it signals the stretching of single chains of fixed contour length. Figure 4.5(a) is indicative of the simultaneous extension of three loops or bridges of different size. As the surfaces are separated, the extensional force of the smallest bridge is dominant while the others remain slack. The stretching force of the smallest bridge grows monotonically until it becomes highly extended and breaks at around 90 nm. From this point the tension in the second bridge grows, releasing at 130 nm. The third bridge detaches at 220 nm. These three bridges may or may not be part of the same chain. That these Langevin events can be fitted to a single force law has served as evidence that these forces are attributable to single chains. In general, such force laws are of the form $f \sim g(x/L, a)$ where f and x are the measured force

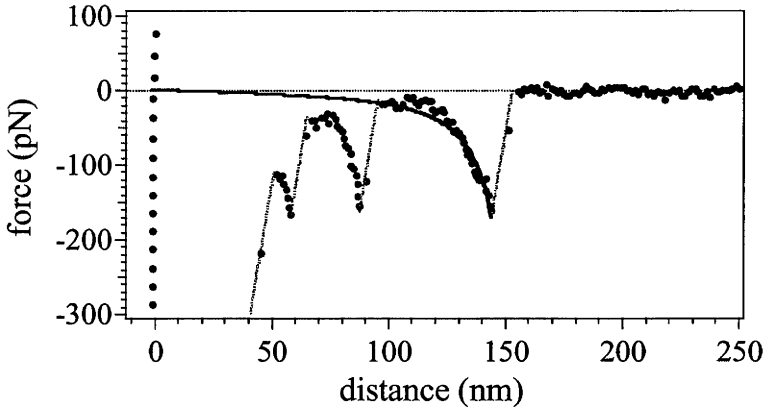

(a)

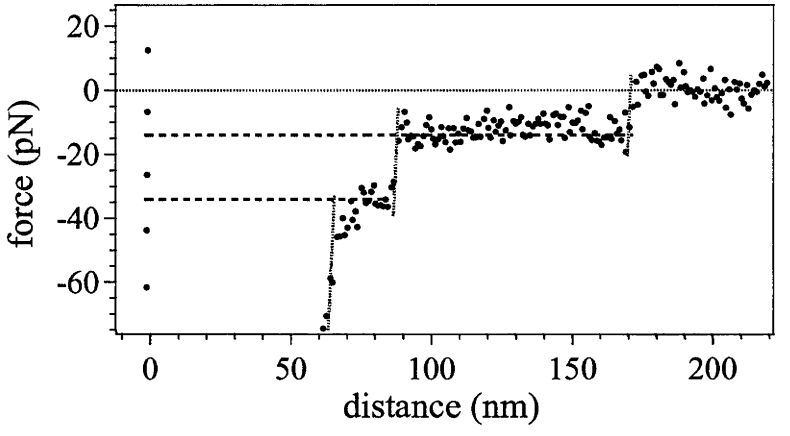

(b)

Figure 4.5: Force versus distance for PNIPAM in aqueous solution at temperatures corresponding to (a) good and (b) poor solvent conditions. For profile (a), the temperature is maintained at 22°C or 12°C below the LCST and corresponds to good solvent conditions in the bulk. The profile shows multiple Langevin events that have been fitted using the WLC model,[7] we show the fit for the longest bridging chain (black solid line). The WLC model is $f = \frac{k_B T}{a}(\frac{1}{4}(1-\frac{x}{L})^{-2} - \frac{1}{4} + \frac{x}{L})$, where f is the force, x is the extension length and the fitting parameters are L, the contour length, and a, the persistence length. For the three Langevin events (L,a) in nanometres are (80.8, 0.1), (99.4, 0.5), and (164.6, 0.4). These chains detach at an average of around 72-88% of their contour length. In profile (b), the temperature is maintained at 39°C, which is above the LCST and corresponds to poor solvent conditions in the bulk. This profile shows multiple Plateau events. The dashed lines are a guide to the eye to highlight the plateau-events. In both (a) and (b), the discontinuities in the force profile have been connected by a grey line of a fixed slope taken to be the spring constant of 0.019 Nm^{-1}. The rms of the baseline noise is 11.0 pN.

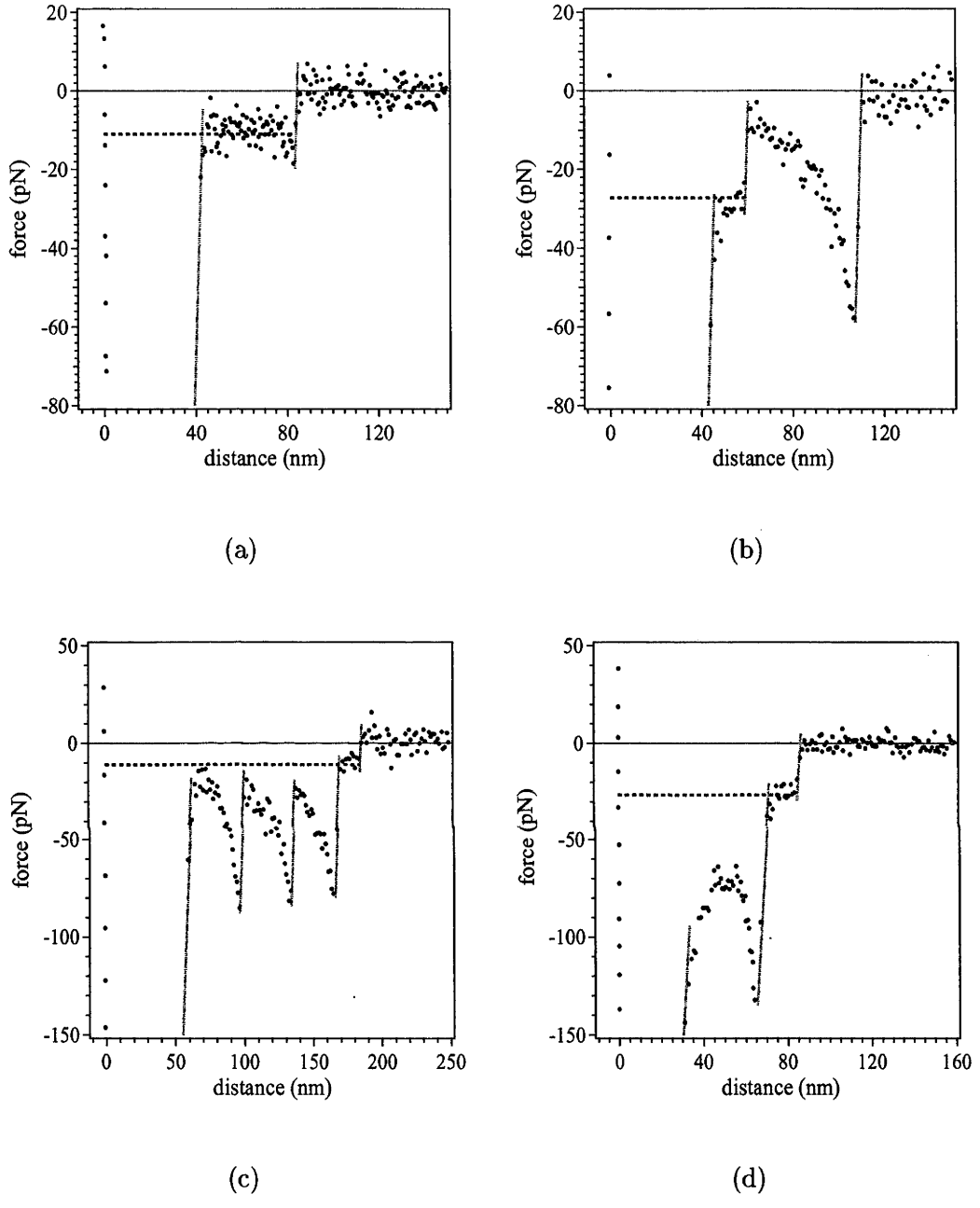

Figure 4.6: Force versus distance for PNIPAM in aqueous solution at temperatures, $T \geq 30°C$, corresponding to poor solvent conditions. Profile (a) shows a single Plateau event. Each of the remaining profiles show combination events, where both Langevin and Plateau events occur. In profile (b), it shows both Plateau and Langevin events. For profile (c), there occurs multiple Langevin events occurring prior to a Plateau event. Profile (d) shows the combination of a Langevin event followed by a Plateau event. The dashed lines are a guide to the eye to highlight the plateau-events. The discontinuities in the force profile have been connected by a grey line of a fixed slope taken to be the spring constant of 0.019 Nm^{-1}. The rms of the baseline noise is 11.0 pN.

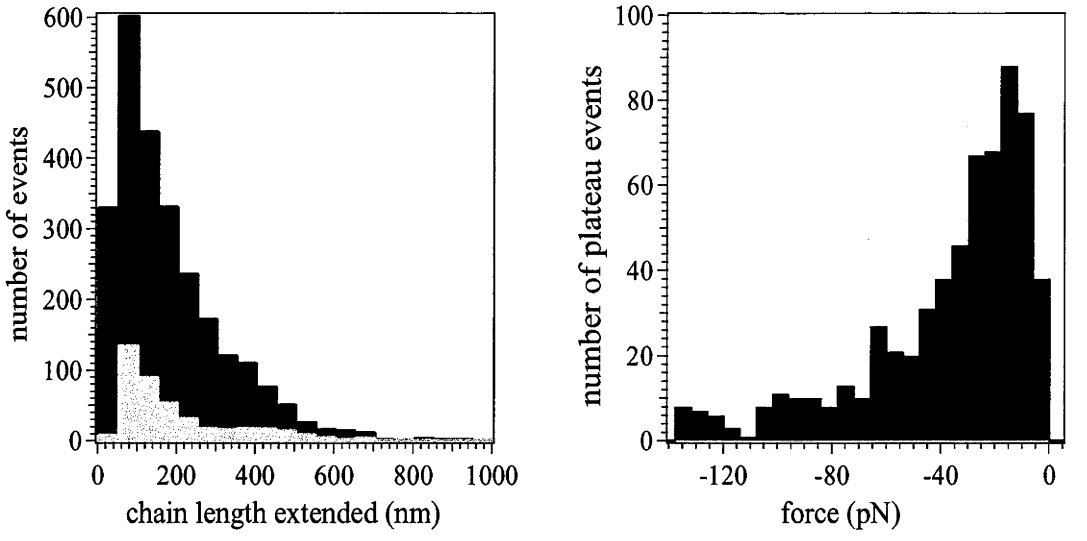

(a) (b)

Figure 4.7: Histograms summarising the statistics of force events for PNIPAM. Histogram (a) shows the frequency of maximum extension distances for both Langevin (black) and Plateau (grey) events that occur under both good and poor solvent conditions for a data set consisting of 1300 force profiles with a bin size of 50 nm. Histogram (b) shows the frequency of the mean force for plateau events collected from 500 force curves, each collected in poor solvent. The bin size is 6.0 pN.

and imposed surface separation and L and a are fitting parameters associated with the contour length and persistence length of the chain. Whether any Langevin event is due to a loop or a tail *cannot* be determined: the tension in a "grabbed" loop is attributed to the shorter side of the loop and cannot be distinguished from the tension of a pulled tail.

When the experiment is conducted under poor solvent conditions, a new type of event is observed in the force profile: a *distance-independent* force or plateau which is typically an order of magnitude smaller than the detachment forces observed in good solvent conditions. Figures 4.5(b) and 4.6 are representative force profiles for the aqueous PNIPAM at temperatures equal to or greater than the LCST for the polymer. These constant force plateaus persist over an extension range (50 to 600 nm) that is similar to Langevin events, suggesting that these Plateau events are also due to single polymer chains. Such Plateau events occur more frequently with increasing temperature (towards poor solvent conditions), but disappear when the temperature is decreased below the LCST or under good solvent conditions. Figure 4.7 gives some statistics of the force profiles of PNIPAM in poor solvent conditions.

When imaging the surface in contact mode at and below the LCST (in good

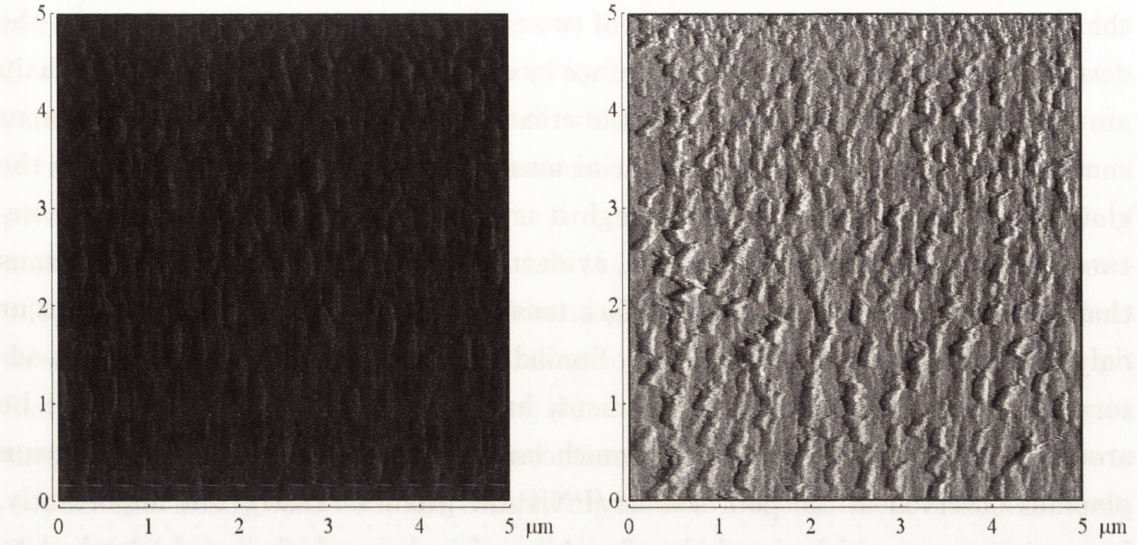

(a) (b)

Figure 4.8: A 5μm $\times$ 5 μm AFM image of PNIPAM adsorbed to a silicon nitride surface at (a) 34°C and (b) 42°C with the grey-scale as black at 0 nm and white at $\sim$ 34 nm. The AFM tip was scanned horizontally, or perpendicular to the surface. In Figure (a) there are no discernible aggregates or globules of the polymer and shows a relatively flat silicon nitride surface with the average height ranging from 4-5 nm. Figure (b) is dramatically different, showing polymer tufts on the surface. The maximum height of the globules is $\sim$ 34 nm, with most globules being 10-20 nm in height.

solvent conditions) the tip simply applies too great a shear force and displaces the adsorbate polymer, Figure 4.8(a). However, as the temperature is increased above the LCST, aggregates or surface-bound "globules" of a few hundred nanometers in width and 10-20 nm in height are observed, Figure 4.8(b). The effective radius of an AFM tip is typically 1$\sim$30 nm[26–28] which is much smaller than the cross section of the surface adsorbed globules. In both imaging and force measurements, the repeated mechanical contact of the tip with the surface aids in collecting and concentrating the polymer into these globular aggregates. Clearly after the tip has scanned a region, that area no longer represents the original state of adsorption. However, this facilitates the formation of the polymer aggregate in the zone of contact.

We can understand these Plateau events, in the most general sense, in terms of a chain pulled monomer-by-monomer from an attractive potential to a zone of zero mean potential with minimal stretching. The filament of polymer between the surfaces is made up of monomers which have been pulled out of a local attractive potential. This bridge grows in number of monomers or chain length with surface separation. Stretching is minimal, as suggested by the small magnitude of the force

plateau in comparison to the larger stretching forces in Langevin events. In principle, the plateaus can be attributed to one of two energy changes upon extension: (a) the destruction of attractive monomer-surface interactions as the monomers of the chain are "ripped" off the surface, or (b) the creation of unfavourable monomer-solvent contacts, characterised by the interfacial tension, as monomers are pulled from the globule into the poor solvent. Although it is difficult to distinguish absolutely between these energies in a force plateau, evidence supports that the PNIPAM plateaus characterise the polymer/solvent surface tension. First, these Plateau events occur only under poor solvency conditions. Second, the force attributable to surface adsorption, that is the force of detachment, has been shown in good solvent to be around a few hundred picoNewton, much larger than the few tens of picoNetwon plateaus observed in the poor solvent/PNIPAM profiles. Lastly, but importantly, Langevin events, which signal the stretching of a chain which is end-adsorbed to *both* tip and substrate, are also seen alongside Plateau events in force profiles at poor solvency Figures 4.6(b)-(d). This suggests that a Plateau event is associated with pull-out of a chain or loop having one end free or unadsorbed to the surface but embedded in the globule. In contrast, a Langevin event is associated with stretching of chains or loops having both ends fixed or adsorbed. Under good solvent conditions, there would be no force for extension of chains with only one end attached to the AFM tip; but in poor solvent an interface is formed between collapsed monomer and poor solvent and work must be done to transfer monomer from globule to filament. The occurrence of both events typifies the aqueous PNIPAM system for poor solvent conditions. Figure 4.6(b) is a force profile showing a Plateau event followed by a Langevin event. The Plateau event persists to an extension distance of 58 nm terminating just outside the primary adhesion and has a mean force of 26 pN. Simultaneously, there occurs a Langevin event which persists until an extension distance of 106 nm. In Figure 4.6(c) the three Langevin events detach at 96 nm, 132 nm and 164 nm. The Plateau event has a mean force of 7 pN that offsets the stretching force and terminates at 183 nm. Figure 4.6(d) also shows the combination of a Langevin event followed by a Plateau event. The extension distance of the Langevin event is 63 nm and the Plateau event is 83 nm. The mean force of the Plateau event was 27 pN.

In any single molecule force measurement, there is always a degree of ambiguity as to the number of chains or loops which are extended. In the case of Langevin events, the fitting of scaled force profiles is taken as sufficient evidence for single chain or loop extension. For the Plateau events here, it is particularly difficult to establish if the plateaus are associated with single chains or bundles of chains, precisely because the force of pull-out is of comparatively small magnitude and is featureless, *i.e.*, it is independent of extension. However, the PNIPAM profiles do

provide some significant clues. First, if we take the pull-out strand to be a cylinder of radius r and the surface energy to be γ, then the energy of pull-out to extension L is $2\pi rL\gamma$. Or equivalently, the force is $2\pi r\gamma$. For PNIPAM, we can adopt a value of γ between 40 and 45 mJ/m^2,[29] which is the range of literature values for PNIPAM. This, together with our measured plateau force of the order of 10s of pNs gives a cylinder of radius r on the order of angstroms, *i.e.*, the cylinder is of molecular dimensions. This suggests that the Plateau event characterises the pull-out of single chains from the surface-bound globule. In addition, we should expect to see stepped force plateaus corresponding to the simultaneous pull-out of multiple filaments. For example, if we are pulling simultaneously 3 filaments from the globule, then the force plateaus should drop discontinuously from $-F$ to $-2/3F$ and then to $-1/3F$ and finally to 0 with the complete pull-out of the different sized filaments. Figure 4.5(b) shows 2 plateaus, although the first plateau terminates at 90 nm, just outside of the primary adhesion zone. This plateau is indicative of a bridge that is completely pulled out of the globule by 90 nm, while a second bridge persists until the surfaces are separated to 180 nm. The mean force of these two events are 34 pN and 14 pN. Figure 4.6(a) also shows Plateau event which terminates at 82 nm and a mean force of 11 pN. However, with over 1300 force profiles examined, the PNIPAM system did not provide sufficient statistics to verify quantised plateaus. Plateau events were rare in the PNIPAM system; for every Plateau event in the set of 1300 profiles there were 10 Langevin events. This might be understood in terms of the low average, but highly polydisperse, molecular weight of PNIPAM. The force events (Langevin and Plateau) arise from the larger chains: these events persist over a hundred or more nanometres indicating that the chains involved are at least that long and considerably longer than the average PNIPAM chain length of tens of nanometres. When a Plateau event occurs, it corresponds to the longest chain pulled out of a globule of more populous smaller chains. Consequently, we anticipate that the frequency of multiple plateaus was much reduced in comparison to what one would expect if the polymer was of high average, monodisperse molecular weight. In the following section, we describe similar experiments with PEO. This system is advantageous in that the polymer is significantly higher average molecular weight.

4.4 Force profiles of PEO

PEO has an aqueous LCST of 96°C,[30] which is not as easily accessible in AFM experimentation. However this critical temperature can be lowered by the addition of various salts, notably K_2SO_4 and KNO_3, to as low as 34°C. Thus, we can change solvency by the addition of salt as well as by temperature. We consider first, salt and temperature conditions for which Plateau events occur alongside Langevin events;

i.e., conditions approaching or at poor solvency. Figures 4.9 and 4.10 are force profiles of PEO in 0.45 M K_2SO_4 at 25 $\pm$ 2°C, selected from a data set of 600 profiles. Figure 4.9(a) is a force profile which shows stepped plateaus, at least 3, arguably 4, extending beyond the primary adhesion region. The force profile Figure 4.10(a) and (d) also shows stepped plateaus. Figure 4.10(a) has at least 5, and arguably 6 Plateau events, while Figure 4.10 has only 2 Plateau events. Many other force profiles in the data set show stepped plateaus, exclusively; however, many more contain both Langevin and Plateau events. The co-existence of both events typifies these systems and indicates that the stretching of doubly end-tethered chains occurs alongside the pull-out of singly end-tethered chains. Figure 4.9(b) is a typical example as it shows a Langevin event followed by a Plateau event. The Langevin event, or stretching of a fixed loop or tail, persists until an extension of 120 nm at which point the chain detaches from one of the surfaces. Simultaneously, there is pull-out of a filament and the force of pull-out, roughly 45 pN, offsets the stretching force. Figure 4.10(b) is a more complicated example consisting of 5 stepped plateaus intermixed with a single Langevin event. Figure 4.10(c) shows the reverse combination of Figure 4.9(b) with a Plateau event of mean force 120 pN followed by a Langevin event. As these figures shows, it is relatively simple to identify and separate Langevin events from Plateau events and to construct a statistical analysis of the Plateau events. From the set of 600 force profiles collected from the PEO/K_2SO_4 system, we have identified over 400 Plateau events in the following way. The distribution of measured force within a candidate Plateau event is fitted to a Gaussian in order to find the mean force and standard deviation. The acceptance criteria for a Plateau event is that the standard deviation from the mean is less than 1.7 pN. We find that Plateau events occur with the same frequency as Langevin events; however multiple plateau events are more likely than multiple Langevin events. Both types of events occur over extensions ranging from 50 nm (the edge of the primary adhesion zone) to 1100 nm.

Figure 4.9(c) provides the statistics on the mean force evaluated over the length of the Plateau events from the complete set of 600 force profiles. Plateaus of 55 pN are the most frequent, with significant populations at double that force or 110 pN, at 185 pN and a discernible population at 250 pN. Thus, the statistics of a large number of analysed force profiles provide evidence of the description suggested by the profiles of Figure 4.9(a) and Figures 4.10(a), (b) and (d): Plateau events are quantised. In addition, there is a discernible population (17 in number) of plateaus of magnitude $\sim$25 pN. This fits with our interpretation of multiple chain pull-out: if we attribute the pull-out force with the highest frequency to the extension of a single loop, then the 25 pN plateaus represents the less likely extension of a single tail. The 25 pN plateau population should also include the short-range extension of

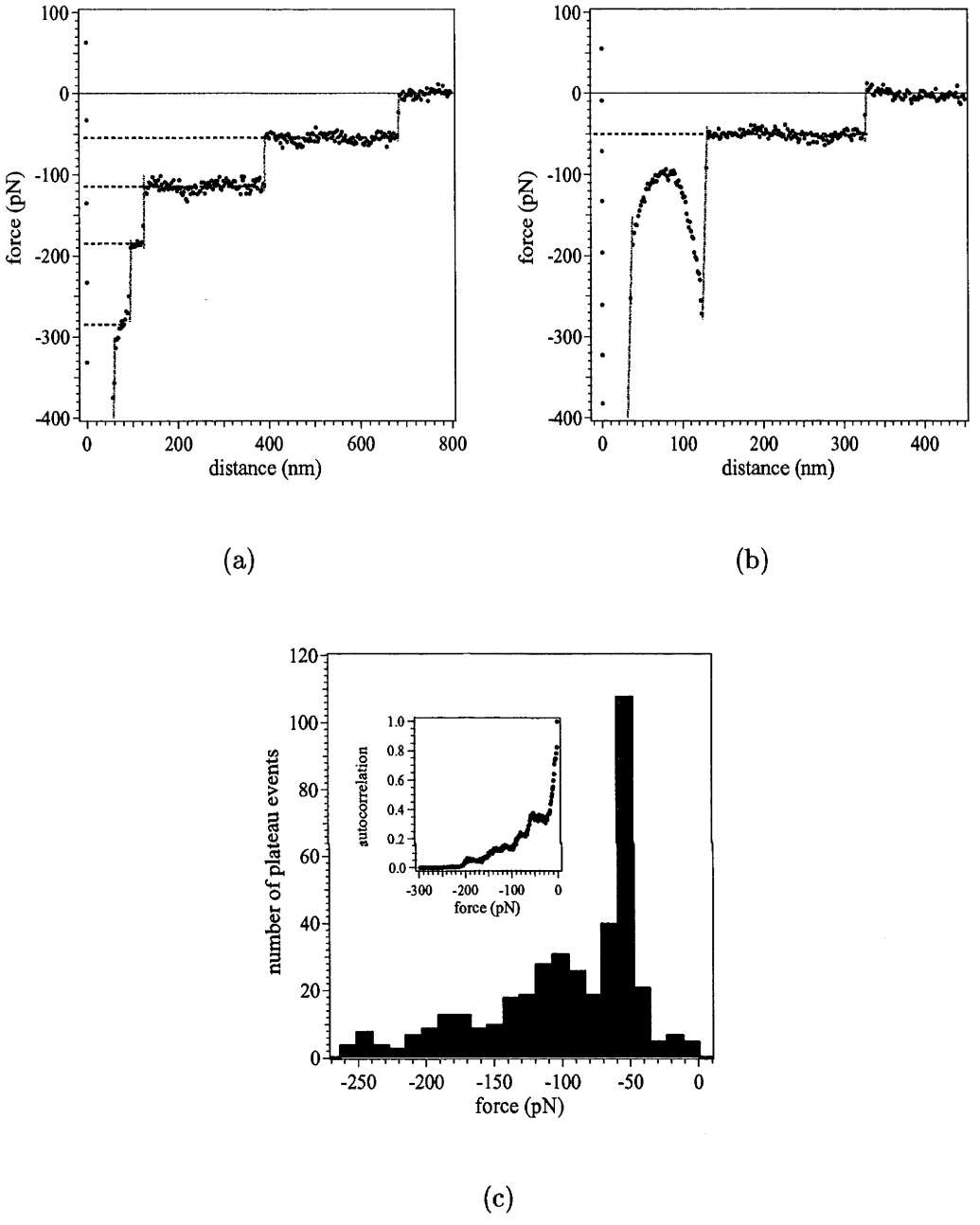

Figure 4.9: Representative force profiles and histogram summarising the set of profiles for PEO in 0.45M K_2SO_4 at 25°C. The spring constant of the cantilever is 0.040 Nm^{-1} and the rms baseline noise is 22.0 pN. The discontinuities in both force profiles have been connected by grey lines of fixed slope. (a) A force versus distance profile shows 4 Plateau events with mean forces of 285 pN, 185 pN, 115 pN and 55 pN. These plateaus persist to extension distances of 80 nm, 120 nm, 391 nm and 679 nm and are highlighted by the dashed lines. (b) A force versus distance profile shows simultaneous Langevin and Plateau events which detach at 120nm and 330 nm respectively. (c) A histogram shows the frequency of plateau forces. It was constructed from 406 Plateau events in a data set of 600 force profiles. The magnitude of the plateau force is the mean of a Gaussian distribution, fitted to the experimental points of the plateau. The bin size of the histogram is 12.0 pN. The inset is an autocorrelation of the data set.

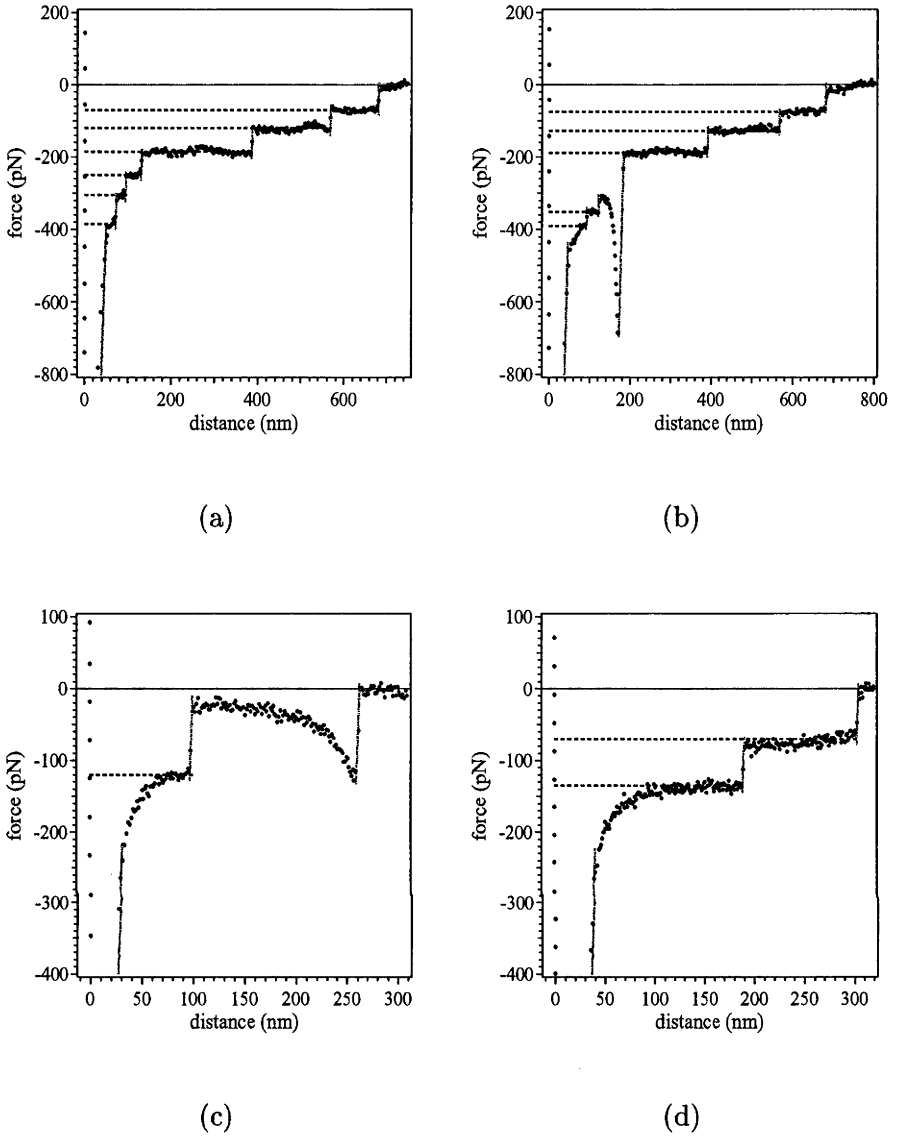

Figure 4.10: Representative force profiles for PEO in 0.45M K_2SO_4 at 25°C. The spring constant of the cantilever is 0.040 Nm^{-1} and the rms baseline noise is 22.0 pN. The discontinuities in both force profiles have been connected by grey lines of fixed slope. (a) A force versus distance profile shows 6 Plateau events highlighted with dashed lines. The mean forces forces are 385 pN, 305 pN, 250 pN, 185 pN, 120 pN and 70 pN. These plateaus persist to extension distances of 68 nm, 93 nm, 124 nm, 384 nm, 570 nm and 683 nm. (b) A force profile shows the combination of 5 Plateau events and a Langevin event. The extension distances of the plateaus are 90 nm, 121 nm, 390 nm, 570 nm and 680 nm. The mean forces are 385 pN, 353 pN, 189 pN, 127 pN and 75 pN. The Langevin event occurs after the second plateau and detaches at 169 nm. (c) The force profile shows simultaneous Plateau and Langevin events which detach at 98 nm and 258 nm. (d) The force profile shows 2 Plateau events with mean forces of 135 pN and 70 pN which detach at 190 nm and 305 nm respectively.

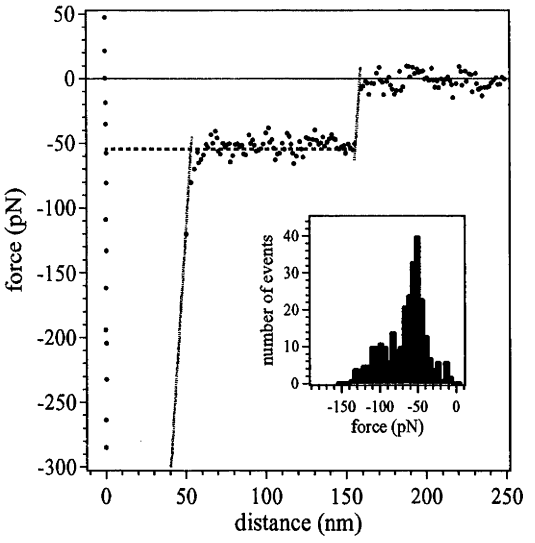

Figure 4.11: Force versus distance for PEO in aqueous no-salt solution at 30°C. This is a typical force profile showing a single Plateau event. The discontinuities in the force profile have been connected by a dotted line and have a fixed slope taken to be the spring constant of 0.019 Nm^{-1}. The baseline noise is 9.8 pN. The inset is a histogram of the frequency of Plateau events as a function of the magnitude of the plateau force, constructed from 280 Plateau events in 1500 force profiles. Plateaus of $\approx$ 55 pN are dominant while there is arguably another smaller population of plateaus of $\approx$ 100 pN. The bin size is 5.4 pN.

an uneven loop where monomers are extracted from the globule on one side of the loop, the other side being slack. The population of Plateau events of roughly 110 pN would then correspond to the extension of two loops. The populations of force plateaus centered at larger forces are more broad and reflect the pulling of more chains. The inset to Figure 4.9(c) is the autocorrelation of the frequency of plateau forces. Despite having only 400 Plateau events, the peak in the autocorrelation near 50 pN lends further evidence of quantisation.

Other PEO studies with different solvent conditions provide fewer profiles and/or fewer plateau events but show similar results. Figure 4.11 and Figures 4.12(a)-(c) are typical profile for aqueous, no-salt PEO at 30°C. The force profile in Figure 4.11 shows a single Plateau with a mean force of 55 pN which detaches at 156 nm. Figures 4.12(a) and (b) shows multiple steps of 2 Plateaus and 3 Plateaus respectively. A combination of a Langevin event followed by a Plateau event is shown in Figure 4.12(c). Both chains are pulled simultaneously and detach at extension distances of 74 nm and 155 nm. The mean force for pulling the filament is 53 pN, which offsets the stretching force corresponding to the Langevin event. Figure 4.12(d) is a typical force profile at 25°C and shows 4 Langevin events. These different sized bridges detach at extension distances of 83 nm, 111 nm, 130 nm and 159 nm. That the Langevin events have been fitted to a force law, indicates single polymer chains

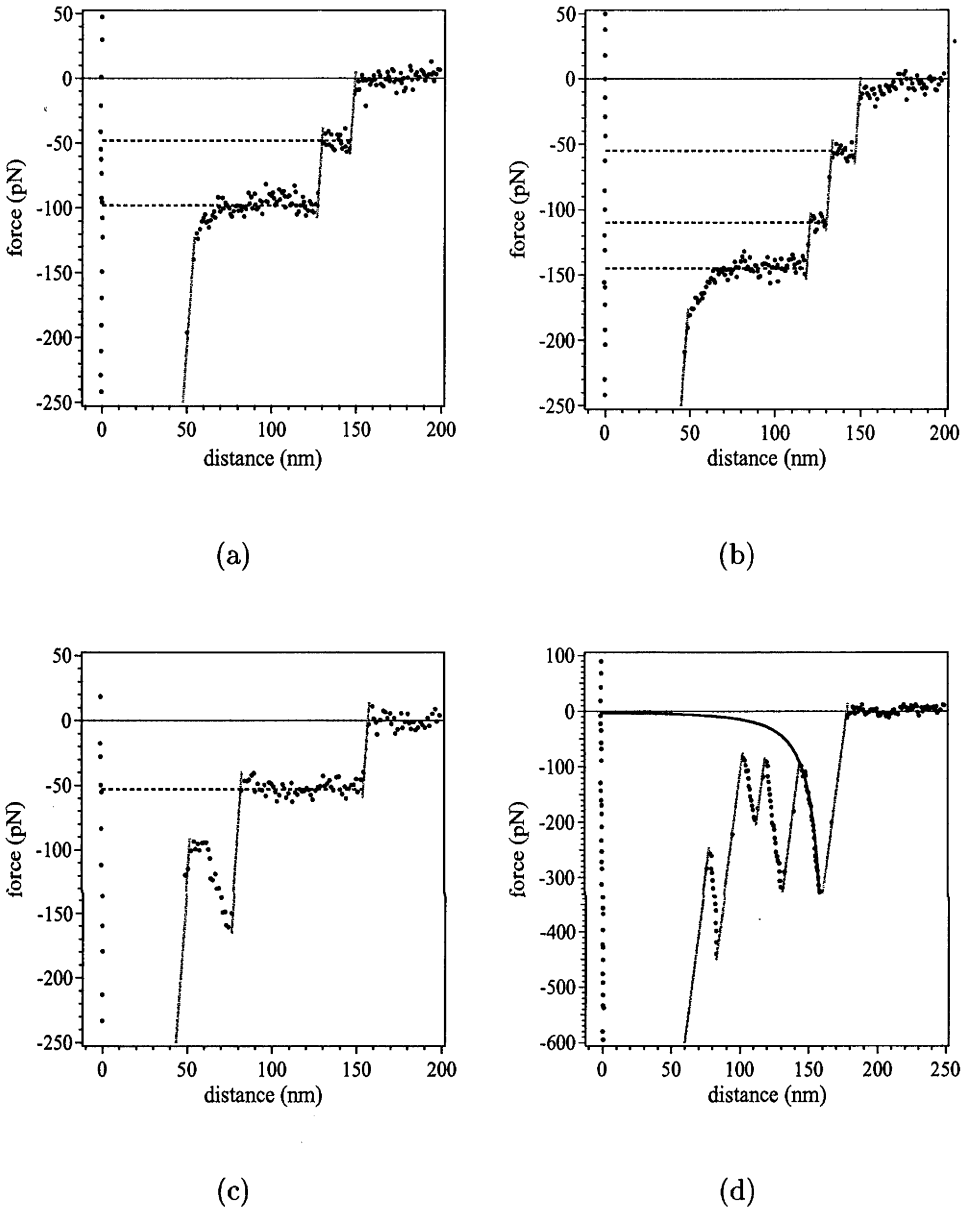

Figure 4.12: Force versus distance for PEO in aqueous no-salt solution at different temperatures. For profiles (a)-(c), the temperature is maintained at 30°C. (a) A force versus distance profile shows 2 Plateau events with mean force of 98 pN and 48 pN. These persist to extension distances of 128 nm and 147 nm. (b) A force versus distance profile shows 3 Plateau events with mean force of 145 pN, 110 pN and 55 pN. These detach at 118nm, 130 nm and 145 nm. (c) A force versus distance profile shows simultaneous Langevin and Plateau events which detach at 74 nm and 155 nm respectively. For profile (d), the temperature is maintained at 25°C and shows multiple Langevin events which have been fitted using the WLC model[7] as shown in Figure 4.5. We show the fit for the longest bridging chain (black solid line). For the four Langevin events (L,a) in nanometres are (178.9, 0.9), (127.3, 0.3), (146.6, 0.3) and (174.9, 0.4). These chains detach at an average of around 46-91% of their contour length.

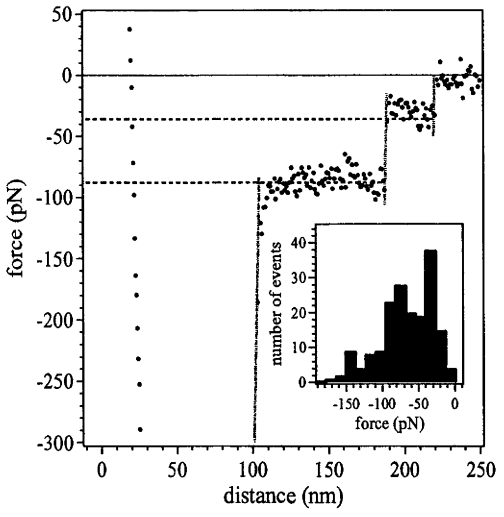

Figure 4.13: Force versus distance for PEO in aqueous 0.25 M KNO_3 solution at 22°C. This is a typical force profile showing a single Plateau event. The discontinuities in the force profile have been connected by a dotted line and have a fixed slope taken to be the spring constant of 0.062 Nm^{-1}. Horizontal dashed lines in profile are used to highlight the constant force of the Plateau events. The rms baseline noise is 25.29 pN. The inset is a histogram of the frequency of Plateau events as a function of the magnitude of the plateau force, constructed from 180 Plateau events in 500 force profiles. The plateau forces range up to 150 pN; however, in comparison to the PEO/K_2SO_4 system, it is difficult to argue that there are interval peaks in the histogram. The bin size is 13.8 pN.

are being stretched. As the first Langevin event is so close to the primary adhesion the number of data points that can be used to fit the force law is reduced, this results in a poorer fit and hence the low percentage of contour length that the chain is extended.

Figure 4.13 and Figure 4.14 are force profiles taken for aqueous PEO with 0.25 M KNO_3 at room temperature. These profiles show the variety of single chain stretching for this system. Figure 4.13 shows 2 Plateau events of mean force 88 pN and 36 pN which detach at 187 nm and 219 nm. The force profiles in Figure 4.14(a) and (b) show a single and double Plateau respectively. Figure 4.14(c) shows a Langevin event followed by a Plateau event. Figure 4.14(d) shows multiple Langevin events which detach at extension distances of 36 nm and 49 nm. This is relatively short when compared to the extension distances of the bridging chains in the other force profiles. Note also that the primary adhesion is also quite small.

Figure 4.11 and Figure 4.13 show single and double plateaus, respectively and each figure provides a histogram of the mean force of plateau events. The maximum extension over which these systems gave Langevin or Plateau events, (the extension at which the force returned to zero) was less than half that of the PEO/K_2SO_4 sys-

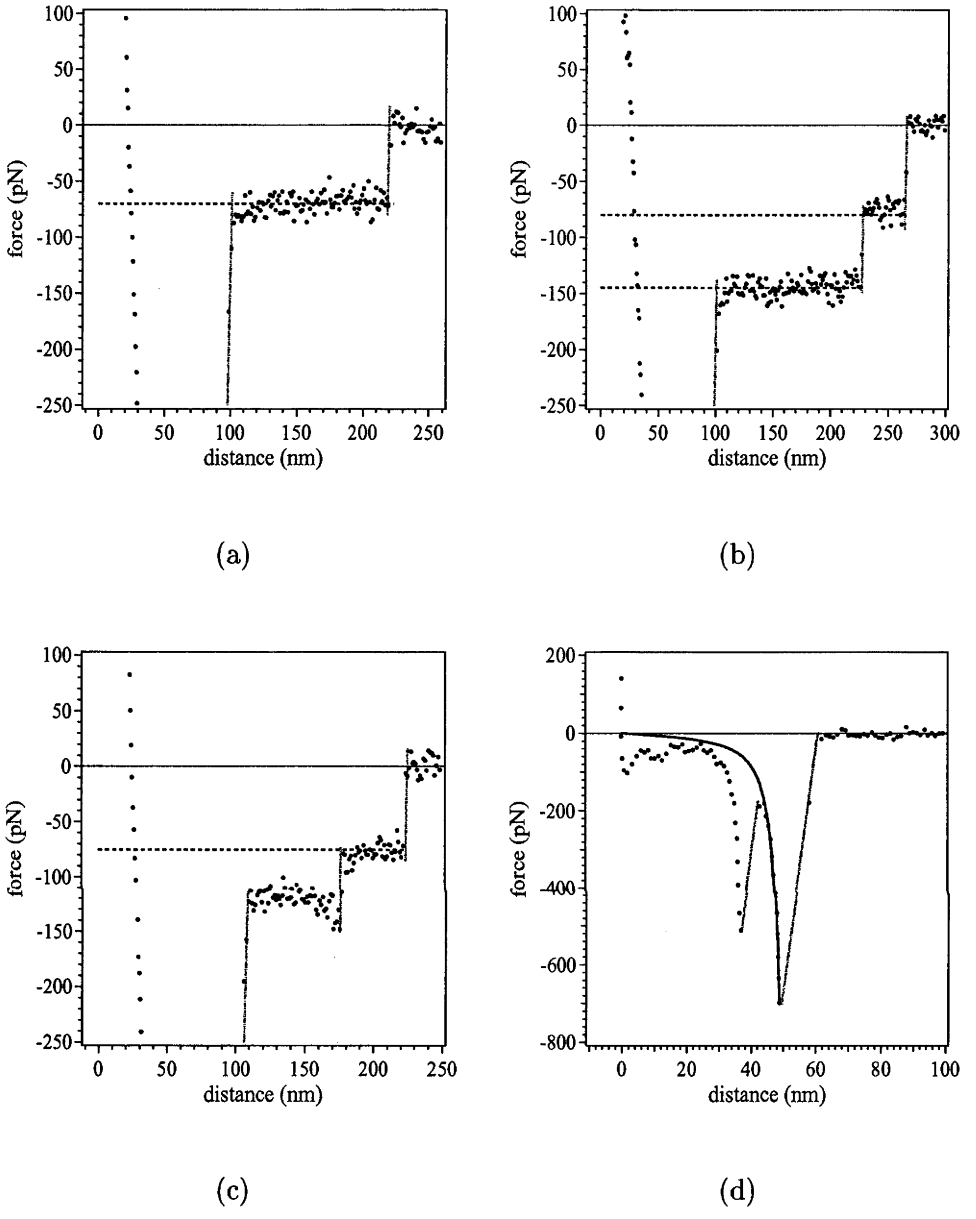

Figure 4.14: Force versus distance for PEO in aqueous 0.25 M KNO_3 solution at 22°C. (a) A force profile shows a single Plateau event with a mean force of 70 pN which detaches at an extension distance of 219 nm. (b) A force profile shows 2 Plateau events with mean forces of 145 pN and 80 pN and detach at 223 nm and 267 nm respectively. The force profile in (c) shows a Langevin event followed by a Plateau event, which detach at 175 nm and 222 nm. The mean force of the Plateau event is 75 pN. (d) A force profile shows 2 Langevin events. These have been fitted to the WLC model[7] (see Figure 4.5), we show the fit to the longest bridging chain (black solid line). For the two Langevin events (L,a) in nanometres are (39.3, 0.4) and (53.0, 0.2). These chains detach at an average of around 92-93% of their contour length. The discontinuities in the force profile have been connected by a dotted line and have a fixed slope taken to be the spring constant of 0.062 Nm^{-1}. Horizontal dashed lines in profile are used to highlight the constant force of the Plateau events. The rms baseline noise is 25.29 pN.

tem. Consequently, for the same number of force profiles, there are far fewer events and the statistical analyses are correspondingly not as clear. The mean force of Plateau events of the aqueous no-salt PEO is predominantly on the order of ~55 pN with a significant population of plateaus with larger force, at roughly 100 pN. Although there is about 1/2 the data of Figure 4.9(c), it appears that the results are similar, suggesting the extension of single and double loops of PEO. The statistics of the PEO/KNO_3 systems are less conclusive. One can argue that there are peaks in the histogram at 40 pN and 90 pN; however, the large rms error in the baseline of the AFM force data, conveyed in the larger bin size used in the histogram, makes the PEO/KNO_3 system less conclusive.

At room temperature and in the absence of salts, the PEO force profiles do not contain Plateau events and consist entirely of Langevin events, Figure 4.12(d), verifying that good solvent conditions prevail. When the temperature is elevated to 30°C or salt is added at room temperature, then we find Plateau events occurring with the same frequency as Langevin events. In the PNIPAM system, the onset of Plateau events occurred when the temperature was elevated just above the literature value of the LCST for bulk PNIPAM solution. However, in the case of no-salt aqueous solutions of PEO, the literature value of the LCST is 96°C and much higher than our temperatures; yet we find the onset of Plateau events as the temperature is elevated slightly from 25 to only 30°C. This is also the case in the salt solutions. Bulk aqueous solutions of PEO in 0.45M K_2SO_4 and 0.25M KNO_3 have reported LCSTs of 34°C and 65°C, respectively. However, we find that the addition of these salts to aqueous solutions of PEO at room temperature are sufficient to cause the onset of these Plateau events. We can presume that the attractive silicon nitride surface plays a role in lowering the effective LCST of the PEO solutions. However, why the effective LCST of the PNIPAM solution is not lowered is not evident to us. When electrolyte is present, the local concentration of electrolyte is significantly larger at the silicon nitride surface than in the bulk due to cation adsorption at the anionic surface, and we can presume that this plays a role in further lowering the effective LCST of the PEO solution. But irrespective of how we describe bulk solution conditions, it is clear that with a slight elevation of temperature or the addition of salt, the pull-out of a free end now requires energy. This enery is is attributed to pulling monomer-by-monomer through a polymer-solvent interface.

4.5 Discussion

To summarise, we have shown that the extension of single PNIPAM and PEO chains in poor, aqueous solution occurs with a force that is independent of extension, *i.e.*, a force plateau. The quantised steps associated with multiple plateaus in

individual force profiles as well as the statistics of a large collection of force profiles strongly suggest that these force plateaus are attributable to single chains. More generally, this force plateau can be understood in terms of the Rayleigh instability for a liquid column: extension of the chain results in monomer-by-monomer pull-out from the condensed globule into the poor solvent. That the plateau is a feature of the dominant surface tension, rather than adhesion of the chain to the substrate, is demonstrated by a number of observations. (1) The force of detachment in the Langevin events is an order of magnitude larger than the plateau force. That is, the force at which one end of the stretched chain is detached from the surface is much larger than the plateau forces. One might argue that elevated temperatures or the addition of salt might lower the affinity between the polymer and surface thereby reducing the force needed to detach a chain from the surface. However, we find that under these conditions, both Langevin and Plateau events occur in the same force profile and that the detachment force in the Langevin events remain at least an order of magnitude higher, and the surface affinity is not diminished. (2) The onset of Plateau events occurs generally with the onset of poor solvent conditions. In the case of PNIPAM, this is attained by elevating the temperature beyond the bulk LCST. However, in the case of PEO, the onset of plateaus occurs before the poor solvent conditions are achieved in the bulk. That is, only slight temperature elevations or salt additions is sufficient to see Plateau events. One might argue that bulk solvent conditions are not expected to accurately describe the polymer-solvent interactions near an adsorbing surface. However, polymer-solvent interactions near the interface will become more unfavourable with the addition of co-solvents/temperature change which bring the bulk solution closer to poor conditions. (3) Plateau events occur simultaneously with Langevin events in the same force profile. This suggests that the plateau force arises from the pull-out of a free chain end from a surface-bound globule while the Langevin event is associated with the comparably high stretching forces of a doubly end-tethered chain.

The aqueous PNIPAM and PEO/salt systems were studied previously by others using AFM and the surface force apparatus. Were force plateaus seen in these studies and, if not, why? In an early study, Braithwaite et al.[31,32] used a colloidal sphere attached to the end of an AFM cantilever to probe PEO in aqueous KNO_3 using similar conditions to ours. Although their probe area is very large, plateaus that range between 750-3800 pN (converted from energy to force using the Derjaguin approximation[33]) are evident in their published profiles. However, because the probe area is so large, it is unlikely that single chains are being pulled out, as also suggested by the large magnitude of the force. Nevertheless, the plateaus are evident. In another study, Oesterhelt et al.[9] added co-solvents to aqueous PEO which was end-tethered to a substrate and probed with an AFM tip. The grafting density was

not reported but Langevin events were recorded at all reported solvent conditions, with fits to the force curves providing evidence of the solvency. No plateaus were reported. However, given that the chains were end-tethered to one surface, we would not expect to discern plateaus even if the grafting density were high. Because all chains were end-tethered to one surface, we would find surface-bound globules mostly on the grafting surface, and not on the AFM tip. Thus, pulling a chain monomer-by-monomer from globule through the polymer-solvent interface and into the solvent could only occur from globules on the grafting surface. A plateau should, under these circumstances occur, but because the chain is end-tethered, the plateau converts smoothly into a saw-tooth stretching profile. The force profiles of Oesterhelt et al. could not contain a plateau with a discontinuous step. Identification of separate Plateau events and Langevin events would be nearly impossible and the best one could do is note changes in the elasticity as evidence by the form of the force at high extension and just before detachment. More recently, Zhang et al,[10] investigated the influence of a co-solvent and thermal treatment on PNIPAM using single chain extension with AFM. Their profiles contained exclusively Langevin events and no plateaus were found. However, these authors have also communicated to us that poor solvent conditions were not tested and the solvent temperature was not maintained *in situ* or during the AFM pulling experiments.

A cantilever which is not sufficiently soft ($k \sim 0$) or stiff ($k \to \infty$) will provide a force profile which details the mechanical properties of both chain and cantilever, particularly at small lengthscales.[35] Thus, it is important to ascertain that the force profiles reported here are indeed representative of the chain and not the cantilever. Consider the case of an infinitely stiff cantilever where we have "magic" detectors for determining the force on the cantilever. This is a perfect, but unrealisable AFM where the measured force is the chain tension as a function of the controlled extension, D. The partition function of the chain is $Z_0(D) = \int_0^\infty d\mathbf{x} \exp(-\beta U(\mathbf{x}))$ where $\beta = (k_B T)^{-1}$, $U(\mathbf{x})$ is the energy of the chain, and $\mathbf{x}$ is the vector of coordinates of the chain which bridges the surface and cantilever tip. Distance D is the experimentally controlled variable and because the cantilever is infinitely stiff, it is also equal to the extension of the chain. The Helmholtz free energy of the system (cantilever and chain) is that of the chain and is $-\beta^{-1} \ln Z_0$. The force exerted by the chain on the cantilever is

$$f_0(D) = \beta^{-1} \frac{\partial \ln Z_0}{\partial D}. \tag{4.1}$$

To describe the forces of chain pull-out, we can express the energy of the chain at extension x as $U(x) = \Delta x$ where Δ is an energy per unit distance associated with pulling the chain monomer-by-monomer through the interface into poor solvent. The bare force of pull-out is then $f_0(D) = \Delta$, *i.e.*, a plateau force.

However, a real AFM does not have a perfectly stiff cantilever. In order to

increase sensitivity in the force measurement, it is most practical to have a soft or compliant cantilever, it i.e., k as small as possible. The experimentally controlled distance D is then the chain extension *and* the cantilever deflection; the measured force will be the bare force, $f_0(D) = \Delta$, plus some correction term. How large is this correction term relative to Δ? To determine this we need to consider the partition function of the entire system, chain plus cantilever. The energy of the cantilever is $\frac{1}{2}k(x-D)^2$ where x is the extension of the chain and the partition function of the system is then

$$Z(D) = \int_0^\infty dx \exp(-\beta\Delta x) \exp(-\frac{\beta k}{2}(x-D)^2). \tag{4.2}$$

The measured force is $f(D) = \beta^{-1}\frac{\partial \ln Z}{\partial D}$, or

$$f(D) = f_0(D) + \sqrt{\frac{2k}{\pi\beta}} \frac{\exp(-\frac{\beta}{2k}(kD-\Delta)^2)}{1 + erf(\sqrt{\frac{2\beta}{k}}(kD-\Delta))}. \tag{4.3}$$

The second term on the rhs is the noise-dependent correction term. We can estimate the magnitude of this term and compare with $f_0(D) = \Delta$. The spring constant of our cantilevers is on the order of a few pN$\mathring{A}^{-1}$ or $\sim 0.1 k_B T \mathring{A}^{-2}$ and the value of Δ or the force plateau that we measure is on the order of 10s of picoNewtons or $\sim 1 k_B T \mathring{A}^{-1}$. Thus, as long as $D >> \Delta/k$ or the controlled distance is greater than 10s of Ångstroms, then the correction term is negligible. As our plateaus persist over a few 100s of nanometers, we can safely say that our plateau forces are representative of the chain pull-out. In addition, it is important to contrast our reported plateau forces with the limit of sensitivity of our AFM. Our AFM has a sensitivity limit of slightly under 10 picoNewtons, but the Plateau events that we report are a few tens of picoNewtons. Figure 4.7 shows that there are some Plateau events in the PNIPAM system which are recorded at or below this limit of 10 picoNewtons. However, plateaus of 15 pN are most populous and the average plateau force is higher and easily detected by the AFM. The PEO systems show larger plateau forces of $\sim$ 50-55 pN, irrespective of the added salt or elevated temperature, and these are well above the sensitivity limit of our AFM. However, in some measurements there is increased baseline noise which we attribute to scattering of the PSD beam by PEO/salt.

There are two other explanations of force plateaus in single chain extension experiments: one based generally upon the rate of extension[34] and another based upon pulling a charged chain.[11,36] Both treatments however, predict force profiles with plateaus exclusively; *i.e.*, Langevin and plateaus do not occur in the same force profile. In a generalised theoretical treatment, Haupt et al.[34] described the force profile of a single chain which adsorbs onto a surface in a series of loops. At ex-

tension rates which are faster than the rate of dissociation of the monomer-surface contact, the force profiles appears as a consecutive series of Langevin events, each corresponding to the stretching of an isolated loop of the chain. However, at slower extension rates where the monomer-surface contact has ample time to detach and reform many times over the timescale of the pulling experiment, the force measured provides information about the strength of the contacts averaged over the length of the chain. Thus, for very slow extension rates, the force will be constant and smaller as the tension is distributed over all of the monomers in the chain. In the second explanation, Châtellier et al.[11] describe the pulling of a single polyelectrolyte chain off an adsorbing, charged surface using scaling arguments; this theoretical work was later expanded in more detail by Johner and Joanny.[36] These researchers showed that the force profile reaches a plateau for extensions beyond the Debye screening length of the solution. The dissociation of electrostatic bonds between the charged groups of the polyelectrolyte chain and the charged surface occurs is much faster than rate of extension of the AFM tip. Consequently, the magnitude of the plateau force indicates the averaged strength of contacts, or equivalently, the energy required to transfer monomers to the bulk solution from the electrical double layer near the surface. These explanations have been experimentally verified using AFM on polyelectrolytes adsorbed onto charged surfaces. Hugel et al.[12] showed the dependence of the magnitude of the force plateau upon the polymer charge and electrolyte concentration. Previously, Châtellier et al.[11] found plateaus when detaching polyelectrolytes from charged surfaces. However, in both of these experimental verifications, plateaus were observed exclusively. The profiles which we presented in this chapter are significantly different. First, our force profiles contain either exclusively Langevin events or Langevin and Plateau events, depending upon temperature and/or co-solute addition. Second, our profiles did not vary in character with rate of retraction of the AFM tip. Finally, we have neutral polymers. Nevertheless, the underlying physics of constant force plateaus is similar: plateaus signify the pulling of a chain monomer-by-monomer from an attractive potential into a zone of zero mean potential. In the Hugel and Châtellier experiments, this potential arises from the electrical double layer. In the experiments that we report here, the potential arises from the local solvency of the chains.

References

[1] Strunz, T.; Oroszlan, K.; Schäfer, R.; H.-J. Güntherodt, H. -J. *Proc. Natl. Acad. Sci. USA* **1999**, *96*, 11277.

[2] Bemis, J. E.; Akhremitchev, B. B.; Walker, G. C. *Langmuir* **1999**, *15*, 2799.

[3] Ortiz, C.; Hadziioannou, G. *Macromolecules* **1999**, *32*, 780.

[4] Marszalek, P. E.; Oberhauser, A. F.; Pang, Y. -P.; Fernandez, J. M. *Nature* **1998**, *396*, 661.

[5] Senden, T. J.; di Meglio, J. -M.; Auroy, P. *Eur. Phys. J. B* **1998**, *3*, 211.

[6] Rief, M.; Oesterhelt, M. F.; Heymann, B.; Gaub, H. E. *Science* **1997**, *275*, 1295.

[7] Bustamante, C.; Marko, J. F.; Siggia, E. D.; Smith, S. *Science* **1994**, *265*, 1599.

[8] Courvoisier, A.; Isel, F.; François, J.; Maaloum, M. *Langmuir* **1998**, *14*, 3727.

[9] Oesterhelt, F.; Rief, M.; Gaub, H. E. *New Journal of Physics* **1999**, *1*, 6.1.

[10] Zhang, W.; Zou, S.; Wang; C.; Zhang, X. *J. Phys. Chem. B* **2000**, *104*, 10258.

[11] Châtellier, X.; Senden, T. J.; Joanny, J. -F.; di Meglio, J. -M. *Europhysics Letters* **1998**, *41*, 303.

[12] Hugel, T.; Grosholz, M.; Clausen-Schaumann, H.; Pfau, A.; Gaub, H. ; Seitz, M. *Macromolecules* **2001**, *34*, 1039.

[13] Oesterhelt, F.; Oesterhelt, D.; Pfeiffer, M.; Engel, A.; Gaub, H. E.; Müller, D. J. *Science* **2000**, *288*, 143.

[14] Carrion-Vazquez, M.; Oberhauser, A. F.; Fowler, S. B.; Marszalek, P. E.; Broedel, S. E.; Clarke J.; Fernandez, J. M. *Proc. Natl. Acad. Sci. USA* **1999**, *96*, 3694.

[15] Rief, M.; Gautel, M.; Oesterhelt, F.; Fernandez, J. M.; Gaub, H. E. *Science* **1997**, *276*, 1109.

[16] Smith, S. B.; Finzi, L.; Bustamante, C. *Science* **1992**, *258*, 1122.

[17] Halperin, A.; Zhulina, E. B. *Europhys. Lett.* **1991**, *15*, 417.

[18] Plateau, J. A. F. *Statique Expérimentale et Théorique des Liquides Soumis aux Seules Forces Moléculaires*; Gauthier-Villars: Paris, 1873; Lord Rayleigh, *Proc. London Math Soc.* **1879**, *10*, 4.

[19] Kreitmeier, S.; Wittkop, M.; Göritz, D. *Phys. Rev. E* **1999**, *59*, 1982.

[20] Maurice, R. G.; Matthai, C. C. *Phys. Rev. E* **1999**, *60*, 3165.

[21] Callen, H. B. *Thermodynamics and an Introduction to Thermostatistics*, 2nd. ed.; John Wilety & Sons: New York, 1985.

[22] Zhou, S.; Fan, S.; Au-yeung, S. C. F.; Wu, C. *Polymer* **1995**, *36*, 1341.

[23] Senden, T. J.; Drummond, C. J. *Colloids Surf. A* **1994**, *87*, 217.

[24] Maeda, N.; Senden, T. J. *Langmuir* **2000**, *16*, 9977.

[25] Schild, H. G. *Prog. Polym. Sci.* **1992**, *17*, 163.

[26] Sheng, S.; Czajkowsky, D. M.; Shao, S. *J. Microscopy* **1999**, *196*, 1.

[27] Albrecht, T. R.; Akamine, S.; Carver, T. E.; Quate, C. F. *J. Vac. Sci. Technol. A* **1990**, *8*, 3386.

[28] Hansma, H. G.; Browne, K. A.; Bezanilla, M.; Bruice, T. C. *Biochemistry* **1994**, *33*, 8436.

[29] Zhang, J.; Pelton, R. *Colloids Surf. A* **1999**, *156*, 111.

[30] Brandrup, J.; Immergut, E. H. *Polymer Handbook*; John Wiley and Sons: New York, 1989.

[31] Braithwaite, G. J. C.; Howe, A.; Luckham, P. F. *Langmuir* **1996**, *12*, 4224.

[32] Braithwaite, G. J. C.; Luckham, P. F. *J. Chem. Soc. , Faraday Trans.* **1997**, *93*, 1409.

[33] Derjaguin, B. V. *Kolloid-Z* **1934**, *69*, 155.

[34] Haupt, B. J.; Ennis, J.; Sevick, E. M. *Langmuir* **1999**, *15*, 3886.

[35] Kreuzer, H. J.; Payne, S. H. *Phys. Rev. E*, preprint.

[36] Johner, A.; Joanny, J. -F. *Macromolecular Theory and Simulations* **1997**, *6*, 479.

Chapter 5

The Detachment of a Polymer Chain from a Weakly Adsorbing Surface using an AFM Tip

5.1 Introduction

The atomic force microscope (AFM) allows one to manipulate single polymer chains and to measure the force required to detach a chain from an adsorbing surface. In many of these studies, the force versus extension profiles obtained exhibit sharp discontinuities which have been interpreted in terms of unadsorbed loops of the chain. A number of different single-chain systems have been studied using AFM and include both synthetic polymers[1–3,5–12,14–17] and biopolymer chains.[4,18–23] Scaling analysis and self-consistent field theory have been used to explain the force profile for pull-off of polyelectrolyte chains.[3,25] The extension of an end-grafted polymer chain in poor solvent conditions has also been studied using scaling analysis for both a neutral polymer chain[26] and a polyelectrolyte chain.[27] The occurrence of plateaus in the force profiles was predicted for neutral polymer chains;[26] while a saw-tooth profile was predicted for the polyelectrolyte chain, which corresponded to the stepwise unfolding of the beads in the necklace structure of the chain.[27] These theoretical treatments focused primarily on large extensions and did not detail the features of loop detachment at shorter extensions, nor did these studies investigate the effect of different rates of extension.

In this chapter we predict force-extension profiles for pulling an isolated polymer from a weakly-adsorbing surface with different rates of pulling or extension. Our theoretical predictions are made using the simplest model: an ideal or Gaussian chain of N statistical monomers of size a (see Chapter 2, Section 2.1.2) where a fraction of the monomers is pinned to the uniformly adsorbing surface with a contact energy $\varepsilon k_B T$. These monomer-surface contacts separate the adsorbed chain into a series

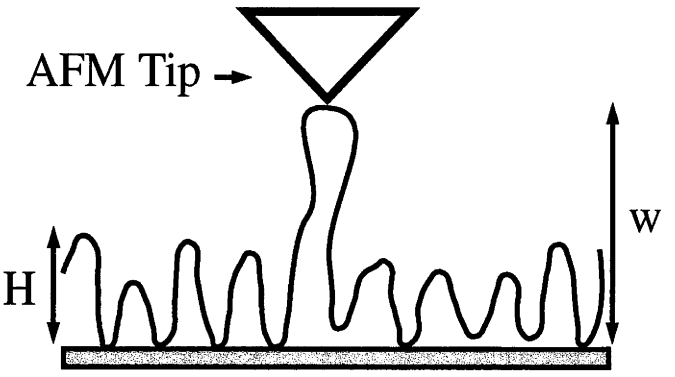

Figure 5.1: Schematic illustration of the "grabbing" and pulling of a loop, referred to as a pulled tether, of a weakly-adsorbed chain on a surface. The pulled tether is extended a distance $w > H$ above the adsorbing surface where H is the equilibrium height of the adsorbed polymer. We consider cases where the pulling rate is very different from the rate of dissociation/association of the surface-monomer contacts.

of loops and tails. We consider "grabbing" a loop or tail and extending this pulled tether a distance w orthogonal to the adsorbing surface as shown in Figure 5.1, while simultaneously measuring the force needed to extend the pulled tether.

In order to rip the chain from the surface, a sequence of surface-pinned monomers must be detached from the surface. Let's first focus upon a single monomer-surface contact and consider the pulled tether as simply a "handle" by which we apply a tension to this surface-bound monomer. An energy path of detachment is $U(z)$ where U is a particular monomer-surface potential energy and z is a distance between monomer and surface. Without specifying an exact form of this potential, we can make general statements using features of the potential such as barrier height, Δ_0, barrier width, δ_0, and well depth, ϵ.[28] First, a surface-bound monomer corresponds to residence in the well or minimum of the potential energy. In order for detachment of occur, the system must overcome the potential barrier, Δ_0, and it does so at a rate $\omega_0 = \omega \exp(-\Delta_0/k_BT)$ where ω is a characteristic frequency. Second, an applied tension, f, on the surface-bound monomer will alter the energy pathway according to $U(z) - fz$, effectively lowering the barrier from Δ_0 to Δ and facilitating detachment of the monomer from the surface. The tension on the surface-bound monomer is the tension of the pulled tether of n statistical monomers and is measured as the force on the AFM cantilever displaced a distance w from the surface.

In an AFM experiment, we control the rate of extension of the tether or $\dot{w}$, measured in units of statistical monomer size, a. Thus, we are applying an increasing tension to the surface-bound monomer according to the prevailing force-law of the pulled tether. We characterise the rate of extension according to the activation kinetics of detachment. A very fast rate of extension is one where the surface-bound monomer has insufficient time to escape the barrier to detachment, even though

the barrier is being continually tension-reduced. In this limit, detachment occurs instantaneously at a large extensional force which reduces the barrier to zero. This yielding force, f_{yield}, is the maximum force sustainable to the monomer-surface contact and no detachment force can exceed this value. On the other hand, a very slow extension provides ample time for the surface-bound monomer to escape the contact without appreciable tension reduction of the barrier. We show that in these two limits the force profiles (i.e. force versus extension curves) are dramatically different. Fast extensions provide a saw-tooth pattern which details each monomer-surface detachment, while the slow extension provides a flat force profile and provides no signature of the detachments. Intermediate extension rates, where detachment occurs with escape over a tension-reduced barrier, provide an interesting combination of these two patterns: a saw-tooth force profile at short extension which diminishes into a characterless force at larger extensions. Our predicted force profiles recover the features of AFM profiles found from different single chain systems.

Our description is organised in the following manner. In the next section we use scaling analysis to describe an equilibrium adsorbed chain and the force required to pull the chain slowly from the surface. In Section 5.3, we consider extension rates which are sufficiently fast that we can probe individual detachments of monomer from the surface, but slow enough that these detachment are activated events, i.e. they proceed with a non-zero, tension-reduced activation barrier. We construct profiles for chains which are homogeneously pinned to the surface, as well as chains which are pinned to the surface with different energies and characterised by the relative rates of monomer-surface detachment and tether pulling. In Section 5.4 we briefly describe the rate-independent force profiles for very fast extension where the detachment is an instantaneous yielding process, rather than an activation process. In conclusion, we summarise and propose extensions to both theoretical and experimental work.

5.2 Slow Extension of a Weakly-Adsorbed Chain

The unadsorbed monomers form a series loops and tails, or an adsorbing layer, of height H. This equilibrium height can be determined from scaling analysis and the chain's free energy,[29]

$$F \cong k_B T \frac{Na^2}{H^2} - \varepsilon k_B T N \frac{a}{H}. \tag{5.1}$$

The first term is the energy penalty associated with the reduction in conformational entropy upon confinement of the chain from solution, where it is of size $R_g \sim aN^{\frac{1}{2}}$, to an adsorbed layer of average height H. The second term represents the favourable

contact energy resulting from Na/H monomer-surface contacts. The equilibrium height of the adsorbed, ideal chain is that which minimises the chain energy and is $H \cong 2(a/\varepsilon)$ and is independent of (large) chain length. As the surface energy decreases, there are fewer monomer-surface contacts, larger loops and trains, and the adsorbed height increases. A lower limit of attractive surface energy for chain adsorption requires that $H < R_g \sim aN^{1/2}$, or $\varepsilon > N^{-1/2}$.

When the extension of a pulled tether occurs at a sufficiently slow rate such that the monomer-surface contacts can detach and reform many times over the timescale of the pulling experiment, the force measured provides only averaged information about the strength of the surface-monomer contacts and not about the detachment process itself. In terms of each monomer-surface contact, the rate of application of tension is so slow that the monomer is able to escape the natural barrier, Δ_0, without the aid of the barrier-reducing tension. In this case, contacts can be lost and reformed many times over an incremental increase in extension or applied force and the chain/surface can be described wholly in equilibrium terms using scaling analysis. The free energy (in units of k_BT) of an adsorbed chain with a tether of n monomers, extended a distance w from the adsorbing surface is

$$F(n) \cong \frac{(N-n)a^2}{H^2} - \varepsilon(N-n)(\frac{a}{H}) + \frac{w^2}{na^2} \tag{5.2}$$

where the last term is the stretching penalty associated with extending a Gaussian loop of n monomers to distance w where the height of the absorbed train is independent of the pulled loop and remains $H \sim 2a/\varepsilon$. The rapid reformation of monomer-surface contacts effectively exchanges monomers across contact or adsorption points and the number of monomers in the extended loop, n, may increase to reduce the stretching penalty of the extended loop. Minimisation of the energy yields $F \cong \varepsilon(w/a) - N\varepsilon^2/4$ and an extensional force, $f_{slow} = \partial F/\partial w \sim \varepsilon k_BT/a$, which is constant throughout the slow pulling process. Thus for very slow extension of the tether, the force will be constant, much like pulling a chain through a viscous medium, and will not signature loss of individual monomer-surface contacts.

5.3 Intermediate Extension Rates of a Weakly-Adsorbed Chain

At higher rates of extensions, the system does not have ample time to trespass over the full detachment barrier. Detachment occurs as an "escape" over a tension-reduced barrier of height $\Delta(f)$, expressed generally to first order in tension as

$$\Delta(f) \approx \Delta_0 - \delta_0 f + O(f^2). \tag{5.3}$$

Each monomer detachment is a stochastic event that occurs after an averaged time, t, determined from

$$1 = \int_0^t dt\omega_0 \exp \frac{\delta_0 f(t)}{k_B T}. \tag{5.4}$$

For a Gaussian tether of n monomers, the force varies with extension, w, according to a simple linear force law, $f/k_BT = w/(na^2)$. The average extension at which the monomer-surface contact is lost is

$$(\frac{w}{a})^{det} = n(\frac{a}{\delta_0}) \ln[\frac{\dot{w}/a}{\omega_0}\frac{1}{n}(\frac{\delta_0}{a}) + 1]. \tag{5.5}$$

and the average detachment force is

$$\frac{f^{det}}{k_BT} = (\frac{1}{\delta_0}) \ln[\frac{\dot{w}/a}{\omega_0}\frac{1}{n}(\frac{\delta_0}{a}) + 1]. \tag{5.6}$$

Upon detachment, the m monomers in the loop adjacent to the contact are added to the n monomers in the pulled tether and the force discontinuously decreases to

$$\frac{f}{k_BT} = \frac{(w/a)^{det}}{(m+n)a}. \tag{5.7}$$

These expressions are valid for detachment forces between the equilibrium force needed to slowly detach the chain and the maximum force at which the barrier to detachment completely disappears, i.e. $f_{slow} < f^{det} < f_{yield}$.

5.3.1 Multiple detachments from a homogeneous surface

We can generalise this description to the pulling-off of a chain adsorbed with multiple monomer-surface contacts. For simplicity, we assume that the chain is initially adsorbed onto the surface with contact points evenly spaced along the chain contour providing loops of fixed number of monomers n. We can assume n is simply the average loop size of the adsorbed chain: The average number of monomers per loop of an adsorbed chain of N monomers with Na/H surface contacts is $n = H/a \cong 2/\varepsilon$. Let k be an index which advances by one with each surface-monomer contact which is lost. Initially, $k = 1$, and the extension and force at the first detachment is given by eqs 5.5 and 5.6. For subsequent detachments, $k \geq 2$, the extension, $(w/a)_k^{det}$, is found from eq 5.4 and $w/a = (w/a)_{k-1}^{det} + \dot{w}t/a$, to be

$$(\frac{w}{a})_k^{det} = kn(\frac{a}{\delta_0}) \ln[\frac{y}{kna} + a_{k-1}] \tag{5.8}$$

with

$$a_k = (\frac{y}{kna} + a_{k-1})^{\frac{k}{k+1}} \tag{5.9}$$

and $a_0 = 1$. We have introduced in the above equation the dimensionless parameter $y \equiv \frac{\dot{w}/a}{\omega_0}(\frac{\delta_0}{a})$. The ratio of barrier width to monomer size, $(\frac{\delta_0}{a})$, is constant and of order unity; consequently, y is the rate of extension relative to that of the detachment kinetics. Values of y range from zero, indicative of very slow pulling, to large positive numbers which indicate fast extension rates. Using eqs 5.8,5.9 and the assumption of Gaussian chains, we find the detachment force from

$$\frac{f_k^{det}}{k_B T} = \frac{(w/a)_k}{kna}. \tag{5.10}$$

After detachment this force is reduced discontinuously by a factor of $k/(k+1)$. Again, these expression are valid for pulling forces between f_{slow} and f_{yield}. These correspond to bounds on the dimensionless pulling rates of $\exp(\varepsilon/k_B T) - 1 < y/n < \exp(\Delta_0/k_B T)$.

Figure 5.2 is the predicted force profile constructed from eqs 5.8-5.10 for the pull-off of a chain of equi-sized loops where the rate of pulling is $y/n = 100$ and $\delta_0/a \equiv 1$. It is important to recognise that this profile is constructed from a sequence of detachment events, each detachment being described in terms of its average or expected lifetime. An experimental force profile, in contrast, is comprised of stochastic detachment events: as such it would retain the discontinuous forces but the magnitude of both force and extension at detachment will vary from the averaged values of our predictions. Figure 5.2 shows that the average detachment force decreases with successive loss of monomer-surface contacts, or $f_k^{det} > f_{k+1}^{det}$. This general decrease in consecutive detachment forces becomes more pronounced at higher pulling speeds. The spring constant, or slope (df/dw) between detachments, diminishes discontinuously with the loss of adjacent contacts due to the increase in the number of monomers in the pulled tether. This decrease in spring constant is most dramatic with the loss of the first few surface contacts with the force attaining a constant-value plateau at large extension of the pulled tether. Clearly, our simplistic assumption of a Gaussian pulled tether can be replaced by an inextensible Langevin tether, or other non-linear spring model. This would result in replacement of the linear force profiles between detachment points with a pulling force which grows more strongly with extension and an increase in the detachment force, according to eq 5.4. Irrespective of the particular model, the tether becomes increasingly compliant with the increase in the number of monomers in the tether that occurs with each lost contact and the detachment force is discontinuous. Our predictions, constructed from averaged detachment events and pulled tethers which are Gaussian, nevertheless capture features of experimentally obtained force profiles. Some of the published work on single molecule force microscopy[1,4,7,16] have found that the spring constant decreases with consecutive discontinuities and that the maximum forces in

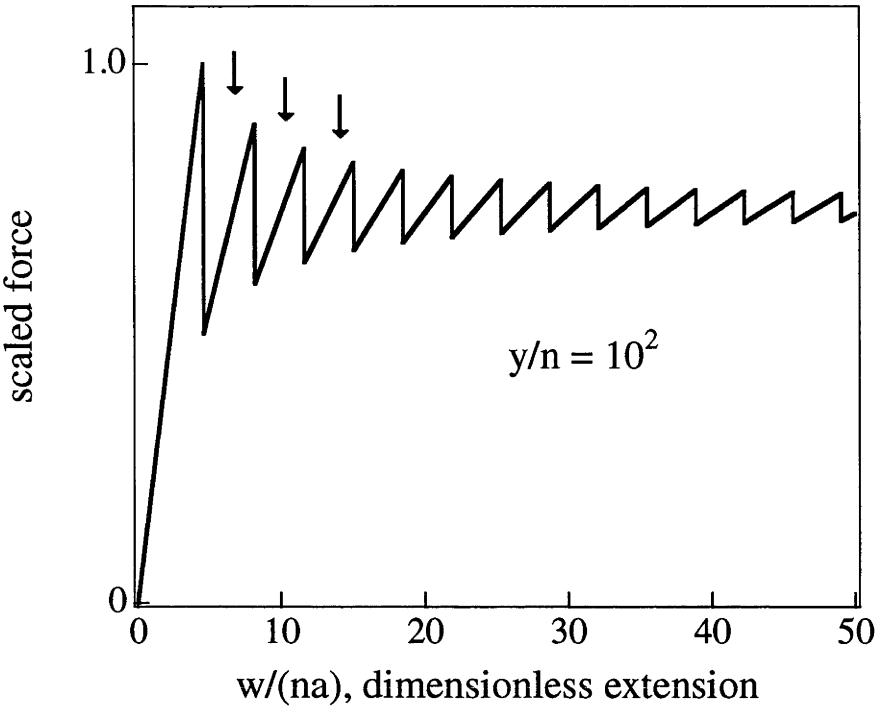

Figure 5.2: Scaled force, $f/f_{k=1}^{det}$, versus dimensionless extension, $w/(na)$, for the detachment of an adsorbed chain with equi-sized loops of n monomers with dimensionless pulling rate of $y/n = 100$. The discontinuities in the profile correspond to detachment of individual contact points which separate the pulled tether from an adjacent loop and the maximum forces in each saw-tooth correspond to the detachment force, f_k^{det}. These contact points are lost or sacrificed according to an activated process with a tension-reduced barrier. The force required for detachment decreases with loss of successive contact points; i.e. pulling becomes easier with the removal of each contact point. Between the detachment of contact points, the force is linear with extension reflecting the Gaussian approximation. The slope of spring constant , df/dw, is inversely proportional to the number of monomers in the pulled tether and this diminishes with loss of successive contact points.

the saw-tooth profiles diminish with extension resulting in a force which is constant over larger extension.

Figure 5.3 shows the effect of extension rate upon the average force profile for a chain of equi-sized loops. With increased rate of extension, the detachment forces increase from $f_{slow} = \varepsilon k_B T/a$, the equilibrium value, to f_{yield}, which we have arbitrarily chosen to be larger than the forces at these extension rates. Moreover, each k^{th} detachment occurs at larger extensions when the rate of pulling is increased.

Some experiments show that the detachment forces may sometimes increase with extension rather than decrease[1,2,13,18,20,22] as shown in our predictions of equi-sized loops. In some instances both decreases and increases in the detachment forces have been observed.[1,4,6,8–10,12–15,17,19,20,22–24] This could be attributed to the stochastic nature of the detachment event or to the likelihood of loops with different sizes.

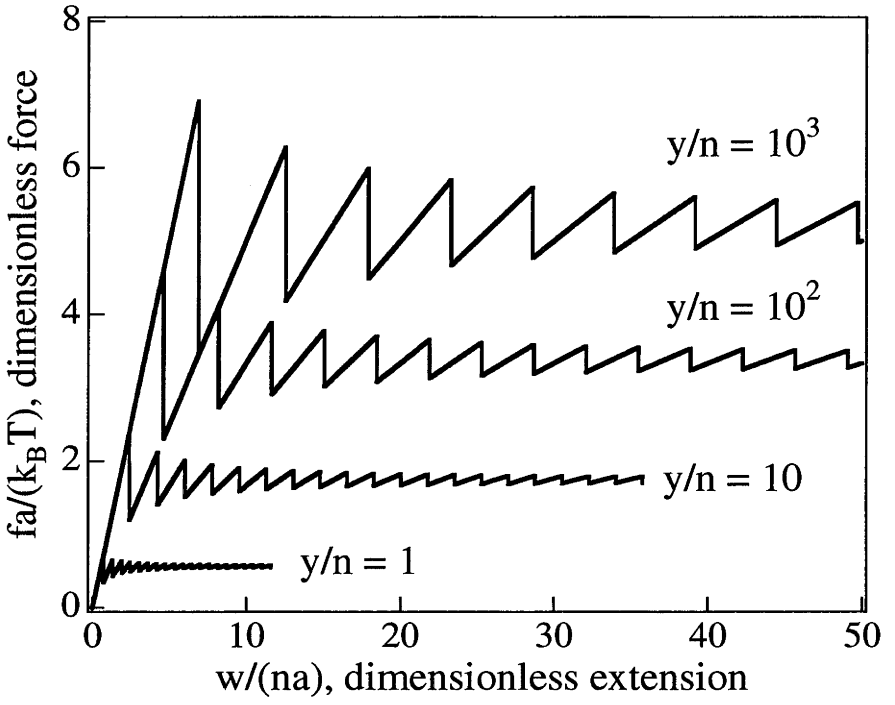

Figure 5.3: Dimensionless force, $fa/(k_BT)$, versus dimensionless extension, $w/(na)$, for the detachment of an adsorbed chain with equi-sized loops of n monomers with dimensionless pulling rates $y/n = 1, 10, 10^2$ Note that as the pulling rate increases, the force increases and larger extensions are required to detach each monomer-surface contact. Moreover, with larger pulling rates, the consecutive detachment forces decrease with each contact lost. The pulling rates are not sufficiently large that tension on the contact reaches the yielding force, f_{yield}.

Experimentally, it would be difficult to distinguish whether the size and breadth of a "tooth" is attributable to loop size or to the stochastic nature of the detachment. We can envision an experiment where the adsorbed chain is comprised of surface "sticky" monomers at known intervals. In this case, an ensemble of AFM force profiles for "ripping-off" of the chain might be used to discriminate loop size in the stochastic, irreversible process. On the computational side, one might construct a stochastic simulation that mimics the stochastic barrier escape to detachment. In this work, we are limited to predicting individual detachment events as averaged events. However, we can show that our description, cast for loops of different sizes, predicts discontinuous forces at detachments and that these detachment forces both increase and decrease with successive detachments, Figure 5.4.

5.4 Fast extension of an adsorbed chain

Consider now pulling rates that are very large such that the tension applied to the monomer-surface contact reduces the barrier height, Δ, to zero. This force

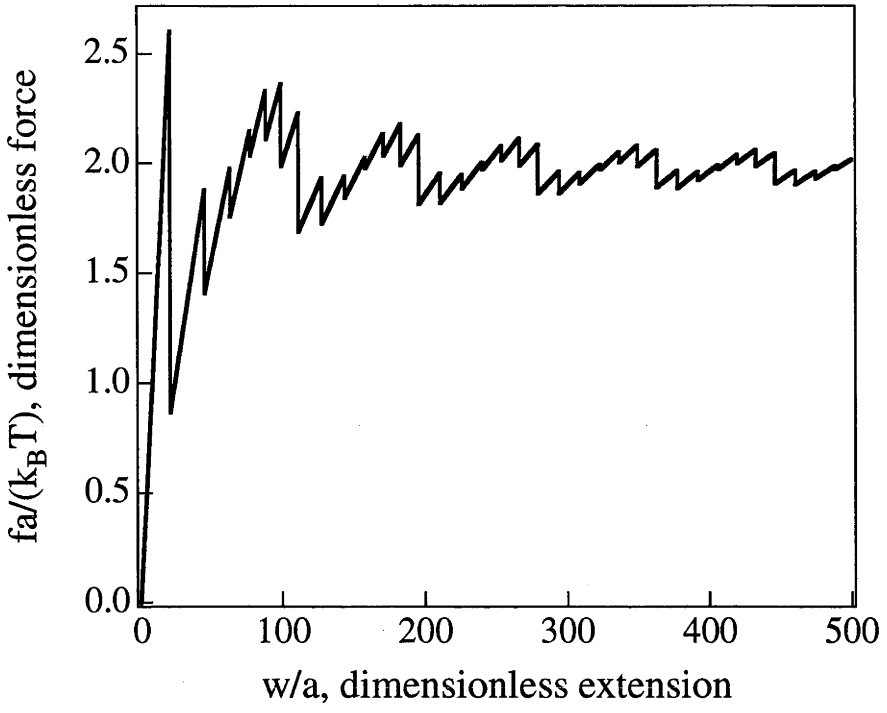

Figure 5.4: Dimensionless force, $fa/(k_BT)$, versus dimensionless extension, w/a, for the detachment of a chain having unequal loops sizes with a dimensionless pulling rate of $y = 100$. We have ordered the loop sizes in the following way. The first loop has 2 monomers and each consecutive loop size is double that of the previous loop until the loop size is 32. Loops following a $n = 32$ loop are 1/2 the size of the previous loop until the loop size reaches 2. The loop sizes thus both increase and decrease according to $m(k) = r * m(k-1)$ where $m(k)$ is the number of monomers in the k^{th} loop and $r = 2$ and 1/2. As a result of this geometric series of loop sizes, the detachment forces of consecutive monomer-surface contacts both increase and decrease in accord with the size of the tether, $\sum_{k=1}^{K} m(k)$, relative to the adjacent loop, $m(K+1)$. Detail in the force profile is more apparent at small extensions when the spring constant, df/dw, and detachment forces are large. However, at larger extension, both spring constant and detachment force diminish and may become indiscernible from experimental noise.

is called the yielding force and, from eq 5.3, is $f_{yield} \approx \Delta_0/\delta_0$. At this tension, detachment is no longer an activated event and occurs instantaneously at f_{yield} which is determined by the exact monomer-surface potential. No force greater than f_{yield} can be maintained by an individual monomer-surface contact.

For a homogeneously adsorbed chain of equi-sized loops of n monomers, fast extension will lead to detachments where the first K detachments occur as barrier-less, instantaneous events at force f_{yield}. The $k > K$ detachments occur with a tension-reduced activation barrier. As the rate of extension is increased, K increases, until all contacts are lost instantaneously at f_{yield}. These $k \leq K$ barrier-less detachments are still marked by discontinuities in the force profile. The barrier-less detachments

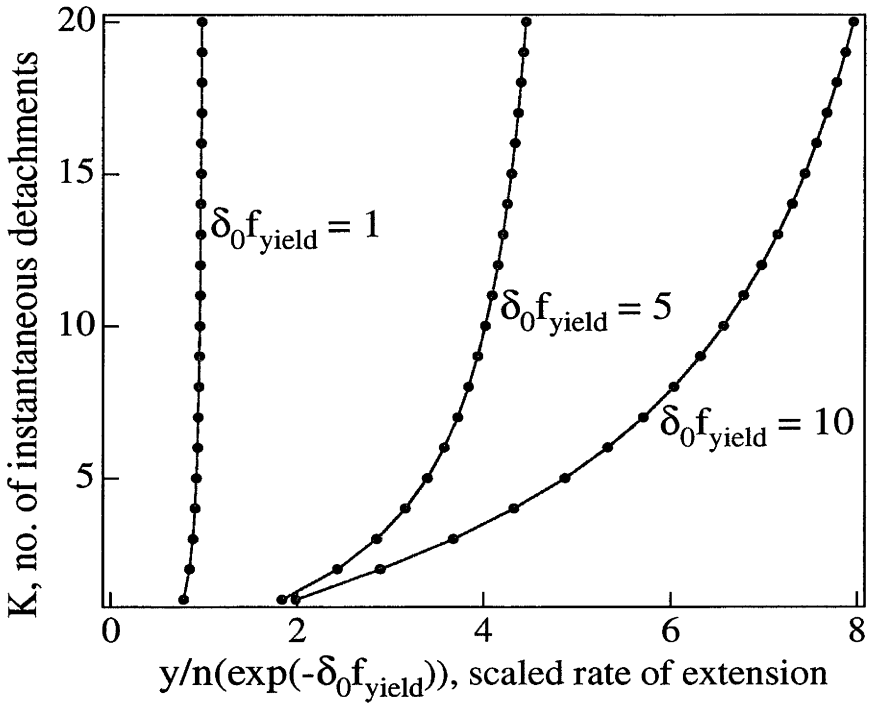

Figure 5.5: The number of instantaneous detachments, K, versus the scaled extension rate, $y/n(\exp(-\delta_0 f_{yield}))$, for surfaces with yielding forces $\delta_0 f_{yield}$ =1, 5, and 10. At any given extension rate and yielding force, the first K detachments occur instantaneously at an applied force equal to f_{yield} while subsequent detachments occur as activated events with detachment forces less than f_{yield}. For any given surface, as the extension rate is increased, a larger number of detachments occur instantaneously at f_{yield}.

occur at extension

$$(\frac{w}{a})^{det}_{k\leq K} = kna(\frac{F_{yield}}{k_B T}) \tag{5.11}$$

and successive, activated detachments ($k > K$) at

$$(\frac{w}{a})^{det}_{k} = kn(\frac{a}{\delta_0})\ln[\frac{y}{kn} + \exp[\frac{\delta_0}{a}\frac{1}{kn}(\frac{w}{a})^{det}_{k-1}]] \tag{5.12}$$

with $f^{det}_{k>K} < f_{yield}$ and given by the force-law, eq 5.10. As the extension rate is increased further, detachments of higher order, i.e. larger K, along with the earlier detachments $k < K$, will occur instantaneously at $f^{det}_{k\leq K} = f_{yield}$. Thus, with fast extension, the force profile is independent of extension rate at low extensions. As the extension rate increases, this range of rate-independent extension grows, as shown in Figure 5.5.

5.5 Conclusion

Using a simple ideal chain model, we have used scaling analysis and activation kinetics to predict force profiles for the detachment of chains from adsorbing surfaces by pulling a loose tether from the surface. Although we do not include detail such as finite extensibility or monomer-monomer interactions, we are able to reconstruct much of the character of experimental AFM force-profiles. Our analysis considers cases where the timescale of equilibration of the monomer-surface contacts is both shorter and longer than the timescale of the pulling experiment. When the extension rate is slow, the monomer-surface contact has ample time to exchange monomers between the pulled tether and adjacent loop and the force is constant as the chain is being ripped slowly from the surface. However, if the extension rate is made faster and commensurate with the kinetic rate of detachment, then the magnitude of the pulling force details individual detachments of monomers from the surface. We have shown that the force profile will be discontinuous marking an individual detachment and that, on average, the magnitude of the detachment force decreases with successive detachments. As the extension rate is increased, the magnitude of the detachment force increases and larger extensions are required for detachment. At very large extension rates, the applied force is sufficiently large to reduce the barrier to detachment to zero and the detachment occurs instantaneously at a yielding force, f_{yield}, which characterises the monomer-surface contact. At these large extension rates the force profile is "saw-tooth" shaped with detachment forces that are equal for successive detachment events and independent of extension rate.

Our results suggest additional experiments where the extension rate of the chain, or probe tip velocity, is varied and the chain is comprised of surface "sticky" monomers spaced at known intervals along the chain backbone, or the adsorbing surface is atomistically patterned. Stochastic simulations are required to construct predictions which are comparable with individual AFM force profiles. Detail such as monomer-monomer interactions, solvency, and inextensibility would be appropriately included in these stochastic simulations. However, in this chapter, our predictions are limited to average detachment events; that is, we construct force profiles as a sequence of detachment events whose lifetime is averaged. Despite our simplistic assumption of Gaussian chains we are able to predict general trends seen in AFM experiments.

5.5.1 Work Since Publication

Since this work has been published, it has been cited by a number of authors.[11,14,30–33] Sano et al.[33] cited this work in order to relate features in force curves in an AFM experiment to the extension of a polymer chain. Al-Maawali et al.[11] used our work to explain experimental data, more specifically that when the

rate of extension is slow compared to the rate of monomer-surface contact reformation, one can expect a constant force with extension. Hugel et al.[14] also cites our work and uses it to explain experimental results: specifically plateau events observed for the detachment of physisorbed polyelectrolytes from a surface. Ennis et al.[30] cites this work as significant work in relation to physics of manipulating single polymer chains. Lubensky[32] have stated their work as being an extension of ours, relating theoretically the unzipping of DNA to the detachment of a heteropolymer from an adsorbing surface in that the number of basepairs broken or monomer/surface contacts lost was dependent on the force applied. Jimenez et al.[31] have also extended this work by using scaling analysis to look at the good solvent case for the detachment of a single polymer chain. They determined the equilibrium force to be $f/k_BT \sim -\varepsilon^{3/2}/a$ for detaching a chain and did not investigate non-equilibrium behaviour.

References

[1] Senden, T. J.; Di Meglio, J. -M.; Auroy, P. *European Physical Journal B* **1998**, *3*, 211.

[2] Kikuchi, H.; Yokoyama, N.; Kajiyama, T. *Chemistry Letters* **1997**, *11*, 1107.

[3] Châtellier, X.; Senden, T. J.; Joanny, J. -F.; di Meglio, J. -M. *Europhys. Lett.* **1998**, *41*, 303.

[4] Rief, M.; Oersterhelt, F.; Heymann, B.; Gaub, H. E. *Science* **1997**, *275*, 1295.

[5] She, H.; Malotky, D.; Chaudhury, M. K. *Langmuir* **1998**, *14*, 3090.

[6] Courvoisier, A.; Isel, F.; François, J.; Maaloum, M. *Langmuir* **1998**, *14*, 3727.

[7] Maaloum, M.; Courvoisier, A. *Macromolecules* **1999**, *32*, 4989.

[8] Li, H.; Liu, B.; Zhang, X.; Gao, C.; Shen, J.; Zou, G. *Langmuir* **1999**, *15*, 2120.

[9] Li, H.; Zhang, W.; Xu, W.; Zhang, X. *Macromolecules* **2000**, *33*, 465.

[10] Bemis, J. E.; Akhremitchev, B. B.; Walker, G. C. *Langmuir* **1999**, *15*, 2799.

[11] Al-Maawali, S.; Bemis, J. E.; Akhremitchev, B. B.; Leecharoen, R.; Janesko, B. G.; Walker, G. C. *J. Phys. Chem.* **2001**, *105*, 3965.

[12] Ortiz, C.; Hadziioannou, G. *Macromolecules* **1999**, *32*, 780.

[13] Garnier, L.; Gauthier-Manuel, B.; van der Vegte, E. W.; Snijders, J.; Hadzioannou, G. *Journal of Chemical Physics* **2000**, *113*, 2497.

[14] Hugel, T.; Grosholz, M.; Clausen-Schaumann, H.; Pfau, A.; Gaub, H.; Seitz, M. *Macromolecules* **2001**, *34*, 1039.

[15] Zhang, W.; Zou, S.; Wang, C.; Zhang, X. *J. Phys. Chem. B* **2000**, *104*, 10258.

[16] Oesterhelt, F.; Rief, M.; Gaub, H. E. *New Journal of Physics* **1999**, *1*, 6.1.

[17] Yamamoto, S.; Tsujii, Y.; Fukuda, T. *Macromolecules* **2000**, *33*, 5995.

[18] Strunz, T.; Oroszlan, K.; Schäfer, R.; Güntherodt, H. -J. *Proc. Natl. Acad. Sci. USA* **1999**, *96*, 11277.

[19] Li, H.; Rief, M.; Oesterhelt, F.; Gaub, H. E. *Advanced Materials* **1998**, *3*, 316.

[20] Rief, M.; Gautel, M.; Oesterhelt, F.; Fernandez, J. M.; Gaub, H.E. *Science* **1997**, *276*, 1109.

[21] Marszalek, P. E.; Oberhauser, A. F.; Pang Y. -P.; Fernandez, J. M. *Nature* **1998**, *396*, 661.

[22] Carrion-Vazquez, M.; Oberhauser, A. F.; Fowler, S. B.; Marszalek, P. E.; Broedel, S. E.; Clarke, J.; Fernandez, J. M. *Proc. Natl. Acad. Sci. USA* **1999**, *96*, 3694.

[23] Oesterhelt, F.; Oesterhelt, D.; Pfeiffer, M.; Engel, A.; Gaub, H. E.; Müller, D. J. *Science* **2000**, *288*, 143.

[24] Haupt, B. J.; Senden, T. J.; Sevick, E. M. *submitted to Langmuir*, 2001.

[25] Châtellier, X.; Joanny, J. -F. *Physical Review E* **1998**, *57*, 6923.

[26] Zhulina, E.; Walker, G. C.; Balazs, A. C. *Langmuir* **1998**, *14*, 4615.

[27] Tamashiro, M. N.; Schiessel, H. *Macromolecules* **2000**, *33*, 5263.

[28] We have not included potential-dependent results in this chapter as our aims are to point out generalised predictions that may be seen experimentally on a number of systems. However, one can simply follow out generalised treatment, extending to higher orders in force if needed, by adopting a specific surface-monomer potential energy function, $U(z)$. Alternatively, one might adopt a simple generalised form, for example, a simple cubic potential of the form $U(z) = A(z - z_0)^3 + B(z - z_0)^2$ with $A < 0$ and $B > 0$.

[29] de Gennes, P. -G. *Scaling Concepts in Polymer Physics*; Cornell University Press: Ithaca, 1979.

[30] Ennis, J.; Sevick, E. M.; Williams, D. R. M. *Physical Review E* **1999**, *60*, 6906.

[31] Jimenez, J.; de Joannis, J.; Bitsanis, I.; Rajagopalan, R. *Macromolecules* **2000**, *33*, 7157.

[32] Lubensky, D. K.; Nelson, D. R. *Physical Review Letters* **2000**, *85*, 1572.

[33] Sano, M.; Okamura, J.; Kanekiyo, Y.; Shinkai, S. *Colloids and Surfaces A* **2000**, *169*, 131.

Chapter 6

The effect of rates on the force profiles for ripping-off a single polymer chain from a surface: A Langevin Simulation Study

6.1 Introduction

Computer simulations complement both theoretical and experimental approaches to studying the behaviour of single polymer chains. This technique is useful in determining properties which may not be able to be probed with current experimental techniques and also in predicting behaviour for experiments not yet conducted. Unlike analytical theory, simulation uses brute force methods to find a solution by performing a large number of calculations and these are often used to verify predictions made by theory.

Simulation has been used to study both the static and dynamic properties of a single polymer chain under tension. Titantah et al[1] used Monte Carlo simulations to investigate the elastic behaviour of a polymer chain in the various force regimes at and above the theta temperature. Nonequilibrium dynamics and static properties of a stretched chain were studied by Sheng et al.[2] The effect of varying the temperature and thus the solvent quality while extending a polymer chain has been studied using Monte Carlo and Langevin simulation.[3–5] These studies found the existence of the ball-string configuration when stretching a polymer chain in poor solvent, and confirmed the predicted behaviour of a chain in good and theta solvents.

This chapter follows on from the previous one and involves the investigation of the dynamics of detaching a single polymer chain from an adsorbing surface. We use Langevin simulation to examine the detachment of the chain and determine its

corresponding force profile, as well as the effect of varying the strength of the surface/monomer interaction, the temperature of the system and the rate of retraction of the AFM tip. Unlike our previous chapters, this work is not yet complete and will be the subject of further research. Consequently, we will only show examples of the possible measures with simulation and, where possible, contrast these results with those of theory and/or experiment. This chapter will proceed as follows, the following section describes the model used for our simulations. The next section details the initialisation and equilibration studies. Section 6.4 presents results from our pulling experiments, where the rate of extension of the tip is constant and Section 6.5 examines the effect of applying a constant force to the end the chain. Lastly, Section 6.6 summarises our conclusions.

6.2 Model for Simulation

We constructed a Langevin simulations of a bead-spring model of a polymer chain consisting of a series of N beads that are connected by $N-1$ springs in three-dimensional space. The Langevin equation, as discussed in Chapter 2, Section 2.3.2, is

$$x(t+\triangle t) = x(t) - \frac{1}{\zeta}\frac{\partial U}{\partial x}\triangle t + G(t) \tag{6.1}$$

where x is the displacement of the beads, t is the time, ζ is the friction constant, U is potential between the beads and the probability distribution function, $G(t)$, has a mean and variance of

$$< G(t) >= 0, < G(t)G(t') >= 2D\delta_{tt'}\triangle t \tag{6.2}$$

where D is the diffusion coefficient and is $D = k_B T_n/\eta$, where $k_B T_n$ is the thermal energy contributing to thermal fluctuations in the random noise term $G(t)$. The interactions between bonded monomers are described by the Finitely Extensible Non-linear Elastic or FENE potential, U_{FENE}, used by Binder et al.,[6–10] with the spring force obtained by differentiating the potential with respect to the bond length, l,

$$f_{spring} = \frac{dU_{FENE}}{dl} = \frac{2 \times K(l-l_o)}{[1-\left(\frac{(l-l_o)}{(l_{max}-l_o)}\right)^2]} \tag{6.3}$$

l corresponds to the length of the spring between two monomers, K is a spring constant, l_0 is the bond length corresponding to the minimum of the potential and l_{max} is the maximum bond length limit. The spring force dictates the length of the bond and is Hookean near l_0. It deviates from this behaviour and approaches infinity as $l \to l_{max}$ and $l \to l_{min} = 2l_0 - l_{max}$, where l_{min} is the minimum bond length limit. In other words, the spring becomes infinitely stiff for bond lengths much smaller or

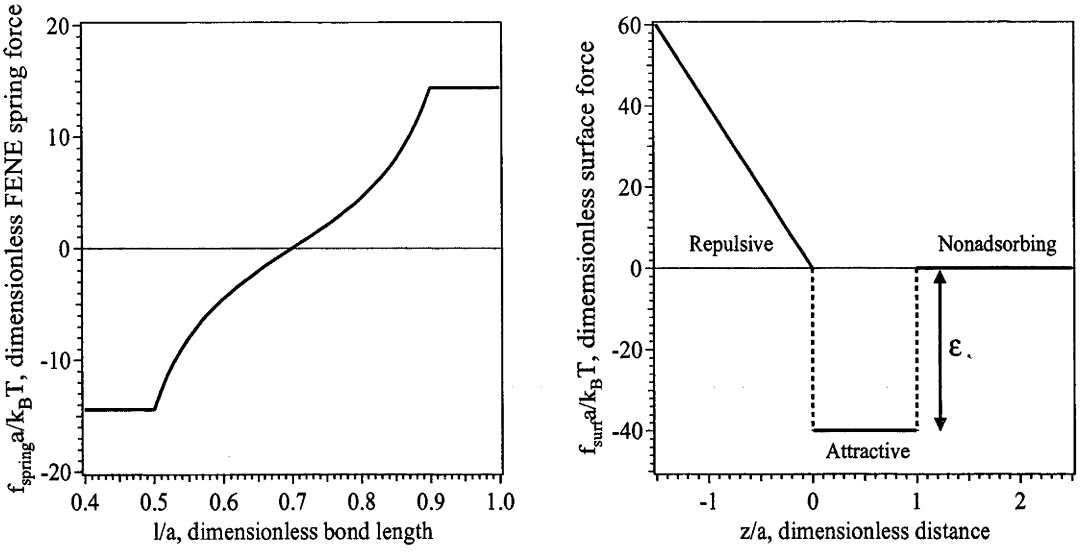

(a) (b)

Figure 6.1: (a) The FENE spring force, $f_{spring}a/k_BT$, (dimensionless units) versus the monomer-monomer bond length, l/a (dimensionless units). The minimum spring force occurs at $l = 0.7$; the maximum force is truncated at $l \leq 0.5$ and $l \geq 0.9$. (b) The surface force, $f_{surf}a/k_BT$, (dimensionless units) versus the z-distance, z/a (dimensionless units) for a monomer above the surface. The surface force is strongly repulsive for $z \leq 0.0$, attractive for $0.0 < z < 1.0$ and nonadsorbing for $z \geq 1.0$.

much larger then l_0. Optimal values for the force parameters have been previously determined Binder and are

$$l_{min} = 0.4; \quad l_{max} = 1.0; \quad l_o = 0.7; \quad K/k_BT = 20.0 \tag{6.4}$$

where k_BT is the thermal energy contributing to the FENE spring force. The value chosen for the spring constant ensures that the spring is stiff so that the limits of the effective bond length are rarely ever met. If the bond length is $l \leq 0.5$, then we set the bond length to $l = 0.5$ and similarly if $l \geq 0.9$, the bond length is set to $l = 0.9$ (see Figure 6.1(a)). This is to avoid extremely large spring forces which would result as the bond length approaches the limits. The model used to describe a polymer chain recovers a Gaussian chain when $k_BT = 0.62$, this model's θ temperature. In our simulations $k_BT = 1.0$, hence we have good solvent conditions.

The surface force, f_{surf}, is the force that results from the interaction of each statistical bead with the surface. We assume that the attractive surface force is short ranged and the repulsive force allows for slight surface penetration, mimicking

surface roughness. The surface force can then be described as,

$$f_{surf} = \begin{cases} 0 & \text{for } z \geq 1.0, \\ -\varepsilon & \text{for } 0.0 < z < 1.0, \\ -40 \times z & \text{for } z \leq 0.0. \end{cases} \tag{6.5}$$

where ε is the depth of the attractive well. Figure 6.1(b) depicts graphically the force applied to an individual monomer at varying distances from the surface with $\varepsilon = 40.0$. In our simulations we have used a range of ε values (*i.e.*, depth of the attractive well) for the attractive surface force, with $\varepsilon = 40.0, 30.0, 20.0, 10.0, 1.0, 0.1$ and 0.01, for polymer chains of length $N(50 \geq N \geq 200)$. Note that one end of the chain is end-tethered to the surface, therefore no surface force is applied to it as it does not move during the course of the simulation.

6.3 Initialisation and Equilibration

In our simulations of single polymer chains, we first must generate the initial configuration of the chain prior to running our pulling "experiments". This is achieved by first generating a structure of an end-tethered chain in close proximity to the adsorbing surface and then allowing it to relax with time in order to equilibrate the chain. Whether the chain has equilibrated or not is determined by calculating its radius of gyration (see Chapter 2, Section 2.3.3) over time. The chain is considered to have equilibrated when these values fluctuate closely around a time averaged mean value. Also, in the initialisation of the chains we are able to find the height of the adsorbed chain and can show its dependence on the surface attraction, ε, and size of the chain, N. Despite definitive evidence of equilibration of the larger chains, these adsorbed chain height agree with the predicted scaling analysis (see Chapter 5, Section 5.2) appropriate to equilibrium chains.

The initial coordinates of the polymer chains were not arbitrarily chosen for our simulations. Instead, we use a toy model to obtain an initial configuration of the chain with one end of the chain end tethered to the surface and with all bond lengths between the monomers set to $l = 0.7$. We chose this value for the bond length based on the FENE spring force equation (see Section 6.2). The coordinates of the chain were then generated by starting at the end tethered monomer and forming surface-bound loops one bond length high and one across in the x-direction, Figure 6.2. This formed the initial configuration of the chain where all monomers were in the attractive region near the surface.

From this initial configuration, the polymer chains were equilibrated over time and the average squared radius of gyration was used to determine whether the chain had equilibrated *i.e.*, that the $< R_g^2 >$ had settled to a constant value in time (see

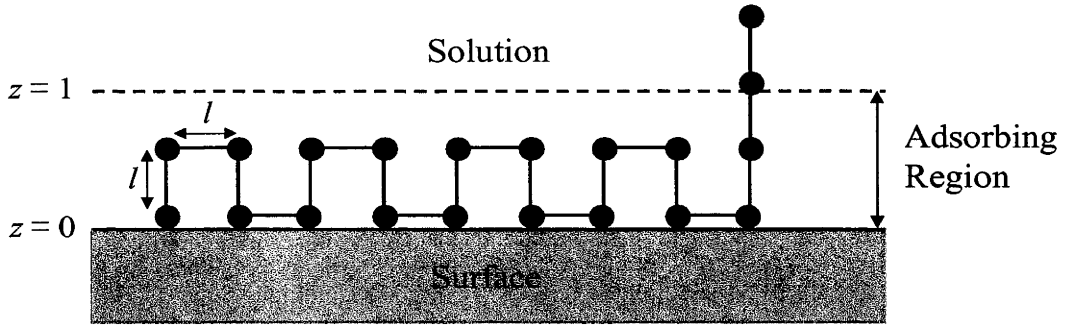

Figure 6.2: The initial configuration of a chain of length $N = 20$ in the z-x plane. All monomer-monomer bond lengths are set to $l = 0.7$, where all but two monomers are within the absorbing region, $0.0 \leq z \leq 1.0$, close to the surface.

Chapter 2, Section 2.3.3). This was determined by first calculating the accumulated average, $< \overline{R_g^2} >_{ac}$,

$$< \overline{R_g^2} >_{ac} = \frac{\sum_{i=1}^{N_t} < R_g^2 >_i}{N_t} \tag{6.6}$$

where N_t is the total number of data points at time, t; and the time interval average, $(< \overline{R_g^2} >_{ti})$,

$$< \overline{R_g^2} >_{ti} = \frac{\sum_{i=t}^{N_{ti}} < R_g^2 >_i}{N_{ti}} \tag{6.7}$$

where N_{ti} is the number of data points in a given time interval, ti. The standard deviation of the time interval average of $< R_g^2 >$ ($\sigma = \frac{\sum_{i=t}^{N_{ti}} < R_g^2 >_i}{N_{ti}}$) was also calculated. The polymer chain was said to have reached equilibrium if the values of $< \overline{R_g^2} >_{ac}$ and $< \overline{R_g^2} >_{ti}$ had converged. The time-step, $\triangle t$, used in these equilibration studies was $\triangle t = 10^{-2} \mu s$ and the time interval over which $< R_g^2 >$ was averaged was 4×10^5 timesteps. The thermal energy, $k_B T_n$, contributing to the random noise in these Langevin simulations was set to $k_B T_n = 0.1$.

For polymer chains of size $N = 50$ and for all the values of ε studied, the chain was allowed to equilibrate for 4×10^6 timesteps. This was repeated for a total of 10 different simulations for a given surface force, each with a different initial random number. Figure 6.3 plots the radius of gyration squared, $< R_g >^2$, versus the number of timesteps and is an example of a single simulation run for a polymer chain of length $N = 50$ with $\varepsilon = 40.0$. It contrasts the raw data with $< \overline{R_g^2} >_{ac}$ and $< \overline{R_g^2} >_{ti}$. Figure 6.3 clearly shows that the different averages quickly converge and that the chain has equilibrated. The final values of $< \overline{R_g^2} >_{ac}$ and $< \overline{R_g^2} >_{ti}$ for all simulations for $N = 50$ are listed in Table 6.1. As there is little difference between the two different averages for all simulations run, we can therefore conclude that simulations of length 4×10^6 timesteps is sufficient to equilibrate chain of length $N = 50$. The final configuration for each simulation was then used as the initial configuration for the pulling experiments.

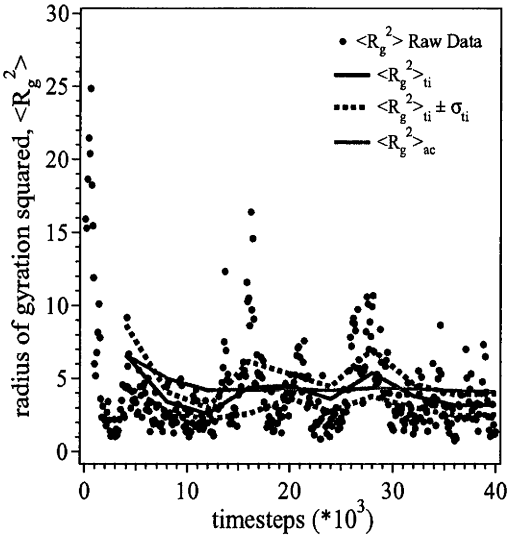

Figure 6.3: Radius of gyration squared, $< R_g^2 >$, versus the number of timesteps for a polymer chain of length $N = 50$, a surface attraction of $\varepsilon = 40.0$ and thermal energy, $k_B T_n = 0.1$. The raw data is plotted as $(\cdots)$, the time interval average, $< R_g^2 >_{ti}$, as ——, with $< R_g^2 >_{ti} \pm \sigma_{ti}$ as - - - and the accumulated average, $< R_g^2 >_{ac}$, as ——.

Polymer chains of size $N = 100$ were also allowed to equilibrate for 4×10^6 timesteps, with a total of ten simulations for each value of ε studied. However, the calculated values of $< \overline{R_g^2} >_{ac}$ and $< \overline{R_g^2} >_{ti}$ shown in Table 6.2, show that these two averages had not converged. Similarly to the chains of size $N = 100$, the polymer chains of size $N = 200$ which had equilibration times ranging from 10^6 to 10^7 timesteps, the calculated $< \overline{R_g^2} >$ values had also not converged (see Table 6.3). Although we could not show conclusively that these larger length chains had equilibrated, their final configurations are significantly different from the toy model initial configurations. Therefore we will treat these chains as "pseudo-equilibrium", *i.e.*, we will continue our analysis of the equilibrium properties of adsorbed chains using these chains, as well as using the final configurations as the starting configuration of the "pulling experiments".

The influence of the surface force on the height of the adsorbed chain was studied by varying ε. Even though the larger chains may not necessarily be at equilibrium, we can show that the conformations of the chain still agree with equilibrium scaling theory. The surface forces studied ranged from $40.0 \leq \varepsilon \leq 0.01$, encompassing very strong to weakly adsorbing forces. For the surface forces ranging from $40.0 \leq \varepsilon \leq 0.1$, there is little variation of the z-height during the course of a simulation for the different size polymer chains. Figure 6.4(a) is an example of a single simulation run with $\varepsilon = 0.1$ for polymer chains of size $N = 50, 100$ and 200. This surface force is so strongly attractive that we are unable to distinguish differences in the z-heights

of the different sized chains. However, for the weak surface forces ($\varepsilon = 0.01$) this is no longer the case. The value of the z-height varies widely during the course of a simulation run and there is a dependence on the size of the chain (see Figure 6.4(b)). The average z-height, z_{avg}, and standard deviation was determined for the different sized chains at the various surface potentials used. This was achieved by averaging the z-height of the chain of a given size for all simulations run at a particular surface force. Figure 6.5(a) shows the average z-height versus the size of the chain N for all values of ε. It can be seen that the height of the adsorbed chain is independent of its size but dependent on the surface forces of $0.1 \geq \varepsilon \geq 1.0$, with average height of the chain increasing with decreasing surface attraction. This is in accordance with theoretical predictions of scaling analysis, *i.e.*, the equilibrium height of the adsorbed chain scaling as $z_{avg}/a \approx 2/\varepsilon$ (see Chapter 5, Section 5.2). That is, the stronger the attraction of a surface, the flatter will be the adsorbed layer. Surface penetration also occurs for $\varepsilon \geq 10.0$, where the average z-height of the adsorbed chain is negative and is a result of the strong surface attraction. For $\varepsilon = 0.01$, the average equilibrium z-height is no longer independent of the size of the chain. The attractive potential is now so weak, that the height, or dimension of the chain follows N dependence of its natural size (*i.e.*, $z_{height} \sim R_g^{1/2} \sim N$).

The effect of varying the temperature of the system has been investigated by varying the thermal energy of the random noise, k_BT_n, with $0.01 \geq k_BT_n \geq 1.0$, for a polymer chain of length $N = 50$. In first instance we used a value for k_BT_n of 0.01, which was 10 times cooler than the systems previously studied. It took 6.25 times longer to equilibrate the chain, taking in total 2.5×10^7 timesteps. The second instance we used a value of $k_BT_n = 1.0$, which is 10 times warmer than the systems previously studied. Equilibration times were twice as fast at this thermal energy than when it was 0.1, with an equilibration taking 2×10^6 timesteps.

The time interval over which $< R_g^2 >$ was averaged for $k_BT_n = 1.0$ was 2×10^5 timesteps and for $k_BT_n = 0.01$ was 2.5×10^6 timesteps. All the values of ε studied, for a total of 10 different simulations for a given surface force, each with a different initial random number. The final values of $< \overline{R_g^2} >_{ac}$ and $< \overline{R_g^2} >_{ti}$ for all simulations for $N = 50$ at $k_BT_n = 1.0$ and $k_BT_n = 0.01$ are listed in Tables 6.4 and 6.5. As there is little difference between the two different averages for all simulations run, we can therefore conclude that the length of time over which the simulations were run was sufficient to equilibrate the chain. The final configuration for each simulation was then used as the initial configuration for the pulling experiments.

Similarly to our previous studies, we also determined the average z-height of the adsorbed chain at different temperatures for a chain consisting of 50 monomers. Figure 6.5(b) compares the average height of the adsorbed ch ain for a number of different surface potentials, with $k_BT_n = 0.01, 0.1$ and 1.0. It is evident from this

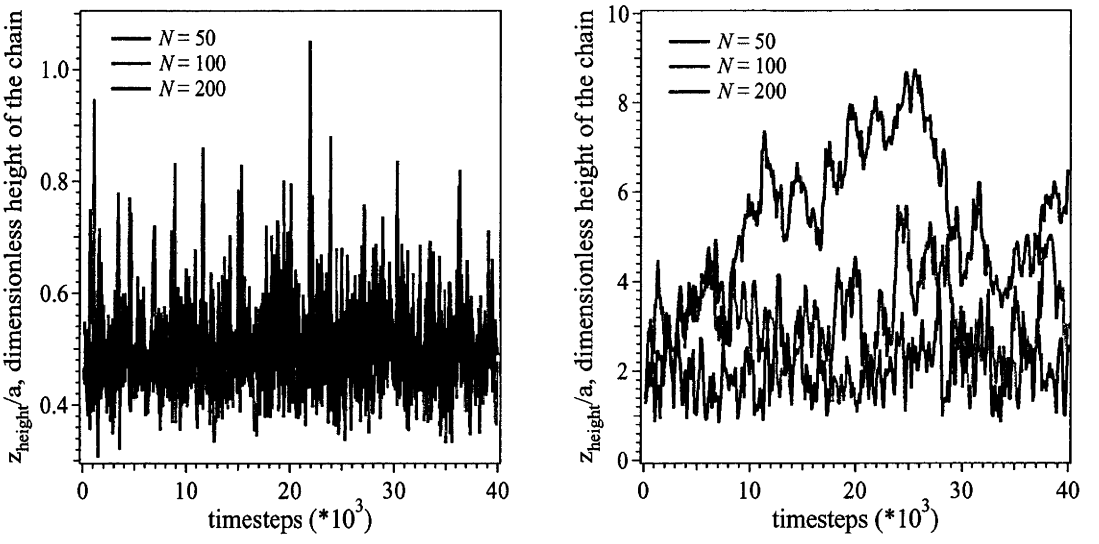

Figure 6.4: The z-height of an adsorbed chain, z_{height}/a, (dimensionless units) versus number of timesteps for polymer chains of length $N = 50, 100$ and 200 at $k_BT_n = 0.1$, with a surface attraction of (a) $\varepsilon = 0.1$ and (b) $\varepsilon = 0.01$.

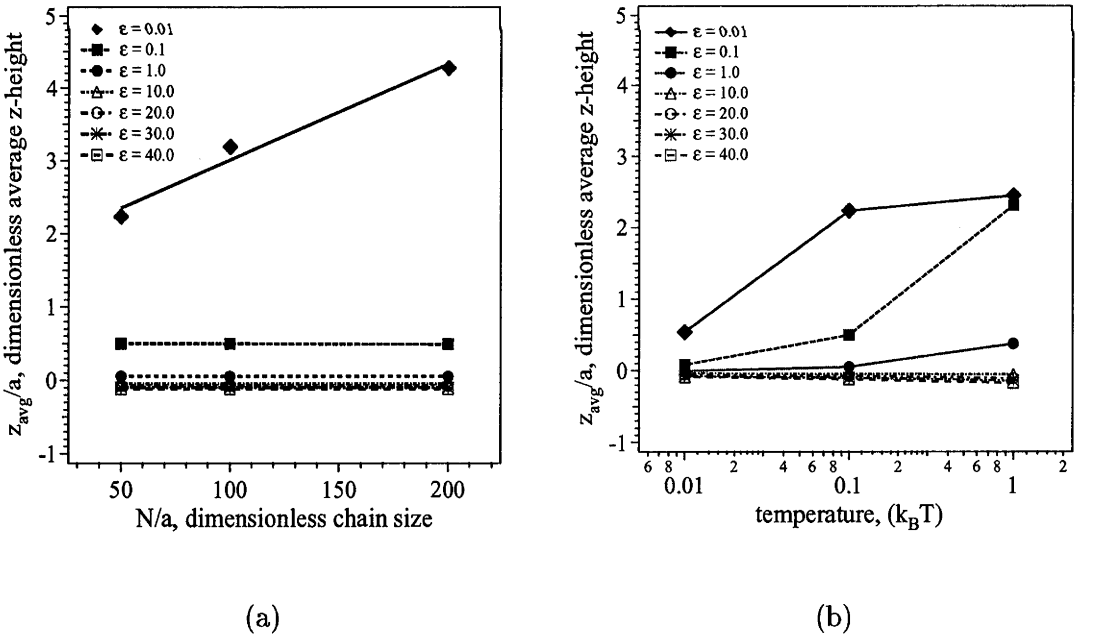

Figure 6.5: (a) The average z-height, z_{avg}/a, versus chain size, N/a, in dimensionless units at $k_BT_n = 0.1$. The height of the adsorbed chains is independent of the chain length for all surface forces except for $\varepsilon = 0.01$, which is very weakly adsorbing. (b) The average z-height, z_{avg}/a, in dimensionless units versus the temperature, in units of k_BT for polymer chains of length $N = 50$. The height of the adsorbed chains increases with temperature. Lines have been drawn through these points and are used as a guide to the eye.

plot that the temperature of the system effects the height of the adsorbed chain, increasing with temperature. As the temperature increases, the system has more thermal energy and the ability of the surface to tightly hold the chain decreases. The most dramatic difference in the average height of the adsorbed chains with temperature are for the weakest attractive surfaces of $0.01 \geq \varepsilon \geq 1.0$. At $\varepsilon = 0.01$, z_{avg} increases significantly when increasing the temperature from 0.01 to 0.1. From Figure 6.5(a), we have shown that at this surface potential and with $k_BT_n = 0.1$, the chain is loosely held by the surface. Therefore we could argue that when the system is at a lower temperature, the effect of the surface is greater and thus the height of the chain is lower. From increasing k_BT_n from 0.1 to 1.0, the increase in the height of the chain at this weak potential is small and is effectively due to the chain already being so weakly bound. At $\varepsilon = 0.1$, the same trend is observed with the height of the chain increasing with temperature. However, it is not until the temperature of the system is at $k_BT_n = 1.0$ for the attractive force of the surface is overcome and the chain is loosely held. For $\varepsilon = 1.0$, the chain remains closely bound to the surface at all temperatures studied. Therefore, the average height of the equilibrated chain is not only effected by the surface potential, but also the temperature of the system.

6.4 Pulling "Experiments"

In our pulling "experiments", the first monomer in a polymer chain is displaced at a constant velocity, v, in the z-direction only. The remainder of the chain, with the exception of the end monomers, is subject to Brownian motion. As the displacement of the first monomer increases, the tension in the chain increases and this results in the detachment of the chain from the surface. As monomers are ripped off to the surface, they are fed into a "pulled tether" which increases in length with the addition of each monomer.

6.4.1 Continuous Pulling Mode in the z-direction

This first example study involves extending a chain vertically so as to rip all of the adsorbed monomers off the surface. We use the final configurations of the initialisation procedure discussed in Section 6.3, as the starting configurations for the pulling experiments. In these pulling experiments, $\triangle t = 10^{-2}\mu$s, $k_BT_n = 0.1$ and the total number of timesteps taken to displace the first monomer a distance $dz = 0.1$nm, is 10^5. Therefore the rate at which the chain is being pulled is $v = dz/time = 1\mu$m/s. This extension rate is comparable to single molecule AFM experiments. In Chapter 4, we used experimental rates ranging from about 0.1μm/s to 10μm/s. Figure 6.6 is a snapshot taken from one simulation where a polymer chain of size $N = 50$ is

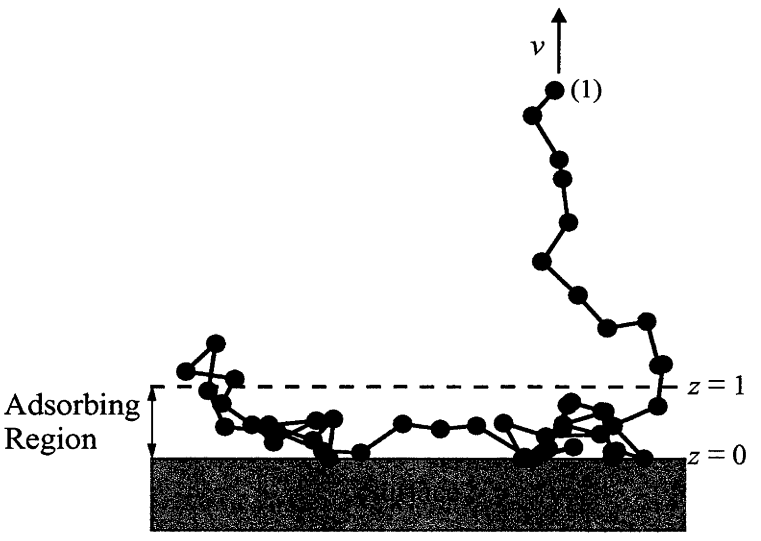

Figure 6.6: A pulling "experiment", where a chain of length $N = 50$ is ripped off an adsorbing surface with $\varepsilon = 0.1$ and $k_B T_n = 0.1$. The first monomer in the chain, labelled (1), is displaced at a constant rate of $v = 1\mu$m/s away from the surface.

being pulled off the surface. The surface potential in this instance is weak, with $\varepsilon = 0.1$, this results in the variation of heights of monomers close to the surface. The first monomer in the chain is labelled (1) and is displaced at a constant rate of $v = 1\mu$m/s. As the displacement of this first monomer increases, the number of monomers in the pulled tether increases. At this point in the pulling experiment, 20% of the monomers in the chain are in the pulled tether.

As the chain is being ripped off the surface, we determine the force experienced by the first monomer in the chain, $fz(1)$, every 10^3 timesteps, thus obtaining a force profile of the pulling experiment. We have chosen to use the same convention of negative force for these force profiles as was used in Chapter 4. In addition we also determine the total number of monomers adsorbed at any time and we record the last time each monomer was still adsorbed to the surface. Figure 6.7(a) depicts how the fraction of adsorbed monomers decreases with time for a chain of length of $N = 50$ and at $k_B T_n = 0.1$. In this instance, the surface is strongly adsorbing, $\varepsilon = 40.0$, and the chain is held tightly by the surface. As the displacement of the first monomer in the chain increases, the tension in the tether increases, with bond lengths overstretching. When this force exceeds that of the surface force, monomers are detached from the surface. Due to the large attractive surface force, monomers are detached sequentially from the surface, resulting in a linear relationship with the fraction of monomers adsorbed to the surface with respect to the total number of timesteps. This is because the work required to detach a certain number of monomers, $N_{detached}$ at a given surface potential, E, is simply the force applied to

monomer (1) integrated over the displacement of the monomer. As the displacement is linear in time, *i.e.*, $z = v \times t$, then the number of monomers detached is also linear with time.

The corresponding force profile is shown in Figure 6.7(b). The saw-tooth profile corresponds to the sequential detachment of monomers from the surface, with the detachment force being a maximum for the detachment of the first monomer. As the chain is extended, the tension in the pulled tether increases until it reaches a maximum detachment force at which point a monomer is ripped off, resulting in a decrease in tension and a sharp drop in the force. The saw-tooth pattern diminishes with the loss of monomers, with only the first few detachments as clear events. The remainder are obscured by the random fluctuations in the system.

Figure 6.7(c) shows the variation in spring force along the contour of the chain at 45.2×10^3 timesteps, denoted by dashed lines and arrows in Figures 6.7(a) and (b). The bond lengths in the chain are numbered from 1 to 49, which corresponds to the bond between monomers j and $j+1$, where j is the bond number. At this point in the pulling experiment 16 bonds have a maximum $f_{spring} = 14.4$ which are overstretched and would suggest that they are part of the pulled tether. This is confirmed by determining the fraction of monomers adsorbed in Figure 6.7(a) at 45.2×10^3 timesteps, at which point $\approx 30\%$ of the monomers in the chain have been detached. The remaining bonds in the chain have a much lower spring force as they are still adsorbed to the surface and do not experience the additional tension from the pulled tether. At weaker surface potentials, the difference in the spring force of the bonds in the pulled tether and those still adsorbed to the surface diminishes. This is because the detachment force is smaller and does not result in overstretching of the bonds in the polymer chain.

Figure 6.8(a) also depicts how the fraction of adsorbed monomers decreases with time. In this example, the chain length is also $N = 50$ and the thermal energy of the noise is $k_B T_n = 0.1$. The difference is that the surface force is much weaker, with $\varepsilon = 0.1$. As a result, the chain is not tightly held by the surface. This is evident in Figure 6.8(a), where the total time taken to detach the chain is approximately a 1/5 of that taken for the previous experiment. Also, there no longer exists a linear relationship between the number of monomers detached and the time. At this weaker surface force, several monomers can be detached at once, as the force required to detach them is much smaller. The corresponding force profile is shown in Figure 6.8(b). The saw-tooth profile corresponds to the sequential detachment of monomers from the surface in Figure 6.7 is not observed. This is due to the detachment force being comparable to the random forces from thermal fluctuations, which effectively obscures any features in the force profile.

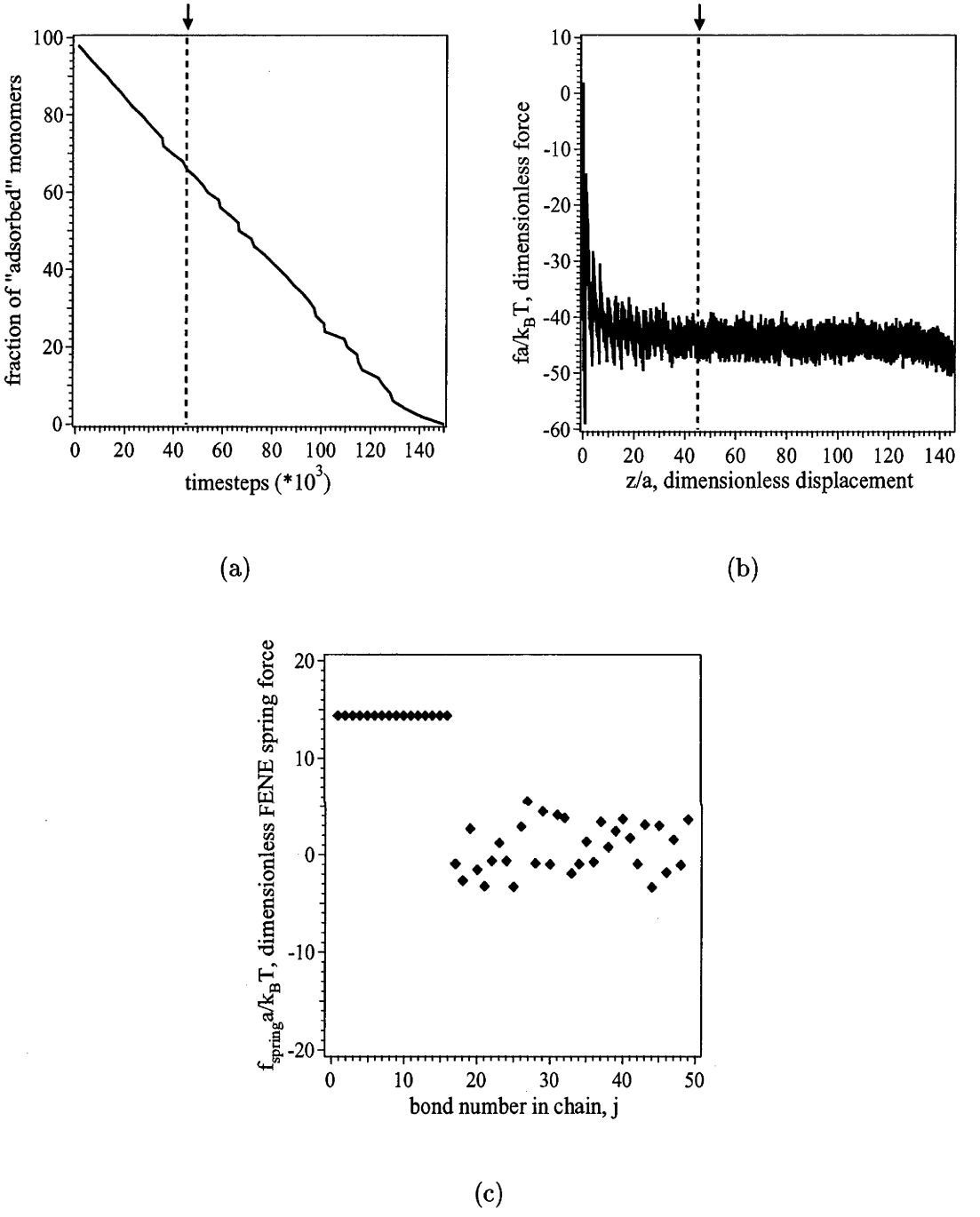

Figure 6.7: (a) Fraction of "adsorbed" monomers versus timesteps for a polymer chain of length $N = 50$, surface potential of $\varepsilon = 40.0$ and $k_BT_n = 0.1$. For this simulation, the loss of monomers is essentially constant with time. (b) Force, fa/k_BT, versus displacement, z/a, profile in dimensionless units for this pulling experiment. (c) Spring force, $f_{spring}a/k_BT$, in dimensionless units versus bond number in chain, j, for a polymer chain of length $N = 50$, surface potential of $\varepsilon = 40.0$ and $k_BT_n = 0.1$. This figure shows the spring force of all bonds in a chain at 45.2×10^3 timesteps and is highlighted in both (a) and (b) with a dashed line and arrow. At this point, approximately 30% of the monomers of the chain have been ripped off the surface resulting in the overstretched bonds that have a maximum spring force of 14.4.

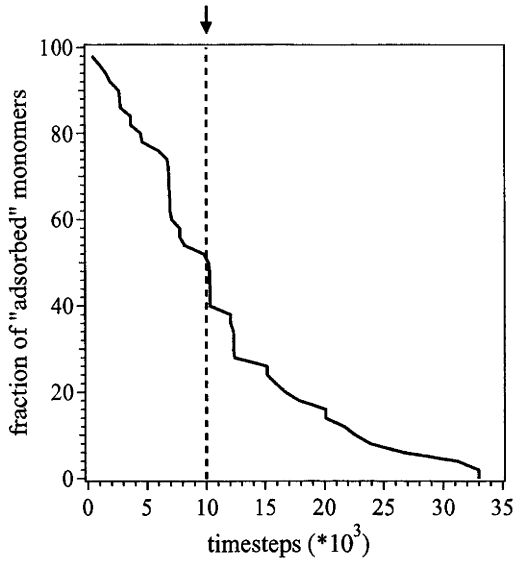

(a)

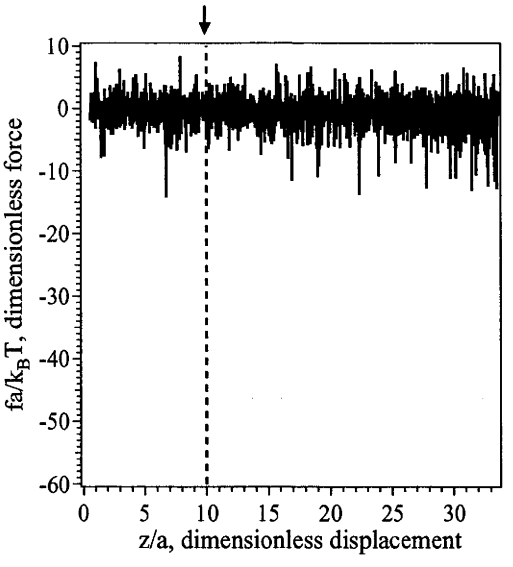

(b)

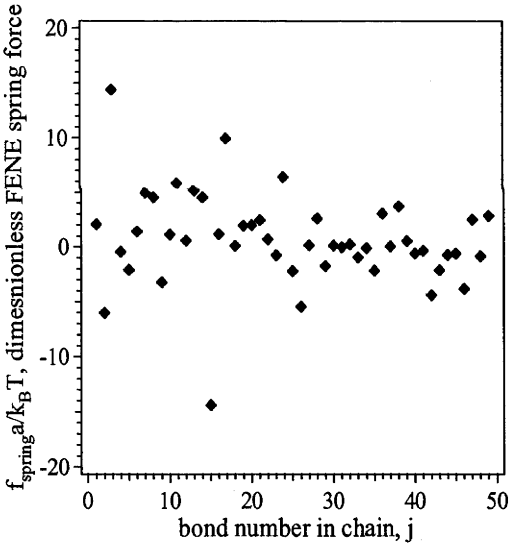

(c)

Figure 6.8: (a) Fraction of "adsorbed" monomers versus timesteps for a polymer chain of length $N = 50$, surface potential of $\varepsilon = 0.1$ and $k_BT_n = 0.1$. For this simulation, the loss of monomers is faster than in the previous figure, where several monomers can be lost at the same time. (b) Force, fa/k_BT, versus displacement, z/a, profile in dimensionless units for this pulling experiment. (c) Spring force, $f_{spring}a/k_BT$, in dimensionless units versus bond number in chain, j, for a polymer chain of length $N = 50$, surface potential of $\varepsilon = 0.1$ and $k_BT_n = 0.1$. This graph shows the spring force of all bonds in a chain corresponding to 10×10^3 timesteps and is highlighted in both (a) and (b) with a dashed line and arrow. At this point, approximately 48% of the monomers of the chain have been ripped off the surface. However, very few of the bonds are overstretched as the force of detachment is much lower at this surface potential.

Figure 6.8(c) shows the variation in spring force along the contour of the chain at 10×10^3 timesteps, denoted by dashed lines and arrows in Figures 6.7(a) and (b). At this point in the pulling experiment only 1 bond has a maximum $f_{spring} = 14.4$. At this point in the simulation $\approx 48\%$ of the chain has detached. The difference in the spring force of the bonds which are part of the pulled tether and those still in the adsorbed chain is not as distinct as in Figure 6.7(c). This is a result of the small detachment force which does not result in the overstretching of bonds.

6.4.2 Temperature

In our temperature studies, we examined the influence of thermal fluctuations in the noise term in eq 6.1 for our pulling experiments. This study is limited in that we only consider chains of length $N = 50$, although we have examined a range of ε, attractive well depths, discussed in Section 6.2. For all pulling experiments, we use the final configuration of the equilibrated chain as the initial configuration of the pulling experiment.

Figure 6.9(a) is a histogram of the detachment forces for the monomers in the chain at $k_BT_n = 1.0, 0.1$ and 0.01. It is evident from this figure that the temperature of the system affects the detachment process. At the coldest temperature, the highest average detachment force of -51.53 and the smallest standard deviation is 1.00, at $k_BT_n = 0.1$, the average detachment force is -45.64 and the standard deviation is 2.17 and at $k_BT_n = 1.0$, the average detachment force is the smallest of the three different temperatures being -34.67 while the standard deviation of 5.78 is the largest.

Figures 6.9(b)-(d) shows representative force profiles for pulling a chain of length $N = 50$, with a strongly adsorbing surface of $\varepsilon = 40.0$ at the three different temperatures studied. Firstly we look at the system where $k_BTn = 1.0$, which is 10 times warmer than the systems previously studied. The increased thermal fluctuations obscures more features in the force profiles, hence instead of the first ~ 10 detachment events being clear when $k_BTn = 0.1$, only the first ~ 5 detachment events are clear when $k_BTn = 1.0$ (see Figures 6.9(b) and (c)). At $k_BT = 0.01$, the system is 10 cooler than in the previous pulling experiments. Figure 6.9(d) shows the force profile for detaching a chain at this temperature and with a surface potential of $\varepsilon = 40.0$. The reduced thermal fluctuations allows more detail to be seen in the profile, with a greater number of detachment events clearly shown than at the other higher temperatures. However, with the reduction in thermal fluctuations, the time and displacement required to detach a monomer from the surface increases.

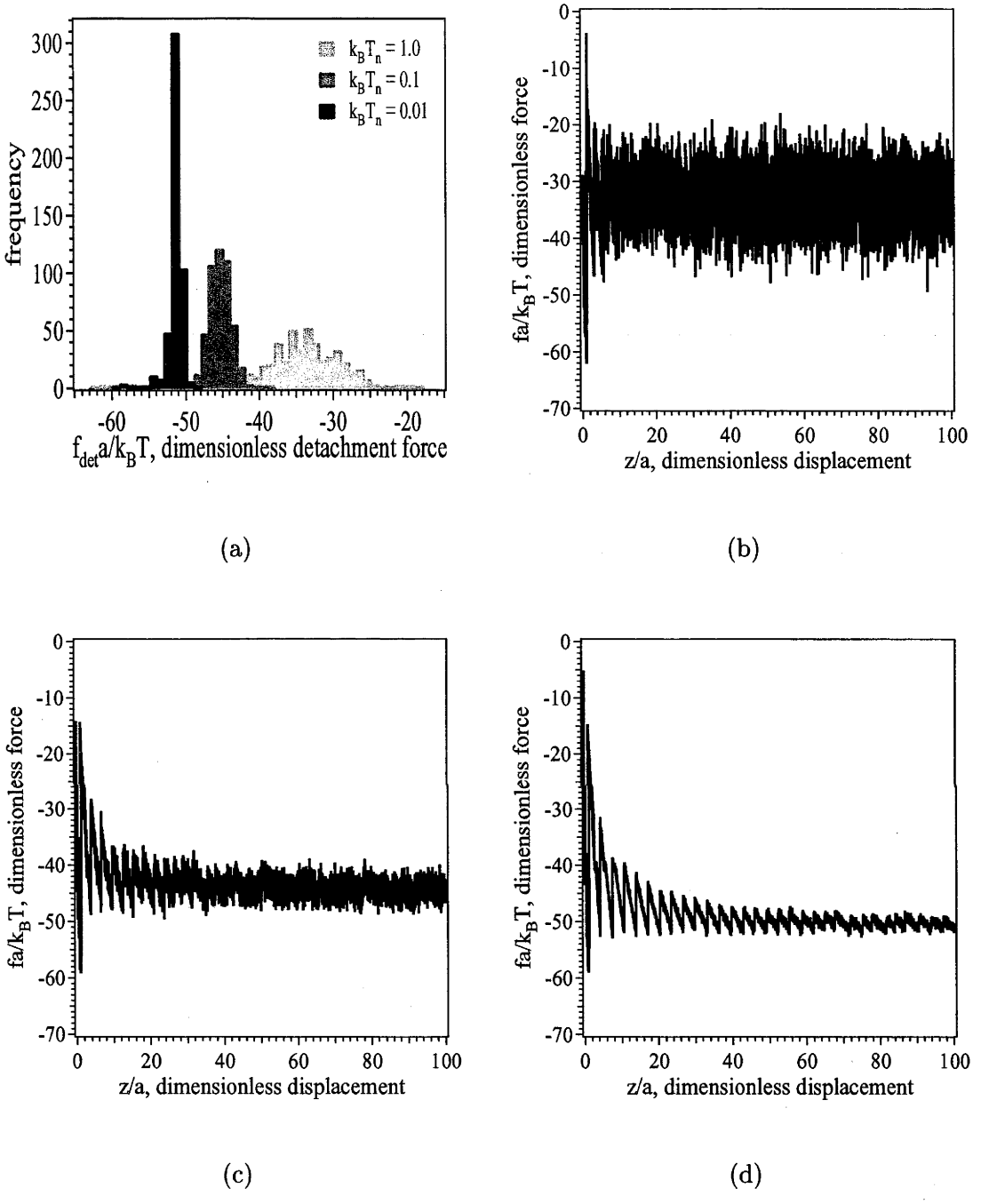

Figure 6.9: (a) Histogram of the detachment forces, $f_{det}a/k_BT$, of monomers in a chain of length $N = 50$ and surface potential of $\varepsilon = 40.0$ at three different temperatures. The spread in the distributions increases with increasing temperature, while the average detachment force decreases. The bin size was arbitrarily chosen to be 1.0. Force, fa/k_BT, versus displacement, z/a, profiles in dimensionless units for a polymer chain of length $N = 50$ and surface potential of $\varepsilon = 40.0$ at (b) $k_BT_n = 1.0$, (c) $k_BT_n = 0.1$ and (d) $k_BT_n = 0.01$. As the temperature is decreased, the number of clear saw-tooth events corresponding to detachment events increases.

6.4.3 Different Rates of Retraction

The next step was to see how the force profiles varied at faster rates of detachment. This was achieved by decreasing the number of timesteps taken to displace the first monomer, this increasing the pulling rate. In total three different rates were studied, $v = 1\mu$m/s, 10μm/s and 100μm/s. Example force profiles are shown in Figure 6.10 for a polymer chain of length $N = 50$, $k_BT_n = 0.1$ and at all surface potentials at the three different pulling speeds. From these force profiles it can be seen that at a given pulling rate, the detachment force of the chain decreases with decreasing surface potential. However, with the increase in the pulling rate, the timescale of the experiment decreases.

At the very fast rates of detachment, the force profiles in Figure 6.10(c) have a negative slope, *i.e.*, the average force increases with increasing number of monomers detached from the surface. This is not seen at the lower pulling velocities in Figures 6.10(a) and (b). A possible explanation for the negative slopes shown in Figure 6.10(c) is (1) if we consider the monomers to be unconnected and at different heights in the adsorbing region above the surface, with those closest to the surface requiring a larger force to detach them from the surface. Therefore as monomers are detached from the surface, we would expect the force to increase as the monomers furthest from the surface would be ripped off first. This explanation is unlikely as it doesn't take in to account the connectivity of the monomers in the chain. Another explanation for the increasingly negative force in these profiles is (2) overstretching of all bonds in the chain as the tether is pulled taut, however we would expect this to decrease with decreasing surface potential. This is not observed to be the case, with all profiles having essentially the same negative slope. Lastly, the negative slope in the profiles can be considered in terms of (3) the pulling rate being too fast for the polymer chain to respond to *i.e.*, that the monomer-surface contacts do not have ample time to adsorb and reform many times over the timescale of the pulling experiment, with the result being an increase in the force as more of the chain is ripped off the surface. This last explanation is the more likely, due to the independence of the slope with respect to the surface potential. However further investigation is required.

6.4.4 A Different Mode of Pulling: Oscillating Tip

AFM single molecule experiments typically involve cycling the AFM tip towards and away from the surface. In this section we perform an analogous experiment, where we displace the first monomer in the chain, which is attached to an AFM tip, a maximum distance from the surface, after which its direction changes and it then approaches the surface. In our pulling experiments the maximum and minimum

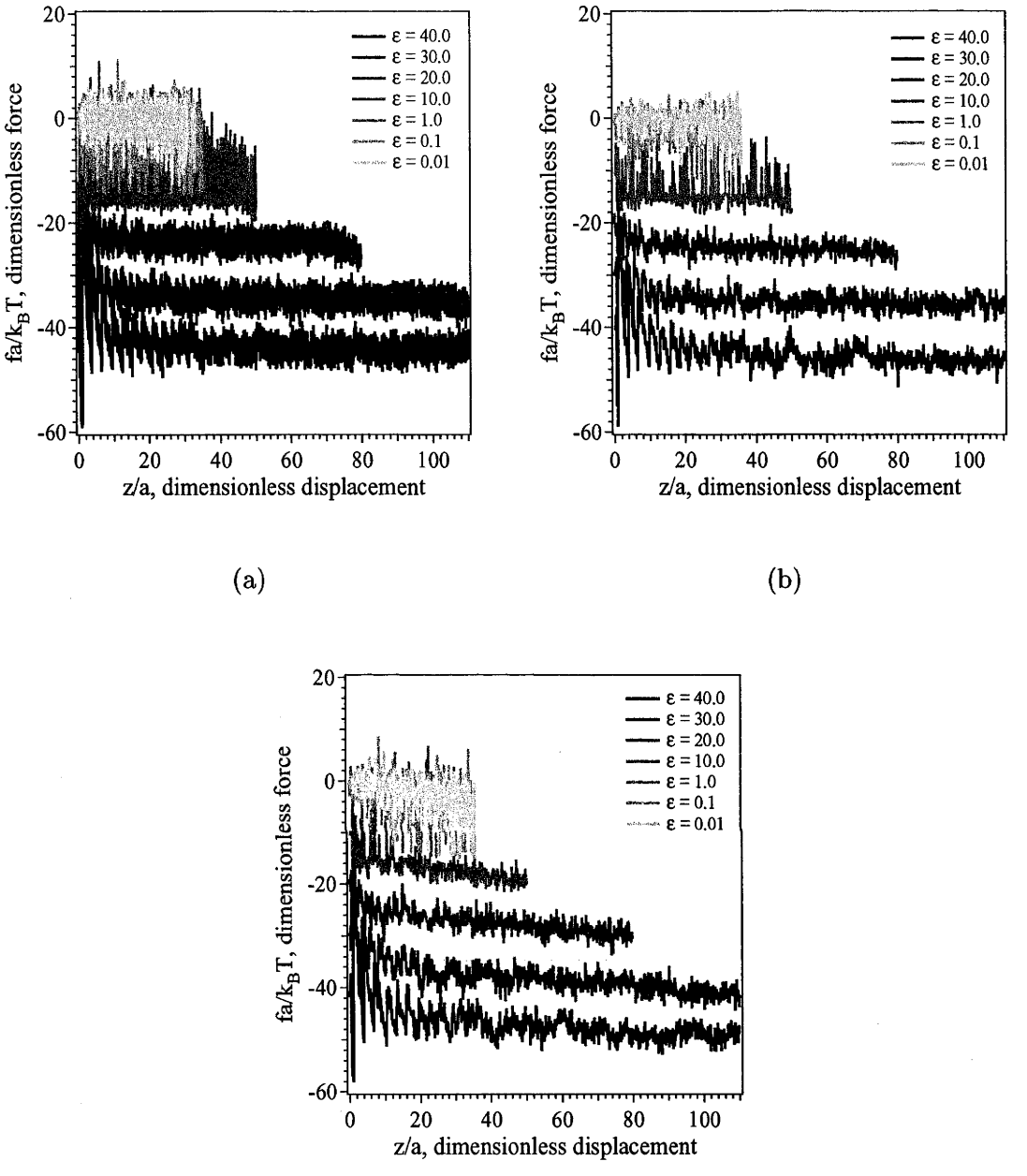

Figure 6.10: Force, fa/k_BT, versus displacement, z/a, in dimensionless units for pulling experiments chains of length $N = 50$ a a range of surface forces. Figure (a) shows the force profiles for pulling a chain at a rate of $v = 1\mu$m/s away from the surface. Figure (b) shows the force profiles obtained when the rate is increased to $v = 10\mu$m/s. At this faster rate, the number of timesteps taken to detach the chain decreases. Figure (c) shows the force profiles obtained when $v = 100\mu$m/s. At this rate, even less time is required to detach the chain. This figure differs to the others in that the force becomes increasingly negative with time and is independent of the surface force.

displacement from the surface of the first monomer in the chain, z, was $0.0 > z > N/2$. At $\varepsilon = 40.0$, the strongest surface force studied, the equilibrium z-height of a chain of length $N = 50$ is $z_{height} = -0.118482$, which is much smaller than the maximum displacement and only slightly less than the minimum displacement of the first monomer in these pulling experiments. Only two retract/approach cycles are completed for these experiments. The thermal energy contributing to thermal fluctuations for all experiments was set to $k_B T_n = 0.1$. We will show representative results from our computer experiments.

Figure 6.11(a) is a plot of the triangular wave displacement of the AFM tip as it cycled away and towards the surface. In this instance, the maximum displacement is $z/a \approx 25$, and the length of the polymer chain studied is $N = 50$. Figure 6.11(b) is the corresponding force profile, with an attractive surface force of $\varepsilon = 40.0$. In this profile we can see the saw-tooth pattern corresponding to the detachment of ten monomers from the surface as the tip is retracted. As the direction of the tip changes direction, the force on the tip decreases as the tension in pulled tether diminishes and the slope of the graph is constant. When the tip is at a height of $z < 10$, monomers readsorb to the surface at a reduced force, again showing the saw-tooth profile. However, this readsorption saw-tooth profile differs in that is much a quicker process and the slope of the curve is positive, and opposite to that for detachment. Once the tip has reached the minimum displacement, it changes direction again and the second cycle begins and has the same characteristics of the first. Figure 6.11(c) is shows the fraction of "adsorbed" monomers versus timesteps for the pulling experiment and suggests that this experiment is completely reversible as the number of monomers which are detached and readsorb is the same for both cycles. Question for future studies: (1) Does the slope of the force profile during the approach cycle indicate the rate of readsorption of monomers? For example, if readsorption was a strong and fast process (relative to detachment) then we would expect that the force would not decrease as much during the initial approach as the readsorption would increase the stretching force in the tether. However, near the end of the approach cycle, that is when the AFM tip is closest to the surface, then the force would be zero if that distance is less than the natural height of the adsorbed chain. This suggests that the force profile might fingerprint the readsorption process.

Figure 6.12 shows the spring force in the bonds along the contour length of the chain and use the same convention as previously described (see Section 6.4.1). Figure 6.12(d) is at a timestep of 10×10^3, when the tip is being retracted and Figure 6.12(e) corresponds to 44×10^3, and the tip is on the approach cycle. The dashed lines and arrows in Figures 6.11(a)-(c) correspond to these two snapshots of a polymer chain and their position relative to the experiment. From these two figures, it is difficult to discern any difference of the behaviour of the chain, as a

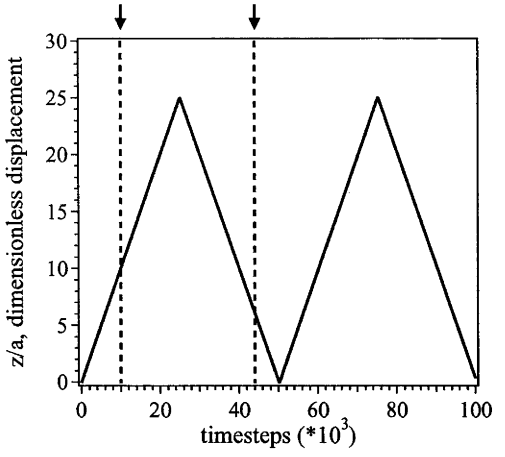

(a)

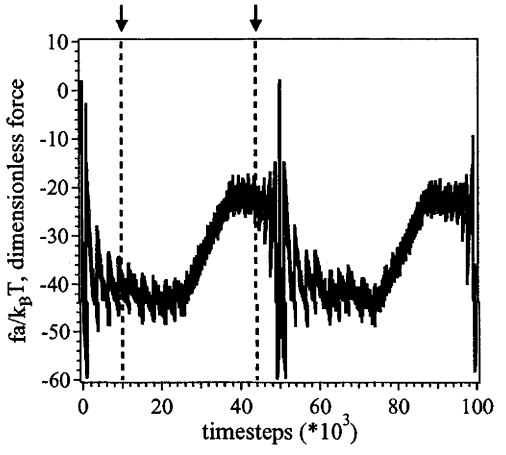

(b)

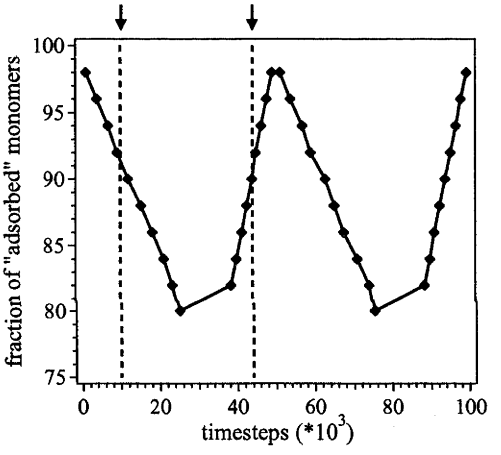

(c)

Figure 6.11: (a) Displacement, z/a, (dimensionless units) versus timesteps plot, depicting the oscillatory motion of the AFM tip as it is cycled away and towards the surface. (b) Force, fa/k_BT, (dimensionless units) versus timesteps profile for this pulling experiment. The size of the chain is $N = 50$, the surface attraction is $\varepsilon = 40.0$ and the thermal is $k_BT_n = 0.1$. The pulling rate in these experiments is $v = 1\mu$m/s. (c) Fraction of "adsorbed" monomers versus timesteps graph. Dashed lines and arrows are used to highlight the timesteps of 10×10^3 and 44×10^3, at which the following figure has calculated the spring forces of the bonds along the length of the chain.

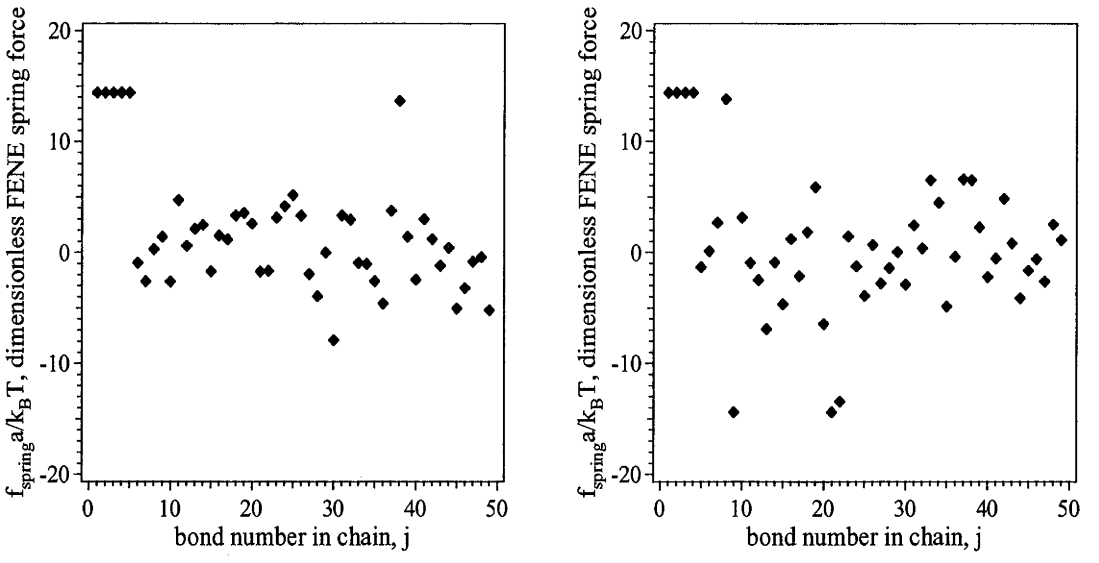

Figure 6.12: Spring force, $f_{spring}a/k_BT$, (dimensionless units) versus the bond number in the chain, j, for a polymer chain of length $N = 50$, with a surface force of $\varepsilon = 40.0$ and thermal energy of $k_BT_n = 0.1$ at (a) timestep= 10×10^3 and (b) timestep= 44×10^3. In Figure (a), 10% of the bonds are overstretched with a total of 4 monomers ripped off the surface. In this part of the experiment, the AFM tip is being retracted from the surface. In Figure (b), there are fewer bonds which are overstretched, with the pulled tether consisting of 5 monomers, as well as a number of bonds which have been compressed. At this point in the experiment, the AFM tip is approaching the surface.

similar number of bonds are overstretched. However, the number of shortened or compressed bonds is larger and could be attributed to the readsorption process. As the number of monomers ripped off the surface is small compared to the size of the chain it is difficult to contrast the retraction and approach cycles. If the maximum height was increased, differences in the cycles may become apparent. This will be the subject of future work and will not be further discussed here.

6.5 Constant Force

Lastly, we will discuss an alternative pulling experiment. Instead of displacing the first monomer at a constant rate, we apply a constant force, f_{apply}, to it in the z-direction adding it to the total force on this monomer. As a result, the first monomer is not held fixed and is affected by the thermal fluctuations in the system. In these experiments, it is not the force on the first monomer that is determined over the timescale of the experiment but the displacement of this monomer in the

z-direction. A number of different applied forces were studied and had the range of $0.5 \geq f_{apply} \geq 20.0$. The thermal energy contributing to thermal fluctuations for the system was $k_B T_n = 0.1$ for all experiments. In this section we will show representative results for a chain of length $N = 50$ at a surface force of $\varepsilon = 0.1$. The initial configurations of the polymer chains used for our constant force experiments were the those obtained from our equilibration studies.

Figure 6.13(a) shows the z-displacement of the first monomer as a function of time for different applied forces. The effect of thermal fluctuations on the motion of the chain is more significant at the smaller applied forces where the fluctuation in the height of the first monomer is more pronounced. All the profiles presented here are the result of a single experiment. Figure 6.13(b) is the average of ten different experiments, at the same applied force and so consequently, the profiles are smoother. Figure 6.13(c) is the equlibrium displacement of the first monomer at a given applied force. It can be seen that the position of the first monomer changes dramatically with the application of a small force of $f_{apply} = 0.5$ to $\sim 50\%$ the contour length of the chain. From $1.0 \geq f_{apply} \geq 15.0$, the displacement of the monomer increases to $\sim 95\%$ contour length of the chain. At $f_{apply} = 15.0$, the chain is almost fully extended. When the applied force is increased to $f_{apply} = 20.0$ the chain is overstretched and is extended to a length of $\sim 120\%$ the contour length of the chain.

In conventional AFM single chain experiments, it is not possible to perform this experiment as it would require a perfectly stiff cantilever which is not practical for probing single polymer chains. However, conventional analysis of AFM force measurements are based upon determining the deflection of the cantilever, which is dependent on the mechanical properties of both chain and cantilever, particularly at small lengthscales.[11] In order to increase sensitivity in the force measurement, it is more practical to have a soft or compliant cantilever, *i.e.*, with the spring constant, k, as small as possible. The experimentally controlled distance D is then the chain extension *and* the cantilever deflection; the measured force will be the bare force, $f_0(D) = \Delta$, plus some correction term. As the controlled distance is typically of the order of the size of the polymer chain studied, $D >> \Delta/k$, and the correction term is negligible.

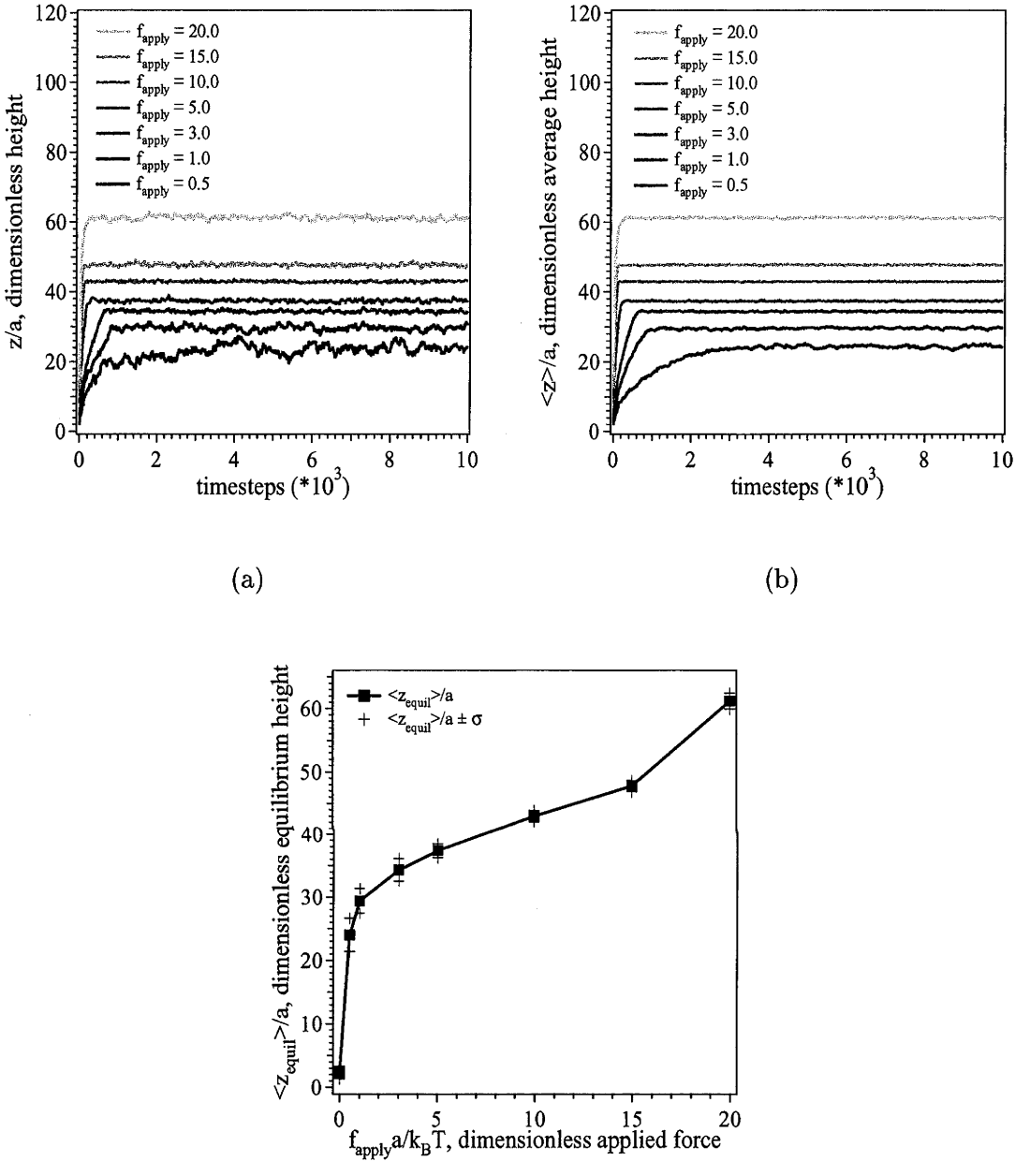

Figure 6.13: (a) The z-displacement of the first monomer in the chain, z/a, (dimensionless units) versus timesteps graph for a single experiment where the applied force, f_{apply}, had values of $0.5 \geq f_{apply} \geq 20.0$. (b) The z-displacement of a chain averaged over ten simulations, $< z > /a$, (dimensionless units) versus timesteps graph again with $0.5 \geq f_{apply} \geq 20.0$. (c) The average equilibrium displacement of chain, $< z_{equil} > /a$, versus the applied force, $f_{apply}a/k_BT$, in dimensionless units graph. The size of the chain was $N = 50$, the surface force was $\varepsilon = 0.1$ and the thermal energy was $k_BT_n = 0.1$.

6.6 Discussion

In this chapter we have highlighted some of the measures possible with our computer experiment. The results to date confirm our expectations on the dependence of the chain length, temperature and surface adsorption upon force profiles. We will use this program in future studies. Some of the practical studies include

(a) Using the retraction/approach cycles to investigate the adhesion of single chains on surfaces

(b) Investigating the effects of varying the rates of pulling on single chain experiments

(c) Contrasting the two different experiment techniques of pulling the chain at a constant rate to the application of a constant force

and

(d) Studying the effects of solvency on features observed in force profiles.

Table 6.1: The $< \overline{R_g^2} >$ for $N = 50$ at $k_BT = 0.1$.

ε	No.	$< \overline{R_g^2} >_{ac}$	$< \overline{R_g^2} >_{ti}$	ε	No.	$< \overline{R_g^2} >_{ac}$	$< \overline{R_g^2} >_{ti}$
40.	1	4.0738	3.2230±0.6966	30.	1	4.7067	3.2568±0.7617
	2	4.3072	5.2306±1.0342		2	5.4490	4.0986±0.9254
	3	4.4421	3.1761±0.5017		3	4.0916	5.4447±2.0599
	4	4.6039	3.8268±0.7664		4	4.3054	3.5755±0.7185
	5	3.9732	5.4948±2.2091		5	4.0420	2.9581±1.2677
	6	4.7398	3.9917±2.0460		6	4.2384	2.9081±0.3654
	7	5.0031	3.7516±1.3824		7	4.8019	3.5388±0.4842
	8	4.3472	5.3974±1.5789		8	4.4209	4.7877±1.4352
	9	4.7832	4.2552±0.8422		9	4.5770	3.2559±0.4130
	10	4.0182	3.1548±1.4260		10	4.1780	2.5456±0.5767
20.	1	3.9951	3.8483±1.7556	10.	1	4.9785	3.5816±1.3033
	2	4.5359	3.2014±0.8014		2	4.3838	6.8144±1.6879
	3	4.6309	3.7588±0.9884		3	4.0587	4.8353±1.1040
	4	4.0472	3.4661±0.5416		4	4.3536	4.3378±1.3538
	5	4.4555	5.1639±1.3588		5	4.8580	6.3115±1.1669
	6	5.6567	7.0951±1.4186		6	5.8658	3.0631±0.6032
	7	4.7030	4.8111±0.6614		7	4.4293	3.5717±1.2401
	8	4.2178	3.4166±0.7618		8	4.4719	3.6469±0.6201
	9	5.4286	4.8502±1.6032		9	4.1258	2.4278±0.3001
	10	4.4432	4.6446±0.7709		10	5.7577	5.6764±1.1028
1.	1	5.2363	3.2222±0.6491	0.1	1	3.6771	2.6273±0.4150
	2	4.7076	4.9613±0.9413		2	3.7907	3.7984±0.4615
	3	3.7800	2.6951±1.1064		3	3.3179	2.8783±0.4435
	4	4.0067	4.8371±0.5542		4	3.7554	4.4494±1.1950
	5	3.5037	2.9853±0.6120		5	3.3704	3.9749±0.5487
	6	3.5273	2.4024±0.3656		6	4.3341	2.9516±1.4111
	7	3.5821	2.2935±0.6318		7	3.4422	3.5960±0.8810
	8	5.6311	5.4534±1.2945		8	3.7875	3.4921±0.6279
	9	4.6210	7.1606±1.1168		9	3.5091	3.1461±0.7521
	10	4.9593	7.3167±2.3755		10	4.8059	5.6854±1.7531
0.01	1	4.4077	4.4745±0.9081				
	2	5.1827	4.6382±0.8871				
	3	4.5449	5.2058±1.1037				
	4	4.9153	5.1648±0.8761				
	5	4.4092	6.1222±0.8685				
	6	4.5906	3.3277±0.5296				
	7	4.2528	4.4702±1.0276				
	8	5.0112	3.2620±0.5221				
	9	4.5407	4.5783±0.8424				
	10	4.5458	5.0893±1.1093				

Table 6.2: The $< \overline{R_g^2} >$ for $N = 100$ at $k_BT = 0.1$.

ε	No.	$< \overline{R_g^2} >_{ac}$	$< \overline{R_g^2} >_{ti}$	ε	No.	$< \overline{R_g^2} >_{ac}$	$< \overline{R_g^2} >_{ti}$
40.	1	13.6913	4.5160±2.1058	30.	1	15.7876	5.1657±0.7008
	2	14.1812	4.7693±0.4599		2	18.0071	7.1856±1.1370
	3	19.2780	8.76538±2.0474		3	12.8373	8.1255±0.9117
	4	17.8648	15.5254±1.7946		4	22.7339	5.2168±0.5779
	5	12.1882	6.8383±1.2497		5	12.1428	5.8604±0.6739
	6	10.4127	4.9052±0.6602		6	11.8280	15.4555±1.6449
	7	13.9399	4.7435±0.7074		7	17.0258	10.6900±1.1458
	8	18.8631	12.3095±2.1083		8	12.0922	4.0187±0.6644
	9	21.4021	5.7421±0.9233		9	18.4260	8.1761±1.0843
	10	20.3349	3.7290±0.4917		10	16.9603	16.9603±1.8933
20.	1	16.5632	6.1616±2.1811	10.	1	19.2693	6.3633±1.1999
	2	24.0733	3.3966±1.3684		2	15.4829	7.0693±0.8795
	3	11.9520	3.4473±0.5710		3	14.5776	10.1726±2.2200
	4	16.8843	6.1430±0.6519		4	16.8463	5.2666±0.7057
	5	15.8900	4.3120±1.1340		5	16.8556	7.6267±0.8771
	6	15.9750	8.0265±1.2909		6	18.7459	9.6069±1.5234
	7	14.4899	9.6153±1.6452		7	20.3227	3.9376±0.5032
	8	11.5810	7.2524±2.7432		8	22.9761	14.6586±1.5041
	9	13.0849	8.8749±1.2698		9	15.8216	9.9511±0.9488
	10	14.0666	8.1074±1.0595		10	12.9166	6.4741±2.2302
1.	1	16.5990	7.6170±1.5848	0.1	1	13.7917	5.2212±1.1580
	2	15.8647	11.2730±1.5772		2	13.9861	3.3135±0.5019
	3	15.8635	4.3128±0.9521		3	11.0934	3.9591±0.5458
	4	16.2647	7.5125±2.0676		4	14.3442	5.2853±0.9373
	5	19.0179	13.4100±1.7070		5	16.2293	6.0007±0.8077
	6	15.2942	9.5554±1.6517		6	10.8470	6.0021±2.0168
	7	16.1880	5.4856±0.8170		7	11.5732	3.5138±0.4607
	8	17.6371	12.2241±1.5836		8	12.7693	5.6300±1.1453
	9	16.9104	4.6014±1.0031		9	12.5141	7.6380±1.0731
	10	15.7391	10.0649±2.1374		10	12.7453	12.0554±0.9103
0.01	1	16.7104	7.9090±0.8986				
	2	15.5894	5.2527±0.5447				
	3	14.3094	10.6006±2.0810				
	4	10.7880	6.0939±1.3025				
	5	15.2380	13.2383±2.3347				
	6	17.2603	5.6290±0.4265				
	7	11.7934	7.1657±1.7385				
	8	14.3856	7.0410±0.6240				
	9	11.8658	7.6099±0.9315				
	10	13.1586	7.5971±1.8017				

Table 6.3: The $< \overline{R_g^2} >$ for $N = 200$ at $k_BT = 0.1$.

ε	No.	$< \overline{R_g^2} >_{ac}$	$< \overline{R_g^2} >_{ti}$	ε	No.	$< \overline{R_g^2} >_{ac}$	$< \overline{R_g^2} >_{ti}$
40.	1	124.592	51.3793±0.8045	30.	1	16.9514	12.9163±1.0209
	2	100.6531	12.2849±0.8737		2	97.0377	13.0953±1.7905
	3	71.9370	18.6622±1.8439		3	103.6358	19.8964±2.2466
	4	126.356	41.9967±2.4506		4	82.2999	9.06461±0.8329
	5	103.2420	14.6820±2.9688		5	97.0174	8.96403±1.2865
	6	78.5387	8.55190±0.9021		6	90.9232	24.2777±3.4807
	7	99.6054	24.6325±1.1169		7	66.8082	27.7133±2.3164
	8	70.0028	6.9170±0.4626		8	99.3166	60.6037±2.3229
	9	63.2576	14.8823±1.4328		9	104.1698	21.9469±2.5269
	10	105.920	6.9319±1.4988		10	114.517	33.1464±7.4781
20.	1	101.0083	11.2435±1.6366	10.	1	216.367	145.747±5.1450 ±
	2	92.5665	19.5857±4.4427		2	65.8621	13.3063±1.2842 ±
	3	81.5033	15.3508±4.6924		3	78.8058	16.2449±3.5889 ±
	4	57.8061	8.6424±1.3185		4	70.0961	9.4461±1.8476
	5	107.131	16.2660±1.6665		5	73.5073	13.8219±2.6897
	6	80.9470	16.5070±1.4444		6	97.1800	19.7023±1.3049
	7	56.9088	23.3429±3.8969		7	67.5532	13.6886±2.8648
	8	79.8103	13.5213±2.0324		8	115.392	39.7365±4.4402
	9	83.4193	8.7432±1.0015		9	79.2955	6.9108±1.2284
	10	94.2270	49.9551±2.3996		10	83.5384	21.7540±4.4562
1.	1	85.1837	14.2753±1.0478	0.1	1	62.5168	9.9689±0.7264
	2	76.6496	11.5235±0.7560		2	66.5440	8.5392±0.8194
	3	81.3426	46.0942±4.8865		3	46.3839	11.5904±2.3189
	4	76.7981	14.8007±2.5582		4	49.1591	8.2937±1.1428
	5	81.2763	15.9573±2.0084		5	42.0751	14.7425±1.1498
	6	71.2902	28.9561±5.7772		6	59.2218	15.0279±1.3967
	7	75.5760	12.9070±5.64316		7	49.9616	10.4100±1.4576
	8	89.9225	34.4145±2.13228		8	45.9631	5.3886±0.8563
	9	70.1602	15.7324±1.6129		9	43.7186	9.1835±2.5898
	10	70.4537	7.3389 ±0.6705		10	54.7692	8.5974±2.406
0.01	1	69.9318	22.0404±3.596				
	2	64.8506	24.8858±1.0802				
	3	57.7514	5.8558±0.4602				
	4	57.8571	13.1188±2.7112				
	5	54.0561	8.907±0.7892				
	6	69.1596	21.6706±3.2721				
	7	60.1116	10.0479±1.6823				
	8	71.0379	16.9126±1.1314				
	9	67.8559	11.9055±1.2017				
	10	61.2607	14.3258±2.0963				

Table 6.4: The $< \overline{R_g^2} >$ for $N = 50$ at $k_BT = 1.0$.

ε	No.	$< \overline{R_g^2} >_{ac}$	$< \overline{R_g^2} >_{ti}$	ε	No.	$< \overline{R_g^2} >_{ac}$	$< \overline{R_g^2} >_{ti}$
40.	1	3.4810	3.5974±2.2378	30.	1	3.8956	3.8657±2.0963
	2	3.9004	3.5322±2.0892		2	3.3265	3.9865±2.3082
	3	4.1443	3.6909±2.0151		3	3.7540	3.6954±2.1574
	4	4.1148	3.4343±2.0416		4	4.0089	3.5998±2.2675
	5	4.1995	4.1572±3.0717		5	2.7176	3.1958±2.1314
	6	3.1114	3.9946±2.1998		6	3.1865	3.7161±2.3344
	7	4.2200	3.5860±2.5012		7	2.6883	3.6309±2.1309
	8	3.1456	3.4974±1.9253		8	4.2590	4.0883±2.2637
	9	4.2706	4.1113±2.5593		9	4.0658	3.8981±2.4420
	10	2.8915	3.8298±2.2882		10	3.6403	4.0058±2.5083
20.	1	3.9316	4.1513±2.5195	10.	1	3.7994	4.3358±2.9450
	2	3.9875	3.8911±2.3693		2	5.1488	4.5464±2.8729
	3	3.3284	3.4092±2.0013		3	3.7985	3.8711±2.6907
	4	2.6822	3.6993±2.5180		4	4.1138	3.6276±2.1511
	5	3.3147	3.6820±2.2415		5	3.8632	4.0584±2.3677
	6	3.2700	3.7802±2.3555		6	4.6834	3.6704±2.3179
	7	3.9865	3.7832±2.2926		7	4.0679	4.0028±2.2859
	8	3.1535	3.8719±2.2427		8	4.3455	3.7166±2.1485
	9	4.0902	3.8405±2.1482		9	5.9314	4.0073±2.7566
	10	3.9908	3.8643±2.1544		10	4.6809	4.0097±2.2830
1.	1	3.4691	3.6937±2.3167	0.1	1	4.4908	4.4297±1.9328
	2	2.4390	3.1004±1.7060		2	5.3610	4.8803±2.1695
	3	3.8197	3.4240±2.4644		3	5.3852	5.4627±2.5666
	4	3.3848	3.6073±2.2397		4	4.3461	4.4655±2.3423
	5	3.0385	3.8408±2.3687		5	3.5303	3.9291±1.7710
	6	2.6008	3.1675±1.8120		6	4.1844	4.9335±2.4975
	7	3.6434	3.3343±1.8804		7	4.4606	5.0932±2.4102
	8	3.9943	3.4884±1.9349		8	3.4020	4.4899±2.1947
	9	2.5771	3.3517±1.9161		9	4.9545	4.6654±2.3528
	10	3.2657	3.2089±1.7409		10	4.9631	4.8908±2.3698
0.01	1	3.9876	4.7486±2.2135				
	2	5.1804	4.8845±2.3812				
	3	3.9915	4.7389±2.3048				
	4	4.4224	4.5998±2.3135				
	5	4.4224	4.5998±2.3135				
	6	4.1234	4.8370±2.3637				
	7	4.6584	4.6249±2.0093				
	8	4.6841	4.8667±2.2692				
	9	3.6756	4.1765±2.0534				
	10	4.0280	4.5399±2.2217				

Table 6.5: The $< \overline{R_g^2} >$ for $N = 50$ at $k_BT = 0.01$.

ε	No.	$< \overline{R_g^2} >_{ac}$	$< \overline{R_g^2} >_{ti}$	ε	No.	$< \overline{R_g^2} >_{ac}$	$< \overline{R_g^2} >_{ti}$
40.	1	3.6975	6.9912±5.2048	30.	1	3.0647	5.4503±4.5080
	2	5.8728	7.3324±4.1818		2	3.2981	5.0466±3.3328
	3	3.6129	6.6044±5.2391		3	4.9250	5.4157±4.0394
	4	6.4607	5.6093±4.7589		4	4.3889	4.9522±3.7581
	5	3.3432	5.7702±5.0355		5	2.6095	4.8094±4.1112
	6	3.1414	5.9012±4.1337		6	3.3297	5.1535±3.7426
	7	6.2626	5.9990±4.6726		7	3.2207	4.1493±3.0043
	8	5.3984	7.4308±4.3399		8	6.1613	5.9370±5.6669
	9	6.5279	6.7626±4.7347		9	5.5785	4.6244±3.5218
	10	3.8805	6.0252±3.5767		10	2.6024	4.0814±2.7494
20.	1	3.1775	5.8933±4.6678	10.	1	4.2154	5.5561±3.7774
	2	3.9263	5.1366±4.2200		2	2.6836	5.0501±4.2929
	3	3.7334	5.8392±4.5438		3	2.7220	5.2124±3.7419
	4	3.7441	6.0532±4.7301		4	4.3316	5.5935±4.4724
	5	5.6579	5.4645±4.5241		5	3.9460	5.3621±4.0197
	6	2.8620	4.5180±3.4231		6	6.3554	5.5158±4.1378
	7	7.4920	6.2895±4.5488		7	6.5682	4.4578±2.8831
	8	2.5674	6.6161±5.4500		8	4.2460	4.4428±3.2216
	9	2.5211	4.7204±4.3131		9	6.4307	4.6361±3.2938
	10	7.7581	5.1894±4.8071		10	3.8741	4.2447±3.5449
1.0	1	5.8102	5.8784±5.0938	0.1	1	6.0615	4.1134±3.3848
	2	3.7395	4.3121±3.1273		2	4.2558	4.9152±3.6438
	3	2.6195	3.2455±2.7023		3	3.0696	4.7642±2.9700
	4	2.2872	4.4590±4.5515		4	3.4493	6.5010±3.6225
	5	2.9651	5.7544±5.3120		5	7.6818	4.5013±3.0979
	6	3.9812	4.9953±3.2336		6	3.0701	4.3667±3.4170
	7	3.7246	5.1312±3.7424		7	5.9789	5.4879±3.6789
	8	5.4479	4.3220±2.9011		8	3.2254	3.7960±3.2253
	9	3.1500	5.1549±3.8380		9	3.2731	3.8798±2.7927
	10	3.0669	5.0618±5.1680		10	3.4820	4.2396±3.8577
0.01	1	2.7534	3.9001±3.1014				
	2	3.1769	3.1479±2.4428				
	3	2.9373	4.4002±3.0685				
	4	2.2984	3.5362±3.0132				
	5	2.2794	3.7770±3.5262				
	6	3.0533	3.4657±3.3675				
	7	1.9663	4.9061±3.7199				
	8	3.5179	4.0670±3.5199				
	9	2.4106	3.5829±2.7384				
	10	2.4773	3.7357±3.2567				

References

[1] Titantah, J. T.; Pierleoni, C.; Ryckaert, J.-P., *Physical Review E* **1999**, *60*, 7010.

[2] Sheng, Y. -J.; Lai, P. -Y.; Tsao, H. -K. *Physical Review E* **1997**, *56*, 1900.

[3] Kreitmeier, S.; Wittkop, M.; Göritz, D. *Physical Review E* **1999**, *59*, 1982.

[4] Wittkop, M.; Kreitmeier, S.; Göritz, D. *Physical Review E* **1996**, *53*, 838.

[5] Maurice, R. G.; Matthai, C. C. *Physical Review E* **1999**, *60*, 3165.

[6] Milchev, A.; Binder, K. *Macromolecular Theory and Simulations* **1994**, *3*, 915.

[7] Milchev, A.; Binder, K. *Macromolecules* **1996**, *29*, 343.

[8] Pandey, R. B.; Milchev, A.; Binder, K. *Macromolecules* **1997**, *30*, 1194.

[9] Binder, K.; Milchev, A.; Baschnagel, J. *Annual Review of Materials Science* **1996**, *26*, 107.

[10] Milchev, A.; Paul, W.; Binder, K. *Journal of Chemical Physics* **1993**, *99*, 4786.

[11] Kreuzer, H. J.; Payne, S. H. *Physical Review E*, preprint.

Chapter 7

Conclusions and Future Work

In this thesis, we have used experiment, theory and simulation to investigate the manipulation of single polymer chains using an AFM. These techniques have been used to study the effect of various system parameters on the detachment process of a single polymer chain from an adsorbing surface. In particular, the theoretical and simulation studies have been used to determine the effects of varying the pulling rates in AFM experiments and make predictions of features observed in the corresponding force profiles, while our experimental study has examined the effects of solvency for single chain experiments.

In our AFM experiments we have investigated the influence of solvency, particularly poor solvent conditions, on features observed in characteristic force profiles. We have shown that the extension of single PNIPAM and PEO chains in poor, aqueous solution occurs with a force that is independent of extension, *i.e.*, a force plateau. The quantised steps associated with multiple plateaus in individual force profiles as well as the statistics of a large collection of force profiles strongly suggest that these force plateaus are attributable to single chains. More generally, this force plateau can be understood in terms of the Rayleigh instability for a liquid column: extension of the chain results in monomer-by-monomer pull-out from the condensed globule into the poor solvent. Plateau events, can be considered in terms of a chain pulled monomer-by-monomer from an attractive potential to a zone of zero mean potential with minimal stretching. The filament of polymer between the surfaces is made up of monomers which have been pulled out of a local attractive potential. In our experiments, the potential arises from the local solvency of the chains. Our force profiles were observed to contain either exclusively Langevin events or Langevin and Plateau events, depending upon temperature and/or co-solute addition, and did not vary in character with rate of retraction of the AFM tip.

We have also used theory to study the effects of rates on AFM single chain experiments. In this study we use a simple ideal chain model, scaling analysis and activation kinetics to predict force profiles for the detachment of chains from

adsorbing surfaces by pulling a loose tether from the surface. Although we do not include detail such as finite extensibility or monomer-monomer interactions, we are able to reconstruct much of the character of experimental AFM force-profiles. Our analysis considers cases where the timescale of equilibration of the monomer-surface contacts is both shorter and longer than the timescale of the pulling experiment. When the extension rate is slow, the monomer-surface contact has ample time to exchange monomers between the pulled tether and adjacent loop and the force is constant as the chain is being ripped slowly from the surface. However, if the extension rate is made faster and commensurate with the kinetic rate of detachment, then the magnitude of the pulling force details individual detachments of monomers from the surface. We have shown that the force profile will be discontinuous marking an individual detachment and that, on average, the magnitude of the detachment force decreases with successive detachments. As the extension rate is increased, the magnitude of the detachment force increases and larger extensions are required for detachment. At very large extension rates, the applied force is sufficiently large to reduce the barrier to detachment to zero and the detachment occurs instantaneously at a yielding force, f_{yield}, which characterises the monomer-surface contact. At these large extension rates the force profile is "saw-tooth" shaped with detachment forces that are equal for successive detachment events and independent of extension rate.

Unlike the experimental and theoretical investigation, our simulation study was not yet complete and will be the subject of further research. Consequently, we have only shown examples of the possible measures with our simulation. The results to date confirm our expectations on the dependence of the chain length, temperature and surface adsorption upon force profiles. We have shown examples of results obtained for pulling an end-tethered polymer chain orthogonal to the surface at a constant rate and the effect of varying the temperature and pulling rates. We also show results for varying the movement of the tip to an oscillatory motion, where the tip is cycled away and towards the surface. Finally we present representative results for applying a constant force to the end of the chain as an alternative to pulling it at a constant rate.

Our experimental study could be extended by investigating the influence, if any, of the cation in the PEO/salt studies and its correlation to the depth of the plateau event in force profiles could be determined. The PNIPAM system could be further explored by studying it in other known poor solvents, *e.g.*, EtOH. In our theoretical study, we could extend this work by examing the effect of solvency, as well as extension rate on features observed in force profiles. A complementary experimental study could be undertaken to determine if the predictions made by our theoretical work are observed in experimental force profiles. Our simulation work will be the subject of future studies. Some of the practical studies which we intend to under-

take include a thorough analysis of the effects of chain length, temperature, surface attraction and pulling rates on the detachment of an end-tethered chain from an adsorbing surface. Using the retraction/approach cycles to investigate the adhesion of single chains on surfaces, contrasting the two different experiment techniques of pulling the chain at a constant rate to the application of a constant force and possibly studying the effects of solvency on features observed in force profiles.